# Université Lille1 Sciences et Technologies

*Laboratoire de Mécanique de Lille (UMR 8107)*

Année : 2009-2010 N° d'ordre: 40170

# Thèse

*Pour obtenir le grade de*
*Docteur de l'Université Lille1 Sciences et Technologies*

Discipline : Génie Civil

## *Modélisation et simulation à l'échelle nanométrique de l'effet de température, de pression et des polluants sur l'argile hydratée de type montmorillonite*

Présentée et soutenue publiquement par

Yuanyuan ZHENG

Soutenue le 10 Novembre, 2009 devant le jury constitué de :

| | |
|---|---|
| M. Isam SHAHROUR, Professeur, Polytech'Lille/ULST (France) | Président |
| M. Rajeev AHUJA, Professeur, Université d'Uppsala (Suède) | Rapporteur |
| M. Artem OGANOV, Professeur, Université de l'État de New York, (États-Unis) | Rapporteur |
| M. Daniel TUNEGA, HDR, Université de Vienna (Autriche) | Rapporteur |
| M. Frédéric PLAS, Directeur Scientifique, ANDRA (France) | Examinateur |
| M. Jean-Claude ROBINET, Professeur, INSA de Rennes (France) | Examinateur |
| M. Ali ZAOUI, Professeur, Polytech'Lille/ULST (France) | Directeur de Thèse |

*A mes parents*

*A Zheng DAI*

# Acknowledgments

This research project would not have been possible without the support of many people. I would like to take this opportunity to thank all colleagues and friends who have given me support and encouragement in my thesis work.

I want to express my deepest gratitude to my supervisor Ali ZAOUI, Professor of Polytech'Lille, whose patience, continuous encouragement, support and guidance from the initial to the final level enabled me to develop an understanding of the subject of my thesis. He gave me the opportunity to discover and to learn this new and very interesting field of research.

It is an honour for me to thank Professor Isam SHAHROUR who has been abundantly helpful and assisted me in numerous ways.

I would like to thank the members of my PhD Committee, Rajeev AHUJA, Artem R. OGANOV, and Daniel TUNEGA for their help and suggestions concerning my research, Jean-Claude ROBINET and Frédéric PLAS for their attentive lecture of my manuscript and examination of my work.

I would like to express my sincere gratitude to my group members: Ibrahim Khalil Benazzouz, Abid Berghout, Ayoub Aaeid, Al-Fach Mohanad for sharing the literature and invaluable assistance.

I would like to thank my friends: PENG Cheng, WANG Xi, QIU Xiang, XU Quan and CAO Jianping, who have given me abundantly help and advices, and accompany me during the hard period.

I wish to express my love and gratitude to my families: my husband DAI Zheng and my parents, for their understanding, endless love, encouragement and support, through the duration of my studies.

Finally, I want to thank all my friends in Lille for their friendship and supports.

# Table of Contents

# List of Figures

# List of Tables

# *General introduction*

Clay mineral is widely distributed over the earth. It impacts a wide variety of environmental and engineering processes. Some clays increase or decrease in volume as they absorb or lose water. The amount of volume change will depend on both the amount and the type of clay minerals present because some clay can absorb more water than others with a proportionally greater effect. These volume changes can cause either swelling or shrinking of clay, which may generate extensive structural damage to constructing engineering which are not sturdy enough and have shallow foundations.

On the other hand, the swelling clay is of great interest in geoenvironmental engineering as liners due to its low hydraulic conductivity, high swelling capacity and high surface area. Clays are used as one of the constituents of engineered barriers around underground storage sites for high-activity radioactive waste due to their low permeability to water and high retention capacity for cations. The storage of nuclear waste imposes elevated temperatures on the surrounding smectite buffer material for about thousands of years. So the effect of temperature on the nature of clay is necessary to investigate. Furthermore, since the storages of radioactive waste are always constructed underground, the mechanic properties of the clay material is of great importance and justify a detailed study.

Montmorillonite, a member of the smectite group, is a naturally occurring swelling clay. This typical 2:1 clay is complex and has diverse kinds of components due to the possibility of extensive isomorphous substitution in the clay's framework. Thereafter, the negative charge resulting from these substitutions in the clay needs to be balanced by adsorbing cations. The interaction between successive clay layers is by van der Waals forces and by cations, so that these bonds are weak and easily separated by cleavage or absorption of water or other polar liquids.

The experimental studies on clay minerals are not always easy because clays are ultra fine grained which require special analytical techniques, and their low permeability of water which needs much time to reach its equilibration. The computer simulations are now the third way of research, which is a necessary complement to experiment and theory. The simulation permits to study the phases that are

inaccessible in laboratory (high temperature, high pressure, etc.). It is a powerful interpretation of the experimental results.

Molecular computer simulations have become extremely helpful in providing an atomistic perspective on the structure and behaviour of clay minerals. These studies have typically used classical Monte Carlo (MC) or molecular dynamics (MD) methods to evaluate the interlayer structure and swelling behaviour of smectite clays.

In this thesis, we will investigate the Wyoming-type montmorillonite by means of Monte Carlo and Molecular Dynamic simulation methods. As shown in figure *i*, we will study the swelling and shrinking behaviours of the clay under the influence of water content, temperature, and different counterions. We will also study the diffusion behaviours of water and counterions in the interlayer space of montmorillonite, considering the effect of hydrated states, existing cations and the temperature. In addition, we will perform simulations to study the evolution of volume of different hydrated clay with increasing pressure to find the bulk modulus of the clay and give a prediction on the phase transition pressure of montmorillonite. Comparing our simulation results with available experimental and other theoretical results, we can extend our investigations to predict the properties of montmorillonite including, especially, some heavy metal cations as pollutants.

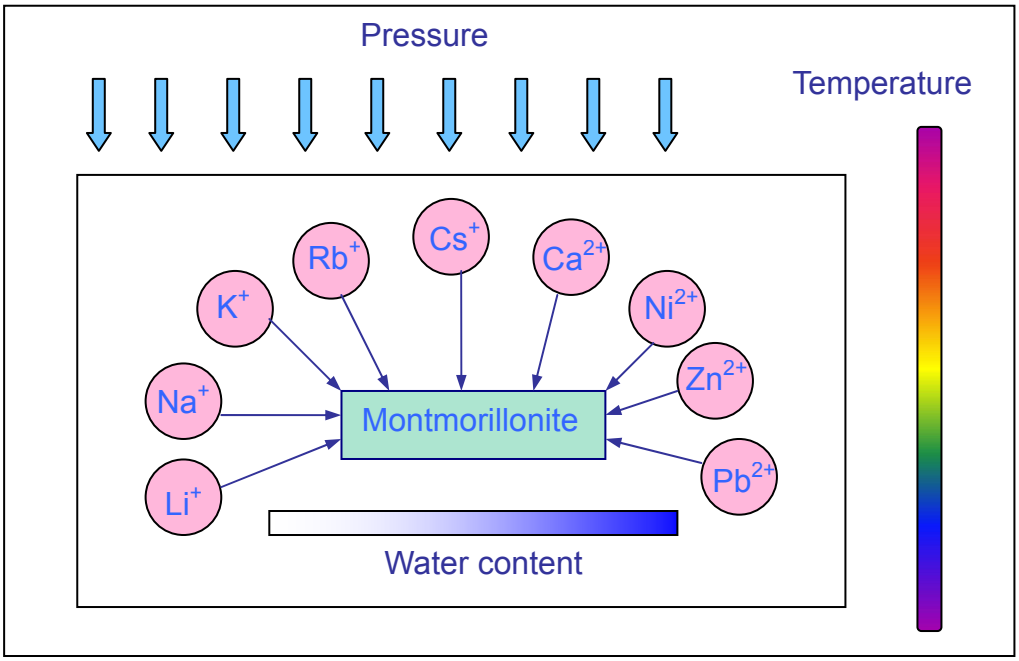


Figure *i*: Influence factors considered in our investigation of montmorillonite.

The first chapter is a summary of the clay minerals, where we will give an overview of the clay minerals concerning their compositions, the atomic structure and the classification, etc.. We will focus on the typical swelling clay, the Wyoming-type montmorillonite, which contains not only some common cations such as $Na^+$, $Li^+$, $K^+$, $Ca^{2+}$, but also some heavy metal cations as pollutant, such as $Rb^+$, $Cs^+$, $Ni^{2+}$, $Zn^{2+}$ and $Pb^{2+}$.

The second chapter focused on the simulation methods that we will use in this work. This section contains two parts: the modelling and the simulation. The modelling part describes the atomic positions and effective charges of a unit cell montmorillonite, a summary of different water models for choice, as well as the interatomic potentials between the components of the water-cation-clay system. In the simulation part, we will introduce first the simulation conditions, the periodic boundary conditions and the ensembles such as NVE, NVT, and NPT. Thereafter, two typical molecular simulation methods, Molecular Dynamic and Monte Carlo, will be presented respectively. We will make a summary on their theory, algorithm and simulation process.

In chapter 3, we will introduce our Monte Carlo simulation results about the swelling and shrinking behaviours of montmorillonite. These simulations will be performed on the montmorillonite including nine counterions respectively to find the effect of cations especially the pollutants on the swelling of this clay. The hydration and dehydration process of montmorillonite will be simulated respectively at 300K to study the swelling and shrinking property of montmorillonite at room temperature. Moreover, simulations will be extended to perform temperature varying from 260K to 400K in order to find the effect of heat on the swelling behaviour of different hydrated montmorillonite. The warming and cooling processes of the clay system will be simulated respectively to investigate their consequences on the evolution of the layer spacing of hydrated clay in different conditions of water content and variety of cations.

The fourth chapter studies the diffusion of water and different counterions in the interlayer space of montmorillonite by means of Molecular Dynamic simulation methods. We want to investigate the diffusion behaviour of the interlayer particles under the influence of hydration degree, and then the effect of different existing counterions especially the pollutants on the diffusion of water. This investigation will be performed at 300K. Moreover, the temperature of this clay system will vary from

260K to 400K to find the effect of temperature on the translation diffusion of water and counterions in the clay.

In chapter 5, we will attempt to provide a detailed study on shrinking behaviour of hydrated montmorillonite under pressure to shed light on the rigidity of this clay affected by the hydrated degree. Simulations will be performed on montmorillonite including different counterions, especially some heavy metal cations, to find the effects on the nature of pollutant on this quantity.

Finally, a summary of the thesis will be given at the end of the manuscript.

# Part I :

# Theory

# Chapter 1

# Overview on the clay minerals

## 1.1. General introduction about the clay minerals

Clay is a naturally occurring material composed primarily of fine-grained minerals, which show plasticity through a variable range of water content, and which can be hardened when dried and/or fired.

Clay minerals are typically formed over long periods of time by the gradual chemical weathering of rocks, usually silicate-bearing, by low concentrations of carbonic acid and other diluted solvents. They are very common in fine grained sedimentary rocks such as shale, mudstone and siltstone and in fine grained metamorphic slate and phyllite.

Clay minerals are hydrous aluminium phyllosilicates, sometimes with variable amounts of iron, magnesium, alkali metals, alkaline earths and other cations. They have structures similar to the micas and therefore form flat hexagonal sheets.

Clay exhibit plasticity when mixed with water in certain proportions. When dry, clay becomes firm and when fired in a kiln, permanent physical and chemical reactions occur. These reactions among other changes cause the clay to be converted into a ceramic material.

Being relatively impermeable to water, clay is used where natural seals are needed, such as in the cores of dams, or as a barrier in landfills against toxic seepage.

Recent studies have investigated clay's absorption capacities in various applications, such as the removal of heavy metals from waste water and air purification.

## 1.2. Characterization of the structure of clays

Clays are commonly referred to as 1:1 or 2:1 which are fundamentally built of tetrahedral sheets and octahedral sheets, as described in the structure section below. A 1:1 clay would consist of one tetrahedral sheet and one octahedral sheet, for example, kaolinite and serpentine. A 2:1 clay consists of an octahedral sheet sandwiched between two tetrahedral sheets, for example illite, smectite and attapulgite.

### 1.2.1. Tetrahedral sheet

In most clay mineral structures, the silica tetrahedrons are interconnected in a sheet structure. Three of the four oxygens in each tetrahedron are shared to form a hexagonal net, as shown in Figure 1-1 and Figure 1-2. The bases of the tetrahedrons are all in the same plane, and the tips all point in the same direction. The structure can be repeated indefinitely and has the composition $(Si_4O_{10})^{4-}$. Electrical neutrality can be obtained by replacement of four oxygens by hydroxyls or by union with a sheet of different composition that is positively charged. The oxygen-to-oxygen distance is 2.55 Å; the space available for the silicon ion is 0.55 Å, and the thickness of the sheet in clay mineral structures is 4.63 Å [1].

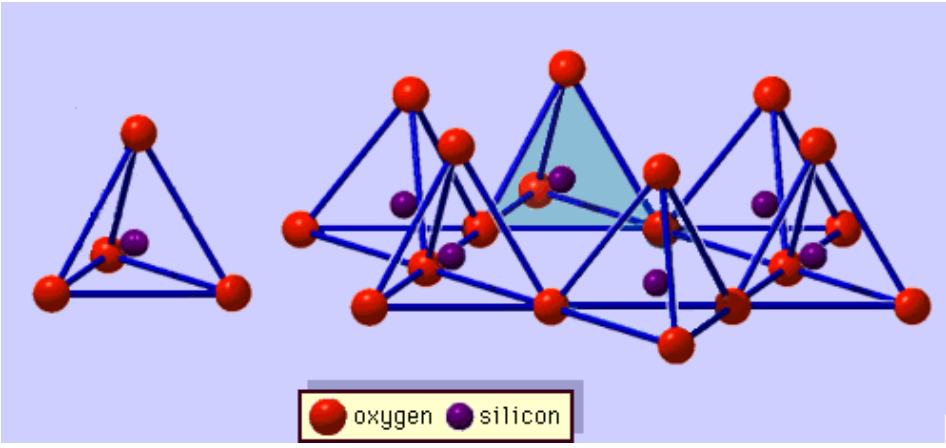


Figure 1-1: Silicon tetrahedron and silica tetrahedra arranged in a hexagonal network.

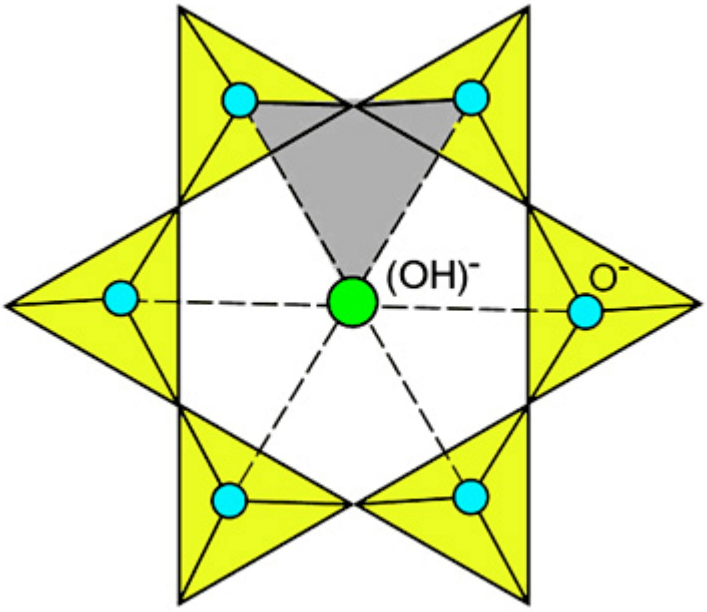


Figure 1-2: Silica sheet in plan view.

### 1.2.2. Octahedral sheet

This sheet structure is composed of aluminium or magnesium coordinated octahedral with oxygens or hydroxyls. In some cases, other cations are present in place of $Al^{3+}$ and $Mg^{2+}$, such as $Fe^{2+}$, $Fe^{3+}$, $Mn^{2+}$, $Ti^{4+}$, $Ni^{2+}$, $Cr^{3+}$ and $Li^{+}$. Figure 1-3 is a schematic diagram of such a sheet structure. The oxygen-to-oxygen distance is 2.60 Å, and the space available for the octahedral coordinated cation is 0.61 Å. The thickness of the sheet is 5.05 Å in clays. [1]

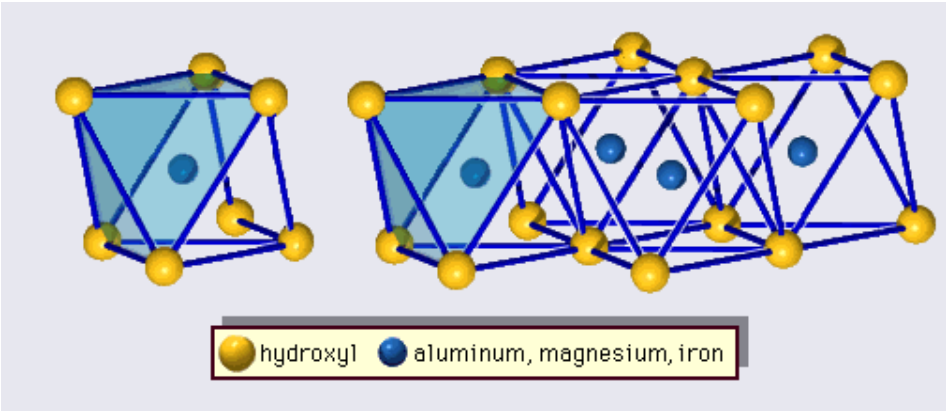


Figure 1-3: Octahedral unit and sheet structure of octahedral units

If the octahedral coordinated cation is divalent, then normally all possible cation sites are filled and the structure is trioctahedral, as shown in Figure 1-4 (a). In the case of magnesium, the composition is $Mg_3(OH)_6$.

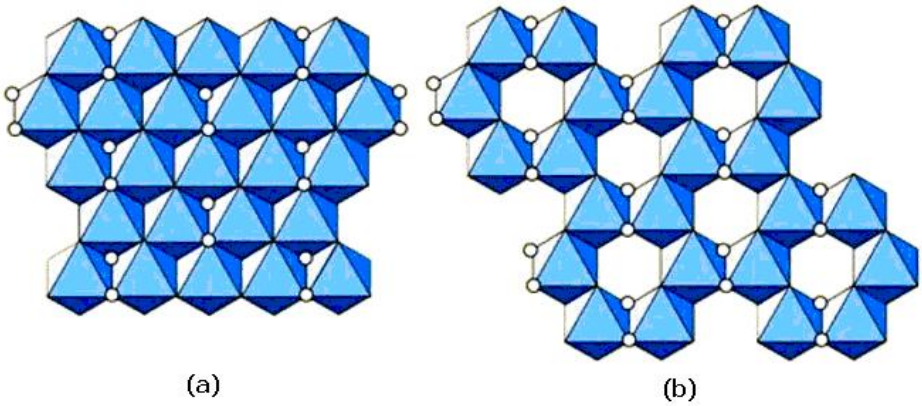


Figure 1-4: Octahedral sheet in plan view. (a) Trioctahedral layer; (b) Dioctahedral layer

If the cation is trivalent, then only two-third of the possible cationic spaces are filled, and the structure is termed dioctahedral, as presented in Figure 1-4 (b). In the case of aluminium, the composition is $Al_2(OH)_6$.

### 1.2.3. Synthesis pattern and classification of the clay minerals

The manner in which atoms are assembled into tetrahedral and octahedral units, followed by the formation of sheets and their stacking to form layers that combine to produce the different clay mineral groups is illustrated in Figure 1-5. The basic structures shown in the bottom row of this figure comprise the great preponderance of the clay mineral types that are found in soils.

Grouping the clay minerals according to crystal structure and stacking sequence of the layers is convenient, since members of the same group have generally similar engineering properties. The classification scheme for layer silicates recommended by the Nomenclature Committee of the Clay Minerals Society[2] (1991) was developed on this basis and is shown in Table 1-1.

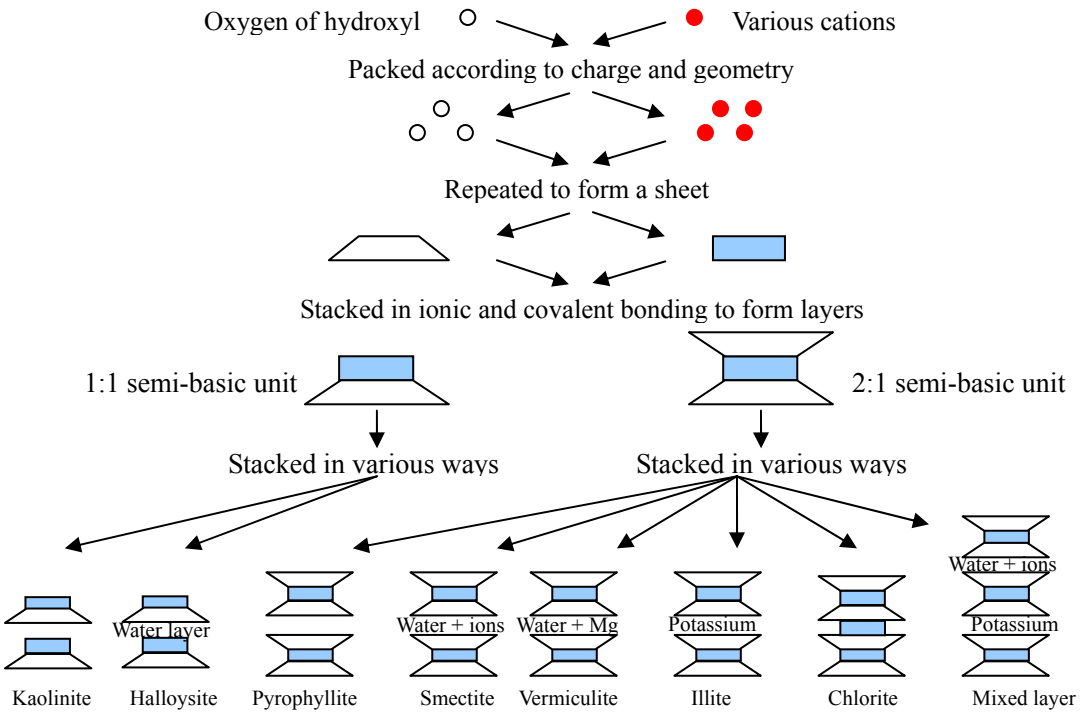


Figure 1-5: Synthesis pattern for the clay minerals [3].

The bottom row of Figure 1-5 shows that the 2:1 minerals differ from each other mainly in the type and amount of “glue” that holds the successive layers together. For example, the smectites have loosely held cations between the layers, the illites contain firmly fixed potassium ions, and the vermiculites have somewhat organized layers of water and cations. The chlorite group represents an end member that has 2:1 layers bonded by an organized hydroxide sheet. The charge per formula unit is variable both within and among groups, and this reflects the fact that the range of compositions is great owing to varying amounts of isomorphous substitution. Because of this the boundaries between groups are somewhat arbitrary.

## 1.3. Damages caused by the swelling and shrinking of clay

Many soils contain clay minerals that absorb water when wet, which makes them swell, and lose water as they dry, which makes them shrink. Many of us see this in our gardens when the ground becomes cracked during the summer, shown in Figure 1-6, yet becomes ‘heavy’ in the winter. This shrink-swell behavior is controlled by the type and amount of clay in the soil, and by seasonal changes in the soil moisture content, also related to rainfall and local drainage. The cracking is an obvious surface

effect. It is not always realized that the fissures may penetrate to a depth of 3 m, and exceptionally, can reach 10 m below the ground surface.

**Table 1-1: Classification of Planar Hydrous Phyllosilicates (from R. T. Martin, 1991[2])**

| Layer type | Interlayer material* | Group | Octahedral character | species |
|---|---|---|---|---|
| 1:1 | None or H2O only ($\chi \sim 0$) | Serpentine-kaolin | Trioctahedral | Lizardite, berthierine, amesite, cronstedtite, nepouite, kellyite, fraipontite, brindleyite |
| | | | Dioctahedral | Kaolinite, dickite, nacrite, halloysite (planar) |
| | | | Di-trioctahedral | Odinite |
| 2:1 | None ($\chi \sim 0$) | Talc-pyrophyllite | Trioctahedral | Talc, willemseite, kerolite, pimelite |
| | | | Dioctahedral | Pyrophyllite, ferripyrophyllite |
| | Hydrated exchangeable cations ($\chi \sim 0.2$-$0.6$) | Smectite | Trioctahedral | Sauconite, stevensite, swinefordite, hectorite, Saponite, |
| | | | Dioctahedral | Nontronite, volkonskoite, beidellite, montmorillonite, |
| | Hydrated exchangeable cations ($\chi \sim 0.6$-$0.9$) | vermiculite | Trioctahedral | Trioctahedral vermiculite |
| | | | Dioctahedral | Dioctahedral vermiculite |
| | Non-hydrated monovalent cations ($\chi \sim 0.6$-$1.0$) | True (flexible) mica | Trioctahedral | Biotite, phlogopite, lepidoilite, etc. |
| | | | Dioctahedral | Muscovite, glauconite, celadonite, paragonite, illite, etc. |
| | Non-hydrated divalent cations ($\chi \sim 1.8$-$2.0$) | Brittle mica | Trioctahedral | Clintonite, kinoshitalite, bityite, anandite |
| | | | Dioctahedral | margarite |
| | Hydroxide sheet ($\chi$ = variable) | chlorite | Trioctahedral | Clinochlore, chamosite, pennantite, nimite, baileychlore |
| | | | Dioctahedral | Donbassite |
| | | | Di-trioctahedral | Cookeite, sudoite |
| 2 :1 | Regularly interstratified ($\chi$ = variable) | variable | Trioctahedral | Corrensite, aliettite, hydrobiotite, kulkeite |
| | | | Dioctahedral | Rectorite, tosudite |

*$\chi$ is net layer charge per formula unit.

Expansive clay is prone to large volume changes when the water content changes. Mitigation of the effects of expansive clay on structures built in areas with expansive clays is a major challenge in geotechnical engineering. Cities built on top of clay compact the clay beneath as groundwater is drawn down and water is wringed out of the clay. Rebound caused by heavy rain can destroy or crack building, and permanent land subsidence may occur in large cities with significant skylines.


Figure 1-6: Cracking at of the ground surface indicating shrink-swell behavior.

Swelling and shrinking of the ground is one of the most damaging geohazards in the world. Swelling soils are a major geologic hazard, and expansive clays and clay-shales cause extensive damage world-wide every year. Figure 1-7 and Figure 1-8 show the damages of houses which are caused by differential heave of the clay in the building's foundation.

Figure 1-7: House damage due to differential heave. Photograph by David C. Noe, Colorado Geological Survey.

Figure 1-8: House damage due to the sinking of the foundation.

Regarded, in France, as a "natural disaster" since 1989, the shrinking and swelling of clay soils causes extensive damage, especially to houses that are, in many cases, not sturdy enough and have shallow foundations, and has recently become the second greatest object of insurance claims, just behind flooding. Extensive damage had been observed during the summer of 2003, which was characterized by very high temperatures, we could assume that the rapid rise in losses attributed to this geological hazard was caused by climate [4].

## 1.4. The swelling clay: montmorillonite

Montmorillonite is a naturally occurring swelling clay and a member of the smectite group which has a prototype structure similar to that of Pyrophyllite, consisting of an octahedral sheet sandwiched between two silica sheets, shown in Figure 1-9. All the tips of the tetrahedral point are towards the centre of the unit cell. The oxygens forming the tips of the tetrahedral are common to the octahedral sheet as well. The anions in the octahedral sheet that fall directly above and below the ditrigonal holes formed by the bases of the silica tetrahedral are hydroxyls [3].

The Smectite minerals differ from Pyrophyllite in that there is extensive isomorphous substitution for silicon and aluminium by other cations. Aluminium in the octahedral sheet may be replaced by magnesium, iron, zinc, nickel, lithium, or other

cations. Aluminium may replace up to 15 percent of the silicon ions in the tetrahedral sheet. Possibly some of the silicon positions can be occupied by phosphorous.

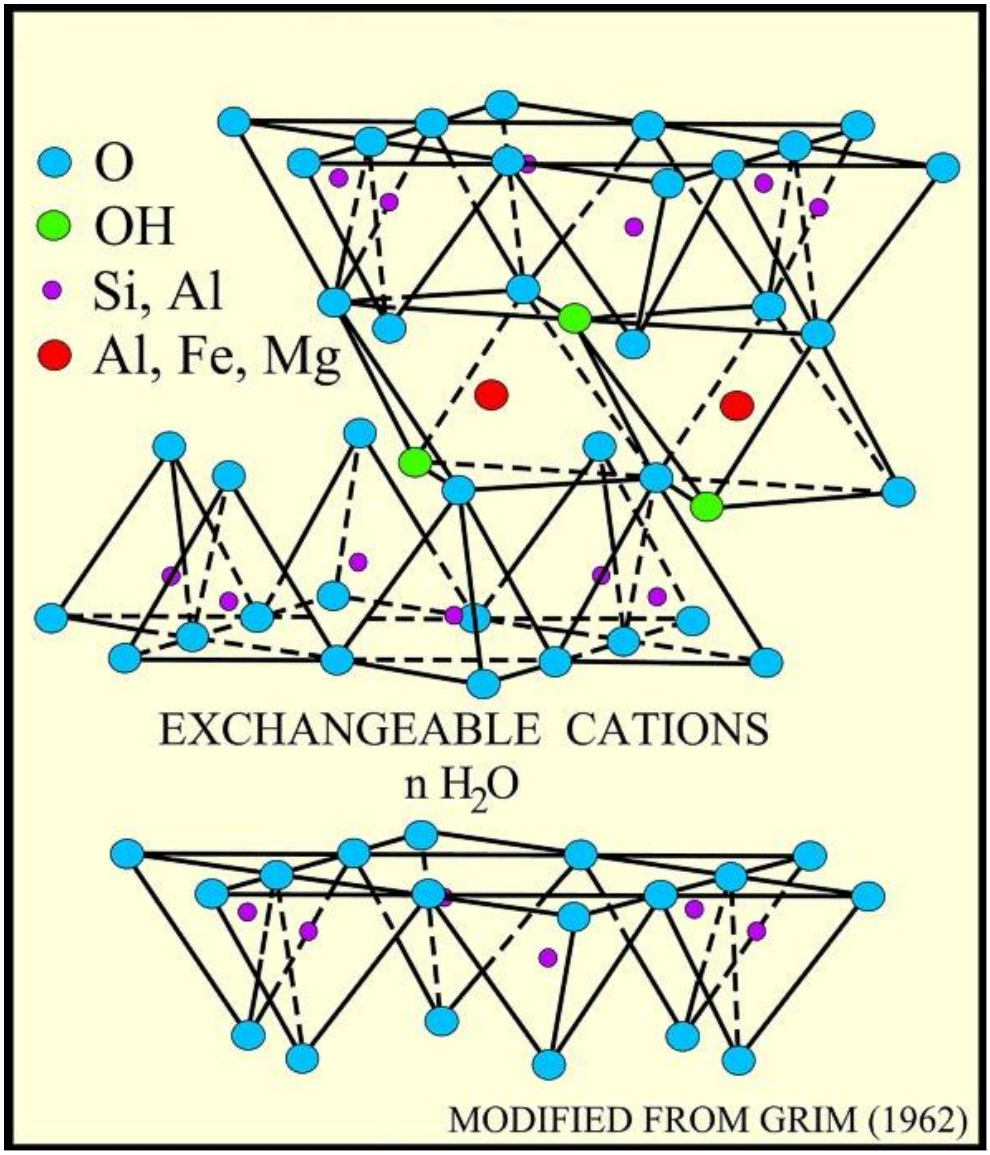


Figure 1-9: Diagrammatic sketch of the montmorillonite structure

Negative charge resulting from these substitutions is compensated by exchangeable cations located between the unit cell layers and on the surfaces of particles. A typical montmorillonite contains $Na^+$, $K^+$, $Mg^{2+}$, or $Ca^{2+}$ as interlayer cations[5, 6], which locate in the interlayer spaces and hold the neighbouring mineral layers together.

# Chapter 2

# Nanoscale simulations

## 2.1. Introduction

Molecular computer simulations have become extremely helpful in providing an atomistic perspective on the structure and behaviour of clay minerals. These studies have typically used classical Monte Carlo (MC) or molecular dynamics (MD) methods to evaluate the interlayer structure and swelling behaviour of smectite clays [7-20]. Successful application of any computational molecular modelling technique requires the use of the interatomic potentials (force field) that effectively and accurately account for the interactions of all atoms in the modelled system [21].

## 2.2. System set up

### 2.2.1. Structure of montmorillonite

In this work, we simulate a Wyoming-type montmorillonite with the unit cell formula

$$M_{0.75}\left[Si_{7.75}Al_{0.25}\right]\left(Al_{3.5}Mg_{0.5}\right)O_{20}\left(OH\right)_4$$

and

$$N_{0.325}\left[Si_{7.75}Al_{0.25}\right]\left(Al_{3.5}Mg_{0.5}\right)O_{20}\left(OH\right)_4$$

where M represents a monovalent cation. In the present work $Li^+$, $Na^+$, $K^+$, $Rb^+$, $Cs^+$ are considered. N represents a double valent cation: such as $Ca^{2+}$, $Ni^{2+}$, $Zn^{2+}$, and $Pb^{2+}$, etc.

The clay simulation models used here is derived directly from empirical models introduced by Skipper and co-workers [10].The coordinates and partial charges of

atoms in the clay crystal structure of one unit-cell of montmorillonite are presented in Table 2-1.

**Table 2-1: Atomic positions and effective charges in the unit cell of a dioctahedral clay mineral layer[10].**

| atom | x (Å) | y (Å) | z (Å) | q (e) | atom | x (Å) | y (Å) | z (Å) | q (e) |
|---|---|---|---|---|---|---|---|---|---|
| O | 2.64 | 0.0 | 3.28 | -0.8 | Al | 7.04 | 6.09 | 0.0 | 3.0 |
| O | 1.32 | 2.28 | 3.28 | -0.8 | Al | 7.04 | 3.05 | 0.0 | 3.0 |
| O | 3.96 | 2.28 | 3.28 | -0.8 | O | 0.88 | 9.14 | -3.28 | -0.8 |
| O(H) | 0.0 | 0.0 | 1.06 | -1.7175* | O | 2.2 | 6.86 | -3.28 | -0.8 |
| H | 0.8815 | 0.0 | 1.434 | 0.7175* | O | -0.44 | 6.86 | -3.28 | -0.8 |
| Si | 2.64 | 1.52 | 2.73 | 1.2 | O(H) | 3.52 | 9.14 | -1.06 | -1.7175* |
| Si | 0.0 | 3.05 | 2.73 | 1.2 | H | 2.6385 | 9.14 | -1.434 | 0.7175* |
| O | 2.64 | 1.52 | 1.06 | -1.0 | Si | 0.88 | 7.62 | -2.73 | 1.2 |
| O | 0.0 | 3.05 | 1.06 | -1.0 | Si | 3.52 | 6.09 | -2.73 | 1.2 |
| Al | 4.4 | 1.52 | 0.0 | 3.0 | O | 0.88 | 7.62 | -1.06 | -1.0 |
| Al | 4.4 | -1.52 | 0.0 | 3.0 | O | 3.52 | 6.09 | -1.06 | -1.0 |
| O | 0.0 | 4.57 | 3.28 | -0.8 | O | 3.52 | 4.57 | -3.28 | -0.8 |
| O | 3.96 | 6.85 | 3.28 | -0.8 | O | -0.44 | 2.29 | -3.28 | -0.8 |
| O | 1.32 | 6.85 | 3.28 | -0.8 | O | 2.2 | 2.29 | -3.28 | -0.8 |
| O(H) | 2.64 | 4.57 | 1.06 | -1.7175* | O(H) | 0.88 | 4.57 | -1.06 | -1.7175* |
| H | 3.5215 | 4.57 | 1.434 | 0.7175* | H | -0.0015 | 4.57 | -1.434 | 0.7175* |
| Si | 0.0 | 6.09 | 2.73 | 1.2 | Si | 3.52 | 3.05 | -2.73 | 1.2 |
| Si | 2.64 | 7.62 | 2.73 | 1.2 | Si | 0.88 | 1.52 | -2.73 | 1.2 |
| O | 0.0 | 6.09 | 1.06 | -1.0 | O | 3.52 | 3.05 | -1.06 | -1.0 |
| O | 2.64 | 7.62 | 1.06 | -1.0 | O | 0.88 | 1.52 | -1.06 | -1.0 |

- The partial charges of O(H) and H depend on the water model used in the clay system. These values are for MCY water model, O(H); for TIP4P model, O(H) will be -1.52, H will be 0.52; for SPC/E model, O(H) will be -1.4238, H will be 0.4238.

### 2.2.1.1. Substitutions in octahedral and tetrahedral sheets of montmorillonite

In our montmorillonite model, one out of eight Al atoms in octahedral sheet is replaced by a Mg atom, likewise, one out of 32 Si atoms in tetrahedral sheet is replaced by a Al atom.

Negative charges resulting from isomorphic substitutions in the octahedral or tetrahedral sheets are placed on specific cation sites within the sheets. To substitute an octahedral Al by Mg in a given site, we simply reduce the charge on that site from +3e to +2e, whereas substitution of Si by Al in the tetrahedral sheet results in a reduction in the charge on the site from +1.2e to +0.2e. The configuration of the layer is not altered to accommodate a cation substitution, but the positions of the tetrahedral substitution sites are chosen so that the top ($z > 0$) and bottom halves ($z < 0$) of the clay layer are structurally equivalent[10].

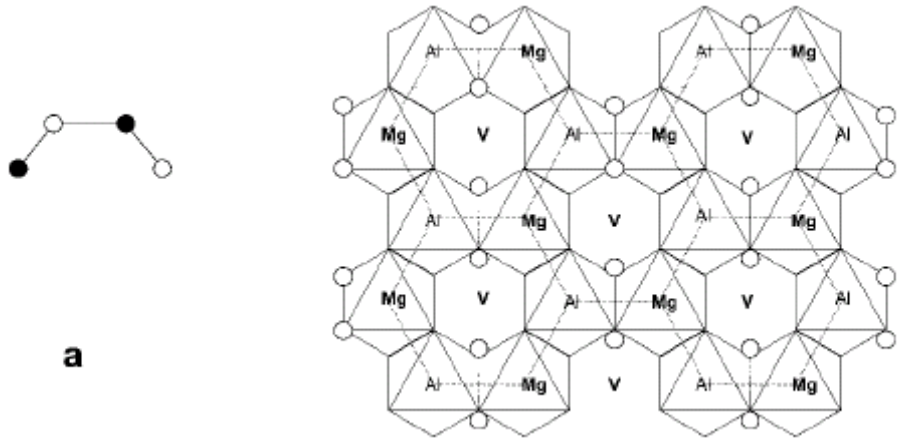


Figure 2-1: Cation distribution models for the octahedral sheet of 2:1 phyllosilicates, in a unit cell and in the crystal lattice[22].

Sainz-Diaz and coworkers have studied on the effect of the distributions of octahedral substitution in smectite clay [22], and they found that the most stable distribution model has no Mg-Mg pair presented in the clay, see Figure 2-1. Experimental studied of cation ordering in smectites and illites gave the same result in that, no Mg-Mg pair was found [23, 24]. According to their DFT simulation results, Sainz-Diaz and coworkers found that the effect of the octahedral cation distribution on the crystallographic parameters is not very significant [22], it should be because of

the locations of the octahedral sites being > 3 Å away from the basal plane surfaces of the clay mineral.

The positions of the substitutions in octahedral and tetrahedral sheets in our montmorillonite model are shown in Table 2-2.

**Table 2-2: Positions of the substitutions in octahedral and tetrahedral sheets of montmorillonite.**

| atom | x(Å) | y(Å) | z(Å) | atom | x(Å) | y(Å) | z(Å) |
|---|---|---|---|---|---|---|---|
| Substitution in octahedral sheet | | | | | | | |
| Mg | 4.4 | -1.52 | 0.00 | Mg | 4.4 | 7.62 | 0.00 |
| Mg | 14.96 | -1.52 | 0.00 | Mg | 14.96 | 7.62 | 0.00 |
| Substitution in tetrahedral sheet | | | | | | | |
| Al | 2.64 | 1.52 | 2.73 | Al | 0.88 | 1.52 | -2.73 |

## 2.2.2. Water model

Montmorillonite is a swelling clay that the existence of water in the clay system is inevitable. Several water molecular models have been developed in order to help discover the structure of water. They are useful given the basis that if the computer water model can successfully predict the physical properties of liquid water then the structure of liquid water is determined.

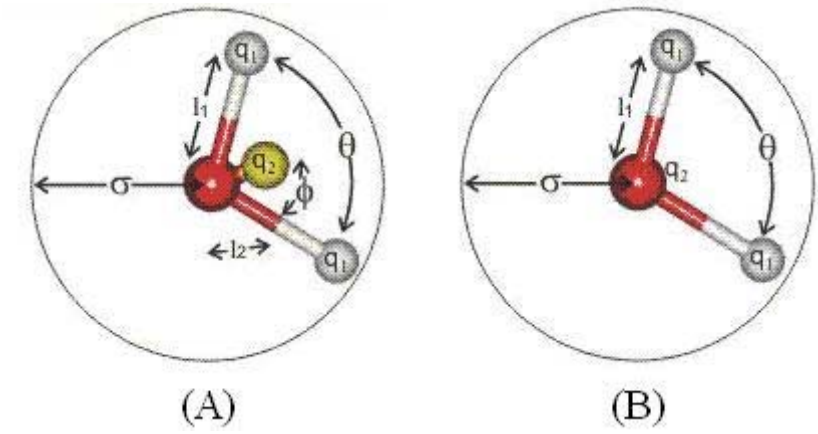


Figure 2-2: Different water models. (A) the four-point model; (B) the three-point model.

The most useful water models are four-point and three-point models as shown in Figure 2-2. The red ball signifies the oxygen, the two white ones are hydrogen, the

yellow one in type A signifies the position of charge; $l_1$ is the distance between O and H, $l_2$ is the distance between O and the charge site, $\theta$ is the angle of H-O-H, $\phi$ is the angle of H-O-charge. $\sigma$ here is Lennard-Jones parameters which signifies the separation between two similar molecules, equivalent to diameter.

Some more successful simple models are presented here: the MCY [25] and TIP4P [26] models which are the type A, four-point model; the SPC/E [27, 28] which is the type B, three-point model. In all these models, the water molecules are rigid. These models meet practical criteria of simplicity of mathematical form, rapidity of numerical evolution, and accuracy of representation of the structure, dynamics, and energetics of bulk liquid water.

### 2.2.2.1. MCY model

The MCY model was developed by fitting *ab initio* quantum chemical calculations of the potential energy $V$ of various configurations of the water dimer to the expression:

$$U^{MCY}(r) = \frac{q_i q_j}{r_{ij}} - A_{ij} e^{-B_{ij} r_{ij}} + C_{ij} e^{-D_{ij} r_{ij}} \qquad (2.1)$$

Where the indices $i$ and $j$ run over four sites on each molecule, $q_i$ is the effective charge on a site and $r_{ij}$ is the intermolecular site separation. Interaction sites ($A_{ij}, C_{ij} \neq 0$) are placed on the H and O atoms. The first term represents coulomb interactions, while the second and third terms represent van der Waals attraction and electron-overlap repulsion, respectively. A charge $q_2$ of -1.43496 e is located at a site 0.2677 Å along the $C_2$ axis, and balancing charges of 0.71748 e are assigned to the H atoms.

### 2.2.2.2. TIP4P model

The TIP4P model was developed by fitting experimental thermodynamic and X-ray structural data for liquid water, at 298 K under 1 atm. Pressure, to a four-site model of a water molecule, in which intermolecular site-site interactions are described by the expression:

$$U^{TIP4P}(r) = \frac{q_i q_j}{r_{ij}} - \frac{E_{ij}}{r_{ij}^6} + \frac{F_{ij}}{r_{ij}^{12}} \qquad (2.2)$$

Where the indices $i$ and $j$ again run over four sites on each molecule. The only interaction site ($E_{ij}$, $F_{ij} \neq 0$) is placed on the O atom, while a charge of 0.52 e is assigned to each H atom, and a charge of -1.04e is located at a site 0.15 Å along the $C_2$ axis.

#### 2.2.2.3. SPC/E model

The SPC/E model is characterized by three point masses with OH distance of 0.1 nm and H-O-H angle equal to the tetrahedral angle, with charges on the oxygen and hydrogen equal to -0.8476 e and +0.4238 e, respectively.

$$U^{SPC/E}\left(r_{ij}\right) = \frac{q_i q_j}{r_{ij}} + 4e_{ij}\left[\left(\frac{\sigma_{ij}}{r_{ij}}\right)^{12} - \left(\frac{\sigma_{ij}}{r_{ij}}\right)^{6}\right] \tag{2.3}$$

A summary of the parameters of the three water models is presented in Table 2-3.

**Table 2-3: Parameters of different water models**

| Model | Type | $l_1$ (Å) | $l_2$ (Å) | $q_1$ (e) | $q_2$ (e) | θ° | φ° | Ref. |
|---|---|---|---|---|---|---|---|---|
| MCY | A | 0.9572 | 0.2677 | +0.71748 | -1.43496 | 104.52 | 52.26 | [25] |
| TIP4P | A | 0.9572 | 0.15 | +0.5200 | -1.0400 | 104.52 | 52.26 | [26] |
| SPC/E | B | 1.000 | - | +0.4238 | -0.8476 | 109.47 | - | [27] |

(A) Four-point model (B) Three-point model (see Figure 2-2)

### 2.2.3. Interatomic potentials

Allen et al. [29] have described the potential energy for a system containing N atoms. The potential energy may be divided into terms depending on the coordinates of individual atoms, pairs, triplets etc.:

$$U = \sum_i U_1\left(r_1\right) + \sum_i \sum_{j>i} U_2\left(r_i, r_j\right) + \sum_i \sum_{j>i} \sum_{k>j>i} U_3\left(r_i, r_j, r_k\right) + \ldots \tag{2.4}$$

The first term $U_1\left(r_i\right)$ represents the effect of an external field (including, for example, the container walls) on the system. The remaining terms represent particle interactions. The second term $U_2$, the pair potential depends only on the magnitude of the pair separation $r_{ij} = \left|r_i - r_j\right|$, so it may be written as $U_2\left(r_{ij}\right)$. The $v_3$ term, three-body contribution have been made for inert gases in their solid-state f.c.c.(face centred cubic) lattices.

Four-body and higher terms in (2.4) are expected to be small in comparison with $U_2$ and $U_3$.

In all terms of equation(2.4), the pair potential is the most important. This is because the calculation of any quantity involving a sum over triplets of molecules will be very time-consuming on a computer, that the three-body and higher terms are rarely included in computer simulations. Fortunately, the pairwise approximation gives a remarkably good description of liquid properties because the average three-body effects can be partially included by defining an 'effective' pair potential. Equation (2.4) can be rewritten in the form

$$U \approx \sum_i U_1(r_1) + \sum_i \sum_{j>i} U_2^{eff}(r_{ij}) \tag{2.5}$$

We have assumed that there is no external potential, no $U_1$ term in equation(2.5). The pair potentials appearing in computer simulations are generally to be regarded as effective pair potentials of this kind, representing all the many-body effects; for simplicity, we will just use the notation $U(r_{ij})$ or $U(r)$. Then this equation will be written as:

$$U \approx \sum_i \sum_j U(r_{ij}) \tag{2.6}$$

A consequence of this approximation is that the effective pair potential needed to reproduce experimental data may turn out to depend on the density, temperature etc., while the true two-body potential $U_2(r_{ij})$ of course does not.

The pair potential consists of two parts, the repulsion and the attraction force. When two atoms approach to each other, the electronic clouds surrounding the atoms start to overlap, the energy of the system increases abruptly. The attractive long-range potential is derived from dispersion interactions. Empirical potential data compared with Lennar-Jones potential result for argon dimer is shown in Figure 2-3. We can see that Lennard-Jones potential curve fit well with the empirical one. It has been proved that the Lennard-Jones model is a good approximation at long and short distances for neutral atoms and molecules.

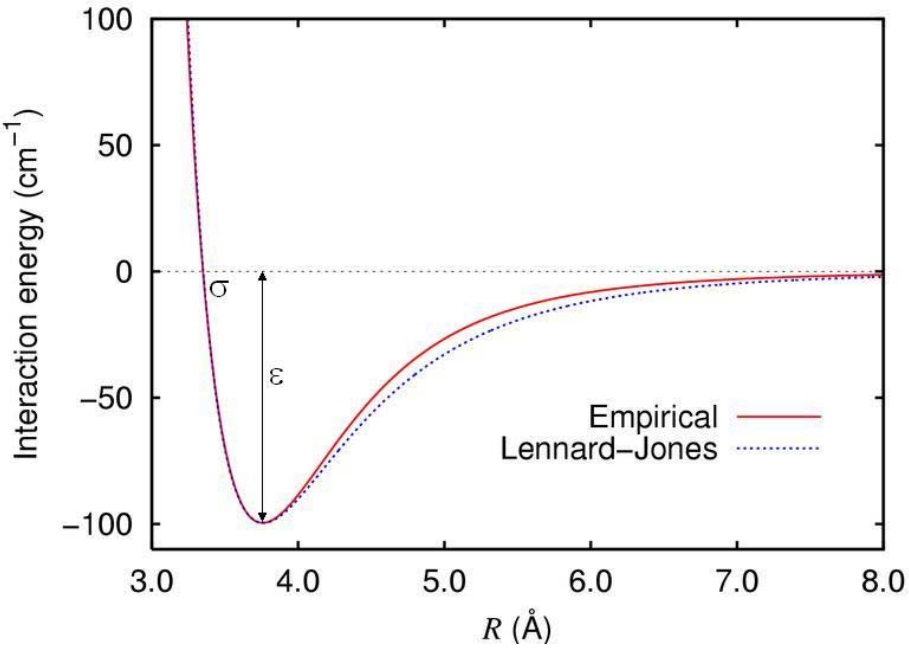


Figure 2-3: Lennard-Jones potential for argon dimer.

The formula of Lennard-Jones potential model is as following:

$$U\left(r_{ij}\right)=4\varepsilon_{ij}\left[\left(\frac{\sigma_{ij}}{r_{ij}}\right)^{12}-\left(\frac{\sigma_{ij}}{r_{ij}}\right)^{6}\right] \tag{2.7}$$

where $\varepsilon$ is the depth of the potential well, $\varepsilon_{ij}=\sqrt{\varepsilon_i\varepsilon_j}$ ; $\sigma$ is the distance at which the interparticle potential is zero, $\sigma_{ij}=\frac{1}{2}\left(\sigma_i+\sigma_j\right)$ ; $r_{ij}$ is the distance between the particles. These parameters can be fitted to reproduce experimental data or accurate quantum chemistry calculations. The $\left(\frac{1}{r}\right)^{12}$ term describes Pauli repulsion at short ranges due to overlapping electron orbitals and $\left(\frac{1}{r}\right)^{6}$ term describes attraction at long range (van der Waals force, or dispersion force).

Several other potential models have been advanced to describe the interaction between two bodies, such as Buckingham, Morse, etc.. Since the calculation of the potential of a system costs a great number of computational times especially for large systems during a simulation, it is necessary and important to choose a simple model which can well describe the interactions between atoms and is simple enough to save computation time. Comparing the potential models presented above, Lennard-Jones model, for its simplicity, is preferable to use in our simulation.

For ions, these potentials are not sufficient to represent the long-range interactions. A simple approach is to supplement one of the above pair potentials with the Coulomb charge-charge interaction

$$U^{Coulomb}\left(r_{ij}\right)=\frac{q_i q_j}{4\pi\varepsilon_0 r_{ij}} \tag{2.8}$$

Where $q_i, q_j$ are the charges on ions $i$ and $j$, $\varepsilon_0$ is the permittivity of free space.

We can see that in section 2.2.2, where we introduce three usual water models, all of their potential functions consist of a Coulomb term and a pair potential term. In the TIP4P and SPC/E function, the pair potential term adopts the Lennard-Jones potential model, whereas the MCY model used a different function to describe the pair interaction.

To describe the atomic interactions in clay systems, the interactions between clay-clay, clay-water, clay-cation, water-water, water-cation and cation-cation should be considered. To simplify the calculation, all these interaction types will be described by a same potential model. Skipper et al. [10] and Park et al. [30] have tried to describe these interactions based on the formula of water potential models, such as MCY and TIP4P. Boek et al. [31] and Chang et al. [16] have studied the clay system based on the TIP4P potential function. Smith [19], Dang et al. [32], Whitley et al. [33] and Koneshan et al. [34] have introduced some parameters corresponding to SPC/E model. The parameters of other cations which have never been introduced in clay system, were taken from UFF fore field, introduced by Rappe et al. [35]. We notice that in the UFF force field, a Lennard-Jones 12-6 type expression (2.9) is used to describe the van der Waals interaction, which is different from the general type we have introduced in equation(2.7).

$$U\left(r_{ij}\right)=\varepsilon'\left[\left(\frac{\sigma'}{r_{ij}}\right)^{12}-2\left(\frac{\sigma'}{r_{ij}}\right)^{6}\right] \tag{2.9}$$

So we need to change the parameters presented in UFF force field to make them useful with equation(2.7).

Comparing equation(2.7) and (2.9), we can obtain:

$$\begin{cases} 4\varepsilon\sigma^{12} = \varepsilon'\sigma'^{12} \\ 4\varepsilon\sigma^{6} = 2\varepsilon'\sigma'^{6} \end{cases} \tag{2.10}$$

So that

$$\sigma^6 = \tfrac{1}{2}\sigma'^6, \qquad \sigma = \sqrt[6]{\tfrac{1}{2}}\sigma', \qquad \varepsilon = \varepsilon' \tag{2.11}$$

The parameters corresponding to TIP4P, MCY and SPC/E model are presented in Table 2-4, Table 2-5, and Table 2-6, respectively. These parameters generally come from *ab initio* quantum chemical calculations and should fit the experimental data.

**Table 2-4: Parameters in the TIP4P potential function**

| Sites | $A_{ij}$ (kcal Å$^4$/mol) | $C_{ij}$ (kcal/mol) | $D_{ij}$ (Å$^{-1}$) | $E_{ij}$ (kcal Å$^6$/mol) | $F_{ij}$ (kcal Å$^{12}$/mol) | Ref. |
|---|---|---|---|---|---|---|
| O-O | 0 | 0 | 0 | 610 | 600000 | [10] |
| H-Na | 0 | 2064 | 3.394 | 0 | 0 | [10] |
| O-Na | 435 | 27343 | 3.5455 | -840 | 0 | [10] |
| Si-Na | 0 | 951.71 | 2.1286 | 0 | 0 | [10] |
| Al-Na | 0 | 951.71 | 2.1286 | 0 | 0 | [10] |
| H-Li | 0 | 1818.732 | 3.9802 | 0 | 0 | [16] |
| O-Li | 411.388 | 12539.952 | 3.3943 | -38.24[a] | 0 | [16] |
| Si-Li | 0 | 204.775 | 1.4010 | 0 | 0 | [16] |
| Al-Li | 0 | 204.775 | 1.4010 | 0 | 0 | [16] |

[a] -3.284 in the ref. [16].

**Table 2-5: Parameters in the MCY potential function.**

| Sites | $A_{ij}$(kcal/mol) | $B_{ij}$(Å$^{-1}$) | $C_{ij}$(kcal/mol) | $D_{ij}$(Å$^{-1}$) | Ref. |
|---|---|---|---|---|---|
| Water-water | | | | | |
| H-H | 0.000 | 0.000 | 666.33 | 2.7608 | [10] |
| H-O | 273.59 | 2.2333 | 1455.4 | 2.9619 | [10] |
| O-O | 0.000 | 0.000 | 1088213 | 5.1527 | [10] |
| Water-cation | | | | | |
| H-Li | 741.667 | 2.5527 | 6662.279 | 3.51582 | [30] |
| O-Li | 192.957 | 1.32063 | 14169.718 | 3.65143 | [30] |
| H-Na | 884.23 | 1.9349 | 2051.9 | 2.36095 | [10] |
| O-Na | 25.948 | 0.77461 | 61888 | 4.0849 | [10] |
| Water-clay | | | | | |
| H-Si | 2.137 | 1.22 | 577.23 | 2.15646 | [10] |
| H-Al | 2.137 | 1.22 | 577.23 | 2.15646 | [10] |
| O-Si | 1345.8 | 2.2671 | 13061 | 3.2037 | [10] |
| O-Al | 1345.8 | 2.2671 | 13061 | 3.2037 | [10] |
| Cation-clay | | | | | |
| Si-Li | 0 | 0 | 151.009 | 1.411 | [30] |
| Al-Li | 0 | 0 | 151.009 | 1.411 | [30] |
| Si-Na | 1505.4 | 1.8652 | 2164.54 | 2.1209 | [10] |
| Al-Na | 1505.4 | 1.8652 | 2164.54 | 2.1209 | [10] |

**Table 2-6: Lennard-Jones parameters used in montmorillonite with SPC/E water**

| Layer | element | q (e) | σ (Å) | ε (kcal/mol) | Ref. |
|---|---|---|---|---|---|
| Water | O | -0.848 | 3.166 | 0.156 | [19] |
| | H | 0.424 | 0.000 | 0.000 | [19] |
| tetrahedral | O | -0.800 | 3.166 | 0.156 | [19] |
| | Si | 1.200 | 1.840 | 3.153 | [19] |
| | Al | 0.200 | 1.840 | 3.153 | [19] |
| apical | O | -1.000 | 3.166 | 0.156 | [19] |
| octahedral | O | -1.424 | 3.166 | 0.156 | [19] |
| | H | 0.424 | 0.000 | 0.000 | [19] |
| | Al | 3.000 | 0.000 | 0.000 | [19] |
| | Mg | 2.000 | 0.000 | 0.000 | [19] |
| Cation | Li+ | +1 | 1.505 | 0.164 | [32] |
| | Na+ | +1 | 2.350 | 0.130 | [33] |
| | K+ | +1 | 3.331 | 0.1 | [36] |
| | Rb+ | +1 | 4.114 | 0.04 | [35] |
| | Cs+ | +1 | 3.830 | 0.100 | [19] |
| | Ca2+ | +2 | 2.869 | 0.1 | [34] |
| | Ni2+ | +2 | 2.525 | 0.015 | [35] |
| | Zn2+ | +2 | 2.462 | 0.124 | [35] |
| | Pb2+ | +2 | 3.828 | 0.663 | [35] |

### 2.2.4. Periodic boundary condition

Computer simulations are usually performed on a small number of molecules, $10 \leqslant N \leqslant 10000$. The size of the system is limited by the available storage on the host computer, and, more crucially, by the speed of execution of the program. However,

this size is not satisfactory for the simulation of a bulk system; moreover, the molecules on the surface will experience quite different forces from molecules in the bulk.

This problem of surface effects and limit of simulation size can be overcome by implementing periodic boundary conditions (PBC), presented by Born and von Karman [37]. Then we can simulate a large system by modeling a small part that is far from its edge. This small part is located in a unit simulation box and replicated throughout space to form an infinite lattice. The copies of the unit cell are called images.

In the course of the simulation, as an object moves in the original box, its periodic image in each of the neighboring boxes moves in exactly the same way. When an object passes through one face of the unit cell, it reappears on the opposite face with the same velocity. A two-dimensional version of such a periodic system is shown in Figure 2-4, where molecules can enter and leave each box across each of the four edges. In a three-dimensional example, molecules would be free to cross any of the six cube faces. During the simulation, only the properties of the unit cell need to be recorded and propagated.

Three-dimension periodic boundary conditions are particularly useful for simulating a bulk system with no surfaces present. Moreover, in simulations of planar surfaces, it is very often useful to simulate two dimensions (e.g. x and y) with periodic boundaries, while leaving the third (z) direction with different boundary conditions, such as remaining vacuum to infinity. This setup is known as slab boundary conditions.

Then the question is how to calculate properties of systems subject to periodic boundary conditions. The heart of the MC and MD programs involves the calculation of the potential energy of a particular configuration, and, in the case of MD, the forces acting on all molecules. Instead of calculating all interactions between a certain molecule and every other molecule in the simulation box and also all their images, Allen et al. have introduced an approximation called ‘minimum image convention’ to simplify this calculation. In this approximation, one consider molecule 1 to rest at the centre of a region which has the same size and shape as the basic simulation box, see Figure 2-4, the red box. Molecule 1 interacts with all the molecules lay within this

region, including the molecules in the basic box and the closest periodic images of the other molecules. This technique, which is a natural consequence of the periodic boundary conditions, was first used in simulation by Metropolis et al. [38].

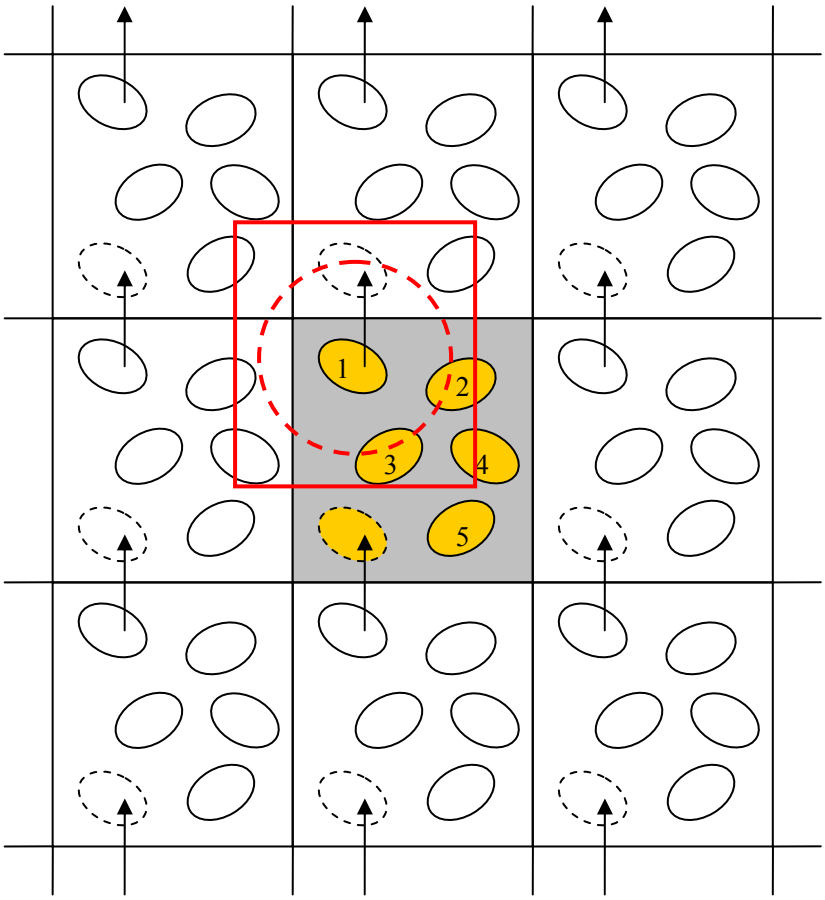


Figure 2-4: A two-dimensional periodic system. Molecules can enter and leave each box across each of the four edges. The dashed circle represents a potential cutoff.

Further approximation called 'spherical cutoff' is used to improve this situation. Because the largest contribution to the potential and forces comes from neighbours close to the molecule of interest, for short-range forces the pair potential $U(r)$ is set to zero for $r \geqslant r_c$, where $r_c$ is the cutoff distance. The dashed circle in figure 2-4 represents a cutoff. The cutoff distance should be sufficiently large to ensure the reliability of the potential calculation. For Lennard-Jones potential, the cutoff distance should be at least $2.5\sigma$. On the other hand, the cutoff distance must be no greater than half of the minimum side of the simulation box for consistency with the minimum image convention.

Of course, the penalty of applying a spherical cutoff is that the thermodynamic properties of the model will no longer be exactly the same as for the non-truncated one. So that it is possible to apply long-range corrections to approximate the desired information. Ewald summation method is used to calculate electrostatic forces in the system.

It is important to ask if the properties of a small, infinitely periodic, system, and the macroscopic system which it represents, are the same. This will depend both on the range of the intermolecular potential and the phenomenon under investigation. If the resources are available, it should be standard practice to increase the number of molecules and the box size.

In simulations containing ionic (Coulomb) interactions, the net electrostatic charge of the system must be zero to avoid summing to an infinite charge when Periodic Boundary Condition is applied.

### 2.2.5. Ensembles

Computer simulation generates information at the microscopic level (atomic and molecular positions, velocities etc.) and the conversion of this very detailed information into macroscopic terms (pressure, internal energy etc.) is the province of statistical mechanics. The thermodynamic state of a system is usually defined by a small set of parameters, such as the number of particles $N$, the temperature $T$, the pressure $P$, the energy $E$, $\sigma$ the stress and $\mu$ the chemical potential. Other thermodynamic properties, such as density $\rho$, heat capacity $C_v$ etc. may be derived through knowledge of the equations of state and the fundamental equations of thermodynamics. Even quantities such as the diffusion coefficient $D$, the shear viscosity $\eta$, and the structure factor S(k) are state functions: although they clearly say something about the microscopic structure and dynamics of the system, their values are completely dictated by the few variables, for example NPT, characterizing the thermodynamic state, not by the very many atomic positions and momenta that define the instantaneous mechanical state.

Four ensembles are in common use: the microcanonical NVE, the canonical NVT, the isothermal-isobaric NPT and NσT, and the grand canonical μVT.

#### 2.2.5.1. Microcanonical ensemble (NVE)

In the microcanonical, or NVE ensemble, the system is isolated from changes in moles (N), volume (V) and energy (E). It corresponds to an adiabatic process with no heat exchange. A microcanonical molecular dynamics trajectory may be seen as an exchange of potential and kinetic energy, with total energy being conserved.

#### 2.2.5.2. Canonical ensemble (NVT)

In the canonical ensemble, moles (N), volume (V) and temperature (T) are conserved. It is also sometimes called constant temperature molecular dynamics (CTMD). In NVT, the energy of endothermic and exothermic processes is exchanged with a thermostat.

A variety of thermostat methods are available to add and remove energy from the boundaries of an MD system in a realistic way, approximating the canonical ensemble. Popular techniques to control temperature include the Nose-Hoover thermostat, the Berendsen thermostat, and Langevin dynamics. Note that the Berendsen thermostat might introduce the flying ice cube effect, which leads to unphysical translations and rotations of the simulated system.

#### 2.2.5.3. Isothermal-Isobaric ensemble (NPT)

In the isothermal-isobaric ensemble, moles (N), pressure (P) and temperature (T) are conserved. In additions to a thermostat, a barostat is needed. It corresponds most closely to laboratory conditions with a flask open to ambient temperature and pressure.

In the simulation of biological membranes, isotropic pressure control is not appropriate. For lipid bilayers, pressure control occurs under constant membrane area (NPAT) or constant surface tension “gamma” (NPγT).

### 2.2.6. Simulation conditions

To model a montmorillonite particle, three-dimensional periodic boundary conditions were applied to a simulation box measured 21.12×18.28 $Å^2$, equivalent to

eight unit cells, four in the crystallographic $a$ direction and two in the crystallographic $b$ direction, interacting with six monovalent cations or three divalent counterions together with varying numbers of water molecules. The layers formed in this way are continuous in the $a$ and $b$ directions and stacked one above the other in the $c$ direction.

Skipper et al. [10] have found evidence that the properties of our relatively small simulation cell are still representative of the macroscopic system and are not influenced by artificial long-range symmetry of the imposed periodic lattice.

In practice, the short range interactions are negligible at distances greater than about 9 Å.

## 2.3. Molecular Dynamic Simulation

Molecular dynamics (MD) is a form of computer simulation in which atoms and molecules are allowed to interact for a period of time by approximations of known physics, giving a view of the motion of the atoms. Because molecular systems generally consist of a vast number of particles, it is impossible to find the properties of such complex systems analytically. MD simulation circumvents this problem by using numerical methods. It represents an interface between laboratory experiments and theory, and can be understood as a “virtual experiment”. MD probes the relationship between molecular structure, movement and function. It is a multidisciplinary method and its laws and theories stem from mathematics, physics, and chemistry, and it employs algorithms from computer science and information theory. It was originally conceived within theoretical physics in the late 1950s and early 1960s, but is applied today mostly in materials science and modelling of biomolecules….

Molecular dynamics is a specialized discipline of molecular modelling and computer simulation based on statistical mechanics. The main justification of the MD method is that statistical ensemble averages are equal to time averages of the system, known as the ergodic hypothesis. MD has also been termed “statistical mechanics by numbers” and “Laplace’s vision of Newtonian mechanics” of predicting the future by animating nature’s forces and allowing insight into molecular motion on an atomic scale. However, long MD simulations are mathematically ill-conditioned,

generating cumulative errors in numerical integration that can be minimized with proper selection of algorithms and parameters, but not eliminated entirely.

### 2.3.1. Equations of motion for atomic systems

The equations of motion for a system of N molecules may be written as

$$m_i \frac{d^2 r_i(t)}{dt^2} = F_i \tag{2.12}$$

Where $m_i$ is the mass of atom $i$, $r_i$ is the Cartesian coordinates and $F_i$ is the force on that atom.

For a system of $N$ particles with coordinates $X$ and velocities $V$, the following pair of first order differential equations may be written in Newton's notation as

$$F(r) = -\nabla U(r) = m\dot{v}(t) \tag{2.13}$$

$$v(t) = \dot{r}(t) \tag{2.14}$$

The potential energy function $U(r)$ of the system is a function of the particle coordinates $r$. It is referred to simply as the "potential" in Physics, or the "force field" in Chemistry.

For every timestep, each particle's position $r$ and velocity $v$ may be integrated with a symplectic method such as Verlet. The time evolution of $r$ and $v$ is called a trajectory. Given the initial positions (e.g. from theoretical knowledge) and velocities (e.g. randomized Gaussian), we can calculate all future positions and velocities.

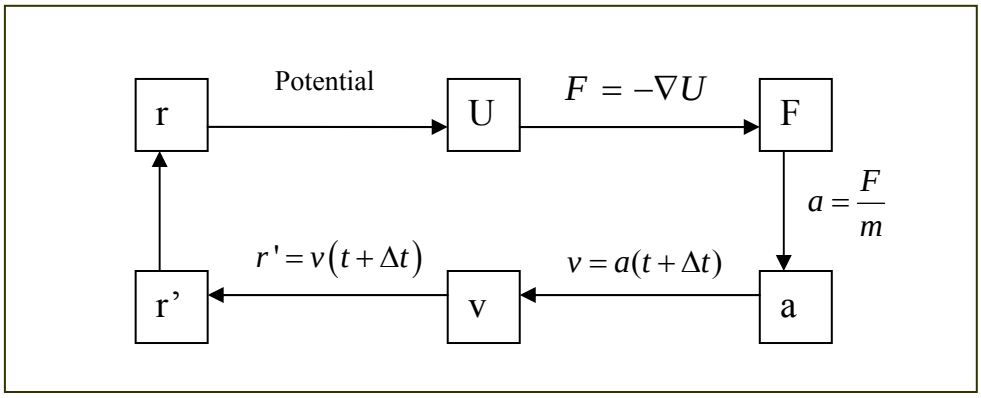


Figure 2-5: The flow diagram of the calculation of Molecular Dynamic simulation.

## 2.3.2. Algorithm

Several algorithms have been developed to treat the great quantity of calculation in molecular dynamics simulation. A successful simulation algorithm might be as follows:

It should be fast, and require little memory;

It should permit the use of a long time step $\Delta t$;

It should duplicate the classical trajectory as closely as possible;

It should satisfy the known conservation laws for energy and momentum, and the time-reversible;

It should be simple in form and easy to program.

### 2.3.2.1. Predictor-Corrector algorithm

The general scheme of a stepwise MD simulation, based on a predictor-corrector algorithm, may be summarized as follows:

- predict the positions, velocities, accelerations etc., at a time $t+\Delta t$, using the current values of these quantities;

$$\begin{aligned} r^p(t+\Delta t) &= r(t)+v(t)\Delta t+\tfrac{1}{2}a(t)\Delta t^2+\tfrac{1}{6}b(t)\Delta t^3+\cdots \\ v^p(t+\Delta t) &= v(t)+a(t)\Delta t+\tfrac{1}{2}b(t)\Delta t^2+\cdots \\ a^p(t+\Delta t) &= a(t)+b(t)\Delta t+\cdots \\ b^p(t+\Delta t) &= b(t)+\cdots \end{aligned} \tag{2.15}$$

Where $r$ and $v$ are positions and velocities, $a$ is acceleration and $b$ denotes all the third time derivatives of $r$.

- evaluate the forces, and hence accelerations $a_i=\frac{f_i}{m_i}$, from the new positions $a^c(t+\Delta t)$ and these can be compared with the predicted accelerations from (2.15), to estimate the size of the error in the predictions step:

$$\Delta a(t+\Delta t)=a^c(t+\Delta t)-a^p(t+\Delta t) \tag{2.16}$$

- correct the predicted positions, velocities, accelerations etc., using the new accelerations;

$$\begin{aligned} r^c\left(t+\Delta t\right) &= r^p\left(t+\Delta t\right)+c_0\Delta a\left(t+\Delta t\right) \\ v^c\left(t+\Delta t\right) &= v^p\left(t+\Delta t\right)+c_1\Delta a\left(t+\Delta t\right) \\ a^c\left(t+\Delta t\right) &= a^p\left(t+\Delta t\right)+c_2\Delta a\left(t+\Delta t\right) \\ b^c\left(t+\Delta t\right) &= b^p\left(t+\Delta t\right)+c_3\Delta a\left(t+\Delta t\right) \end{aligned} \tag{2.17}$$

Where $c_0$, $c_1$, $c_2$, $c_3$ are coefficients with their values are proposed by Gear [39, 40].

- calculate any variables of interest, such as the energy, virial, order parameters, ready for the accumulation of time averages, before returning to a) for the next step.

### 2.3.2.2. The Verlet algorithm

The most widely used method of integrating the equations of motion is that initially adopted by Verlet [41] and attributed to Störmer [40]. This method is a direct solution of the second-order equations(2.12).

The method is based on positions $r\left(t\right)$, accelerations $a\left(t\right)$, and the positions $r\left(t-\Delta t\right)$ from the previous step.

The development in Taylor series around r in time past and future is written as:

$$\begin{aligned} r\left(t+\Delta t\right) &= r\left(t\right)+v\left(t\right)\Delta t+\tfrac{1}{2}a\left(t\right)\Delta t^2+\cdots \\ r\left(t-\Delta t\right) &= r\left(t\right)-v\left(t\right)\Delta t+\tfrac{1}{2}a\left(t\right)\Delta t^2+\cdots \end{aligned} \tag{2.18}$$

Then we can obtain the equation for advancing the positions reads as follows:

$$r\left(t+\Delta t\right)=2r\left(t\right)-r\left(t-\Delta t\right)+a\left(t\right)\Delta t^2 \tag{2.19}$$

It will be seen that the velocities do not appear at all.

The velocities are not needed to compute the trajectories, but they are useful for estimating the kinetic energy and the total energy. They may be obtained from the formula:

$$v\left(t\right)=\frac{r\left(t+\Delta t\right)-r\left(t-\Delta t\right)}{2\Delta t} \tag{2.20}$$

### 2.3.2.3. Verlet Leapfrog algorithm

Based on the Verlet scheme, Hockney [42] and Potter [43] have proposed a modification called half-step 'leap-frog' scheme. The algorithm is as following:

$$v\left(t+\tfrac{1}{2}\Delta t\right)=v\left(t-\tfrac{1}{2}\Delta t\right)+a\left(t\right)\Delta t \tag{2.21}$$

$$r\left(t+\Delta t\right)=r\left(t\right)+v\left(t+\tfrac{1}{2}\Delta t\right)\Delta t \tag{2.22}$$

The stored quantities are the current positions $r\left(t\right)$, accelerations $a\left(t\right)=\dfrac{F\left(t\right)}{m}$ and the mid-step velocities $v\left(t-\tfrac{1}{2}\Delta t\right)$. The velocity equation (2.21) is implemented first, and the velocities leap over the coordinates to give the next mid-step values $v\left(t+\tfrac{1}{2}\Delta t\right)$. During this step, the current velocities may be calculated as the average of the velocities half a timestep either side of time t:

$$v\left(t\right)=\tfrac{1}{2}\left[v\left(t-\tfrac{1}{2}\Delta t\right)+v\left(t+\tfrac{1}{2}\Delta t\right)\right] \tag{2.23}$$

Molecular dynamics simulations normally require properties that depend on position and velocity at the same time, such as the sum of potential and kinetic energy.

### 2.3.2.4. Velocity Verlet algorithm

The Velocity Verlet algorithm assumes that positions, velocities and forces are known at each full timestep. The algorithm proceeds in two stages as follows.

In the first stage a half step velocity is calculated:

$$v\left(t+\tfrac{1}{2}\Delta t\right)=v\left(t\right)+\frac{1}{2}\Delta t\frac{F\left(t\right)}{m} \tag{2.24}$$

And then the full timestep position is obtained:

$$r\left(t+\Delta t\right)=r\left(t\right)+\Delta t v\left(t+\tfrac{1}{2}\Delta t\right) \tag{2.25}$$

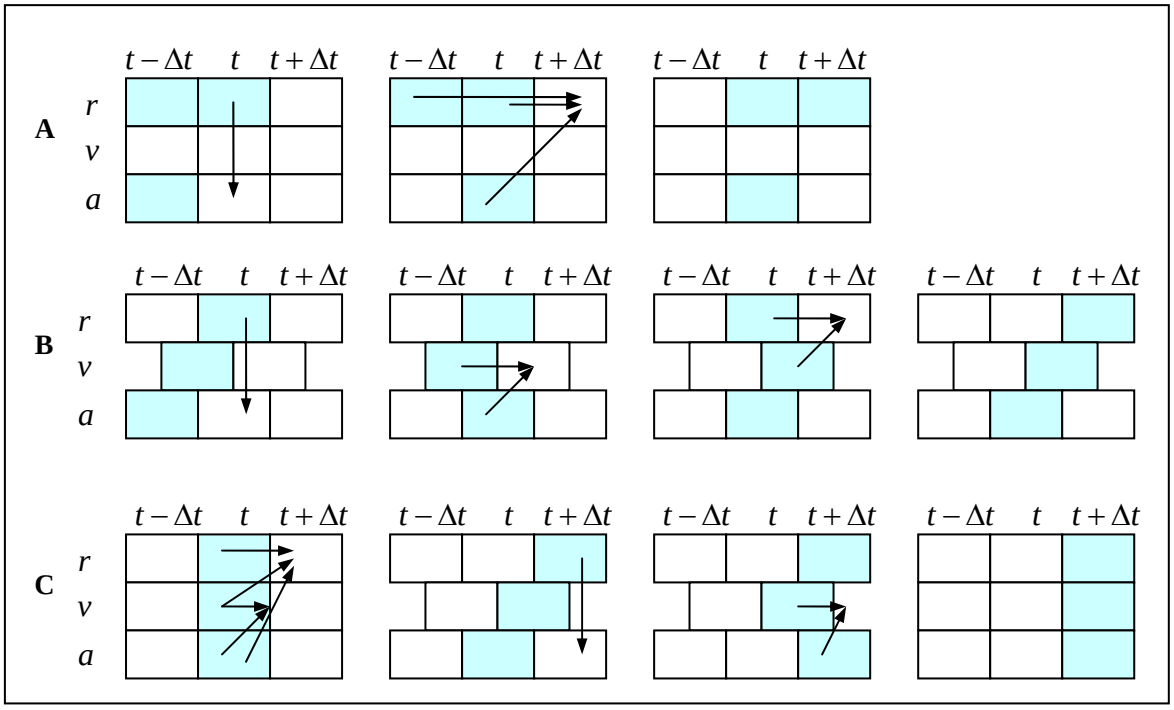


Figure 2-6: Various forms of the Verlet algorithm. (A) Verlet's original method. (B) The leap-frog form. (C) The velocity form. We show successive steps in the implementation of each algorithm. In each case, the stored variables are in cyan boxes.

In the second stage, using the new positions, the next update of the forces $F(t+\Delta t)$ is obtained, from which the full step velocity is calculated using:

$$v(t+\Delta t) = v\left(t+\frac{1}{2}\Delta t\right) + \frac{1}{2}\Delta t\frac{F(t+\Delta t)}{m} \tag{2.26}$$

Thus at the end of the two stages full synchronisation of the positions, forces and velocities is obtained.

The difference of the three verlet algorithm is shown in Figure 2-6.

## 2.4. Monte Carlo Simulation

The Monte Carlo method was developed by von Neumann, Ulam, and Metropolis at the end of the Second World War to study the diffusion of neutrons in fissionable material. The name "Monte Carlo" is chosen because of the extensive use of random numbers in the calculation.

It is a statistical method where a class of algorithms for sampling from probability distributions based on constructing a Markov chain that has the desired distribution

as its equilibrium distribution. The Markov chain means that future states depend only on the present state, and are independent of past states.

Metropolis [38] method has been employed to treat the transition matrix between states.

### 2.4.1. Algorithm

In a Monte Carlo simulation, the process is as following:

Step 1: An atom or a molecule is selected randomly in the system and given a uniform random displacement along each of the coordinate directions. All molecules in the system have an equal chance of selection. This displacement is small enough that about half the attempted moves will be accepted, but no so small that the system can get stuck in a local energy minimum. The maximum displacement $\Delta r_{\max}$ is an adjustable parameter that governs the size of the region $R$ and controls the convergence of the Markov chain, as shown in Figure 2-7.

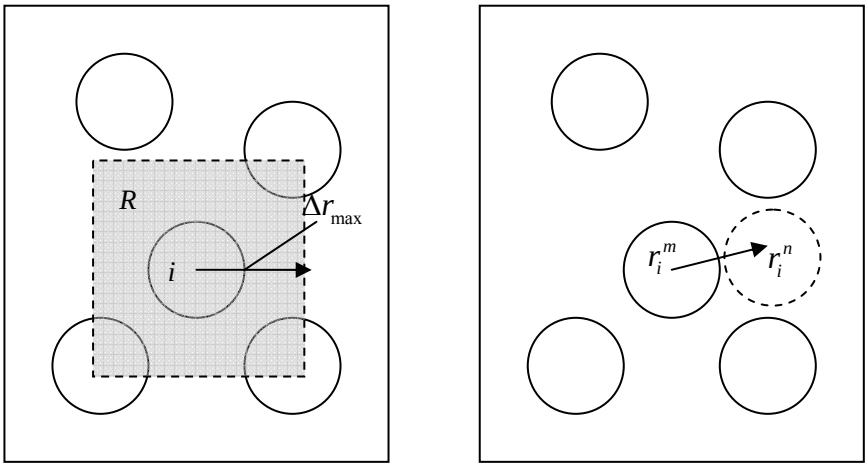


Figure 2-7: Movement of particles in Monte Carlo simulation. State n is obtained from state m by moving atom *i* with a uniform probability to any point in the shaded region *R*.

Step 2: The difference of configurational energy of the system is calculating just the changes associated with the moving atom.

$$\Delta U_{nm} = \sum_{j=1}^{N} U\left(r_{ij}^{n}\right) - \sum_{j=1}^{N} U\left(r_{ij}^{m}\right) \tag{2.27}$$

Where $m$ means the initial state and $n$ is the final state. The sum over the atoms excludes atom $i$. In calculating the change of energy, the explicit interaction of atom i with all its neighbours out to a cutoff distance is considered.

For NVT ensemble, the difference of total energy is:

$$\Delta H_{nm}^{NVT} = U_n - U_m \tag{2.28}$$

While for NPT ensemble, the difference of total energy is:

$$\Delta H_{nm}^{NPT} = \left(U_n - U_m\right) + P\left(V_n - V_m\right) - \frac{N}{k_B T}\ln\left(\frac{V_n}{V_m}\right) \tag{2.29}$$

Where, $U$ is the potential energy, $P$ is the pressure, $V$ is the volume and $N$ is the number of molecules.

Step 3:

If $\Delta H_{nm} \leqslant 0$ then the probability of state $n$, $p_n$, is greater then that of state $m$, $p_m$, and then the new configuration is accepted.

If $\Delta H_{nm} > 0$, then the move is accepted with a probability $\frac{p_n}{p_m}$. This ratio can be expressed as the Boltzmann factor as:

$$\frac{p_n}{p_m} = \exp\left(-\frac{\Delta H}{k_B T}\right) \tag{2.30}$$

Where, $T$ is the temperature and $k_B$ is the Boltzmann constant.

To accept a move with a probability shown in equation(2.30), a random number $\xi$ is generated uniformly on (0, 1).

Comparing this random number with the probability:

If $\xi < \exp\left(-\frac{\Delta H}{k_B T}\right)$, then this move is accepted;

If $\xi > \exp\left(-\frac{\Delta H}{k_B T}\right)$, then this move is rejected.

This procedure is illustrated in Figure 2-8.

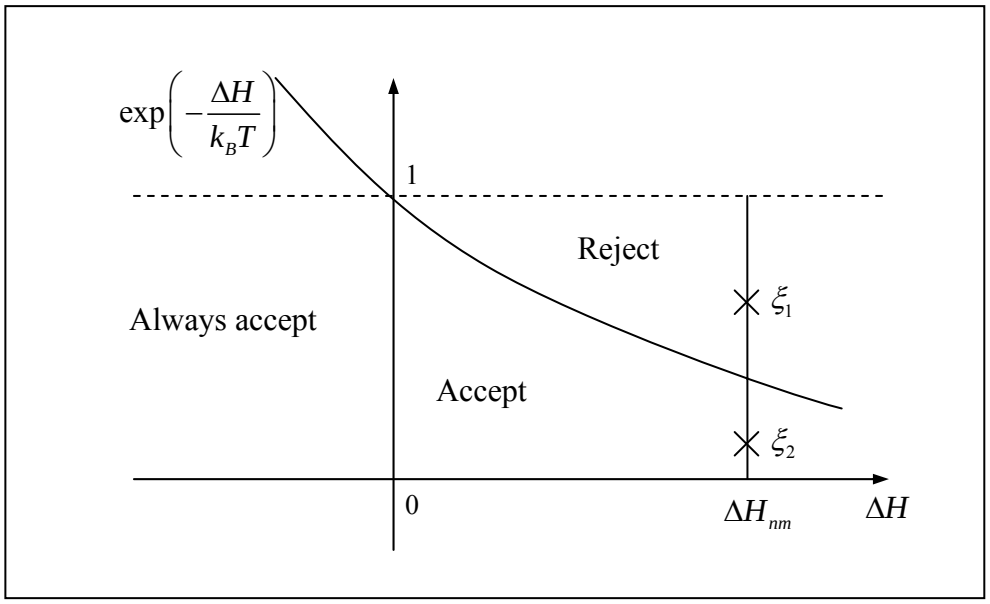


Figure 2-8: Accepting moves in the MC simulation.

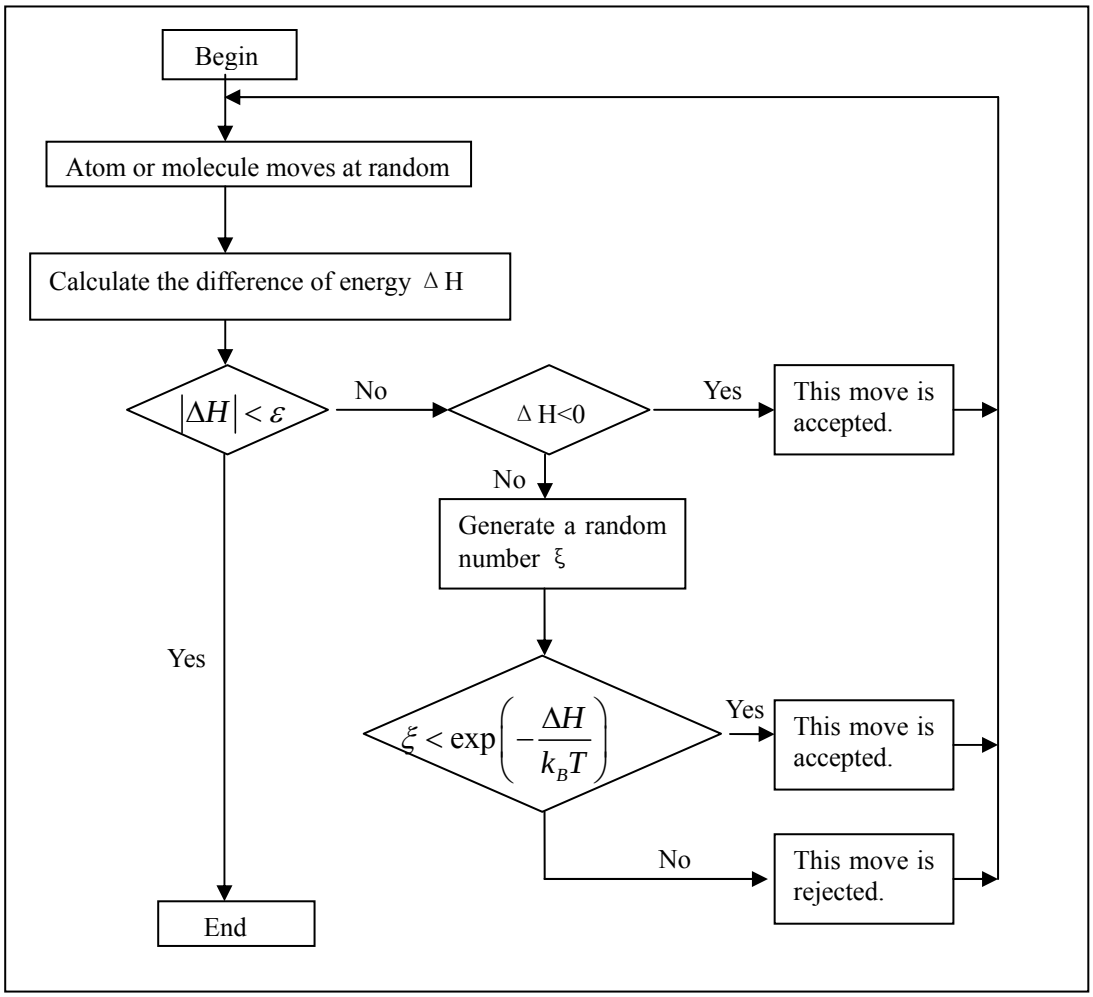


Figure 2-9: The procedure of Monte Carlo simulations.

Return to step 1 till that the energy difference between new and old configurations is small enough. So the system achieves its minimum energy and we can say that the system is stable.

This process is illustrated in Figure 2-9.

### 2.4.2. Procedure of Monte Carlo simulation

In the beginning of each simulation run, the water molecules are placed randomly within the interlayer region and the cations are placed in the mid-plane of the simulation box, following the suggestion of Chang et al. [15]. During the first optimizing run, only water molecules are permitted to move, while the layer and the interlayer cations' positions remain in their initial positions. In this step, 100000 to 1000000 moves were attempted depending on the number of water molecules included in the clay.

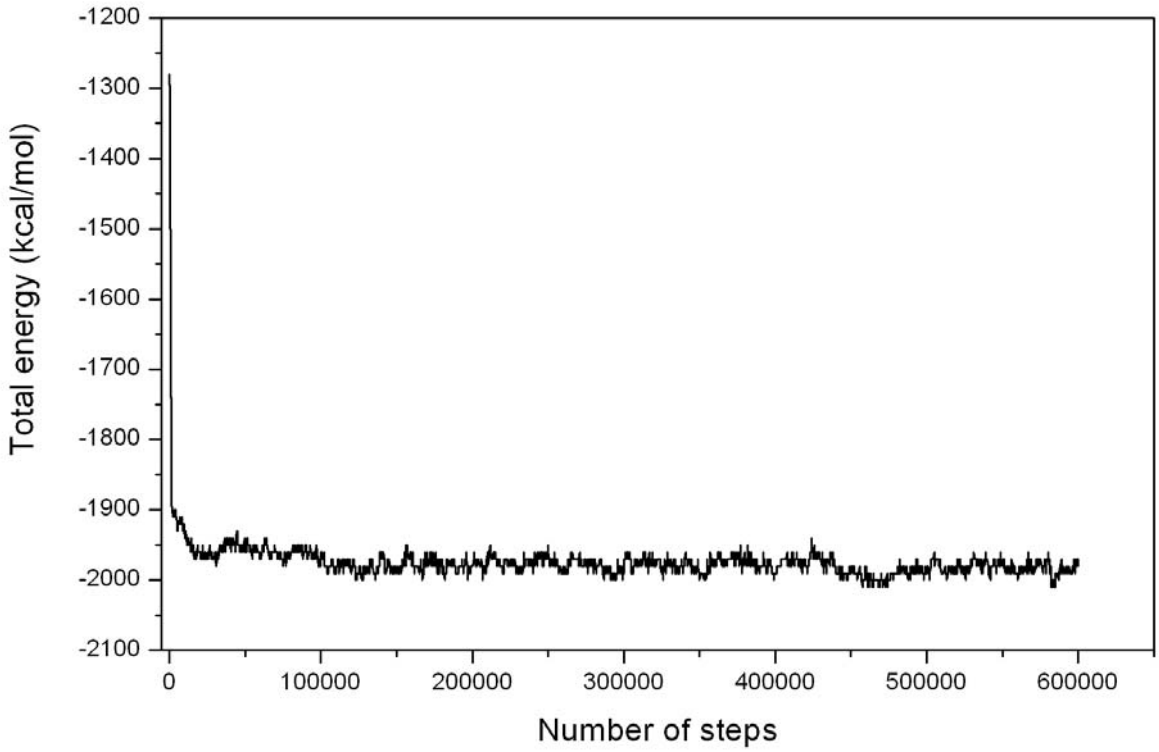


Figure 2-10: Equilibration of the total energy of 1-layer hydrated Li-montmorillonite.

In the second optimizing run, involving 100000 to 2000000 attempted moves, water molecules move and the layer spacing is permitted to vary only in the z-

direction, so that all interlayer cations become hydrated, before they start to move [10].

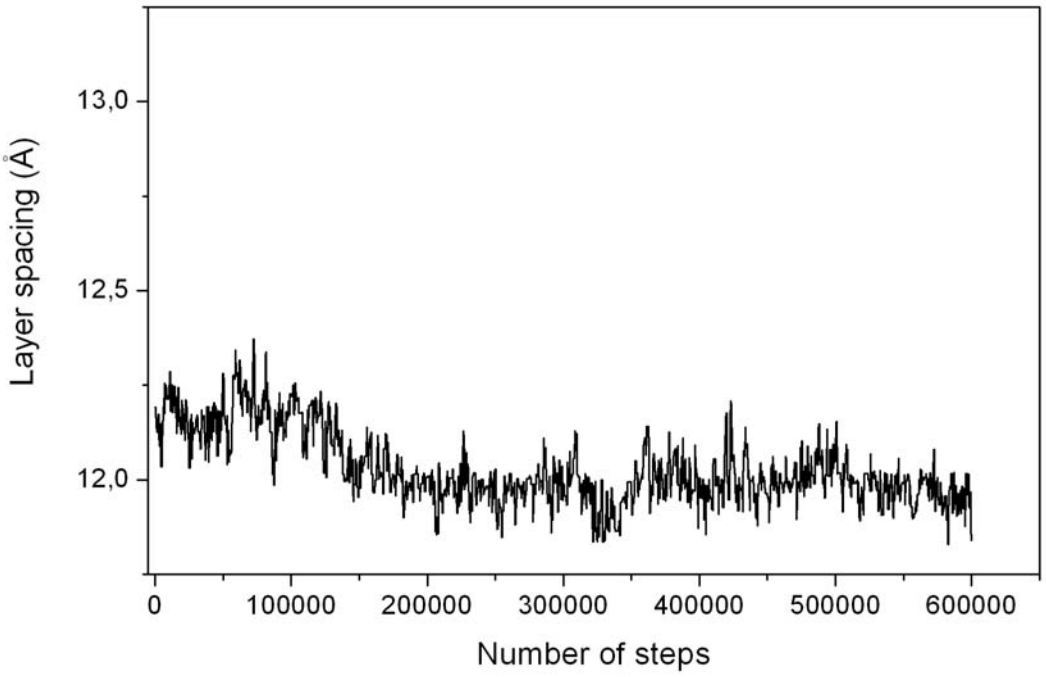


Figure 2-11: Equilibration of the layer spacing of 1-layer hydrated Li-montmorillonite.

Thereafter, the upper clay mineral layer is allowed to move one step in any direction for approximately every five movements of interlayer water molecules [15], where 600000 to 2000000 attempted moves are involved ensure that the structure is well equilibrated. Equilibration of the clay system is considered to have taken place when the average potential energy and the z-dimension of the simulation cell tend to constant values. The equilibration of the total energy, as well as the layer spacing of 1-layer hydrated Li-montmorillonite is shown in Figure 2-10 and Figure 2-11.

# Part II:

# Results

# Chapter 3

# Swelling and Shrinking of Montmorillonite

## 3.1. Introduction

As it is well known, montmorillonite is a swelling clay which has a variable volume corresponding to the water content it has. When the water content in the clay increases, montmorillonite will swell; while the water content decreases during to transpiration, the clay will shrink, in same case, the soil will split.

As described in section 1.4, montmorillonite has a lamellar structure. In Figure 3-1 we show the structure of Li-Wyoming as prototype, in different hydrations. We can see that the Oxygens stay on both sides of the clay's surfaces so that the VDW interactions between layers are weak. The existence of counterions in the interlayer space has the role of joining the clay layers together. The influence of different counterions included in the clay is necessary to be studied.

The layer spacing of a montmorillonite denotes the distance between neighbouring mineral layers plus the thickness of one mineral layer. This distance is variable upon the cations and the number of water molecules contained. Several experimental [44-49] and theoretical [10, 17, 19, 31, 50-54] studies have been devoted to the description of the swelling behaviour in smectite clay. Fu et al. [45] have studied experimentally the absorption and desorption of water in Na-saturated montmorillonite. Berend [44] presents some experiment curves about the relations between the relative pressure, water content and layer spacing of Wyoming-type montmorillonite with several counterions. Boek et al. [31] present the simulation swelling curves of Na-, Li- and K-montmorillonite. Meleshyn et al. have studied on the

crystalline and osmotic swelling of Na-montmorillonite [51] and the swelling of the clay with mix counterions, Na/Mg-montmorillonite [52]. The important role of interlayer ion size and charge in smectite swelling has been reported by Heather, D.W. et al.[33].

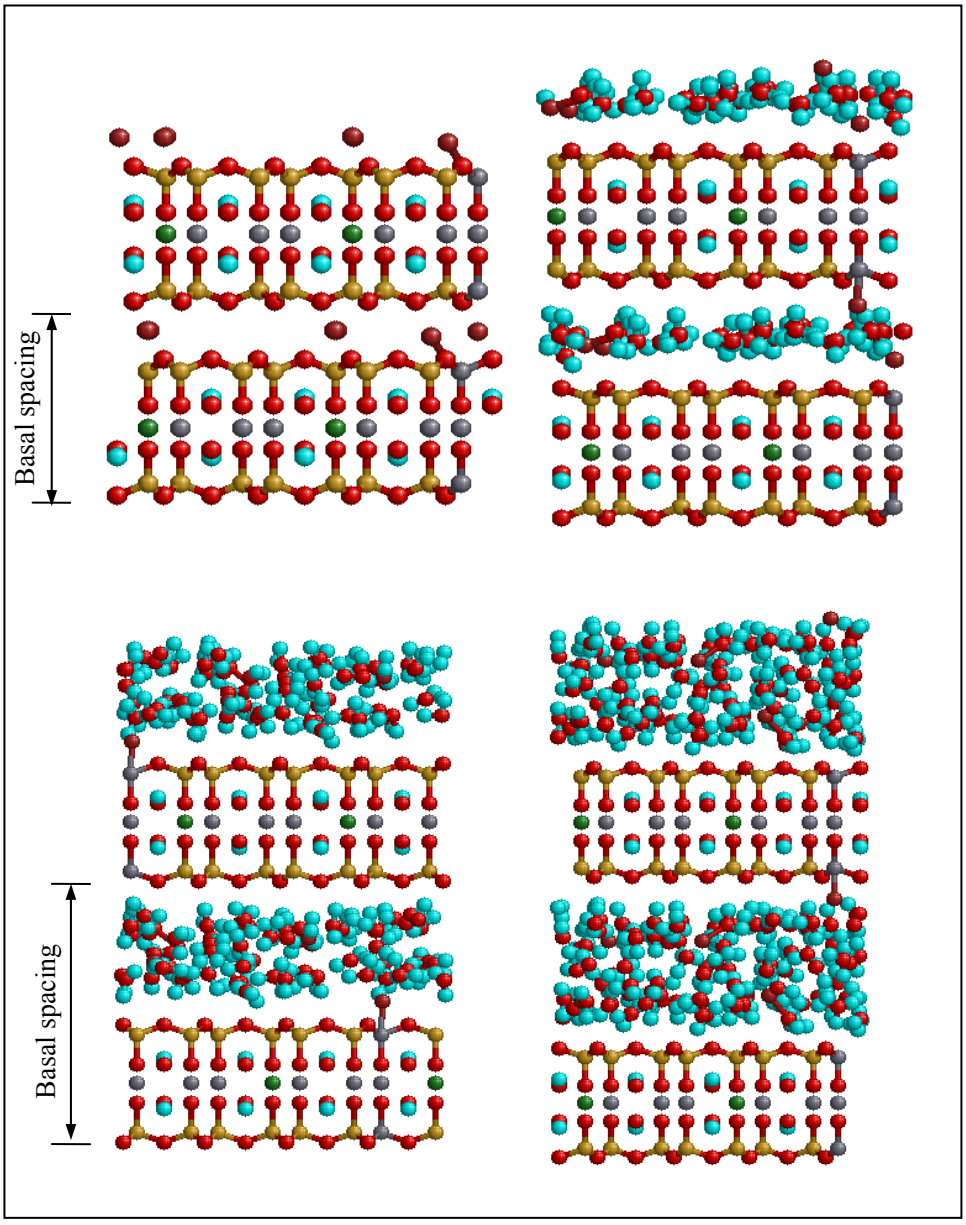


Figure 3-1: The relaxed structure of dehydrate, monolayer hydrate, two-layer hydrate and three-layer hydrate Li-Wyoming montmorillonite: O-red, H-cyan, Si-golden, Al-grey, Mg-green, Li-brown. (results of SPC/E type simulatons)

The layer spacing for a smectite clay depends upon several variables: the temperature, applied pressure, water chemical potential, the magnitude and location of the negative clay layer charge, the identity of the charge-balancing cations that

reside in the interlayer. Mooney et al. [48] and Brindley et al. [55] have found that in the presence of water these cations tend to hydrate, thereby forcing the clay layers apart in a series of discrete steps. At increasing relative humidity, smectite absorb water vapour and form one-, two-, and three-layer hydrates [55-57]. The experiments of Fu [45] and Berend [44] have shown a hysteresis curves, nevertheless, preceding simulation studies show only the swelling process. This motivated us to simulate both the swelling and the shrinking process of the clay.

On the other hand, a number of studies claim that the sorption of water into the interlayer spacing is mainly determined by the size and charge of the counterions [33, 48, 58], which means that swelling behaviour of clay depends on the type of cations. This gives us the idea to study the interlayer structure with wide variety of cations including especially some pollutants.

Monte Carlo simulations have been successfully employed on the study of equilibrium clay-water system [10, 15, 31, 50]. So this method is used to study the swelling and shrinking behaviour of clay.

In this work, we will study first the swelling and shrinking behaviours of montmorillonite at 300K. Based on this study, the temperature factor will be added into the simulations to find the influence of temperature on the swelling of this clay at different hydrated states.

In the first part, we test first the swelling and shrinking of Li- and Na-montmorillonite by using MCY, TIP4P and SPC/E water potential models. With the best model, we describe the swelling and shrinking behaviours of montmorillonite including $K^+$, $Rb^+$ and $Cs^+$. Then we perform the same simulation in montmorillonite with divalent cations such as $Ca^{2+}$, and some heavy metal ions such as $Ni^{2+}$, $Zn^{2+}$ and $Pb^{2+}$ to predict the swelling and shrinking behaviours in the case of the polluted clay.

In the second part, simulations have been performed on these montmorillonites at 1-, 2- and 3-layer hydrated state. The temperature of the clay system varies between 260K and 400K. Comparing the behaviour of 1-, 2- and 3-layer hydrate states of the same clay, we can find the role of water molecules in this process. Comparing the curves of the nine montmorillonite at the same hydrate state, we can then find the influence of counterions in the swelling clay.

## 3.2. Simulation methods

Our Monte Carlo simulations were performed using the computer program MONTE [59], as described by Skipper et al. [13]. This code, which uses the Metropolis algorithm [29, 38], has been designed primarily to simulate molecular liquids (e.g. water and aqueous solutions) between solid surfaces. Liquid molecules are treated as rigid bodies, and molecular orientations are stored as quaternions [31]. Van der Waals interactions are treated within an all-image regime [29], with a cut-off radius of 9 Å. The Ewald sum method [29] was applied to handle the long-range electrostatic interactions in the simulation system.

Our simulations were performed in the isothermal-isobaric (NPT) ensemble, more strictly a constant (NσT) ensemble, in which a uniaxial stress $\sigma_{zz}$ was applied perpendicular to the clay layers. This ensemble can well represent the experimental swelling procedure. The volume of the system is allowed to vary, and the simulation will predict the layer spacing. The pressure is fixed at $10^5$ Pa. No flexibility in the clay lattice was allowed during the simulation [10].

### 3.2.1. Simulation details of swelling and shrinking at 300K

Monte Carlo simulations were carried out with steps of four water molecules (from 0 to 16) or eight water molecules (from 16 to 96), as propose of Boek et al. [31]. For our montmorillonite simulation box, 0 to 96 water molecules correspond to 0 to 0.3g/g of clay, which are the values typically encountered experimentally.

The procedure of the simulations is seen in section 2.4.2. To begin the Monte Carlo simulation, the initial layer spacing of the clay system should be set first. Chang et al. [15] have proposed 10 Å for dehydrated Na-montmorillonite, 13 Å layer spacing for monolayer hydrated, 16 and 19 Å for two- and three-layer hydrated respectively. In this work, we aim to simulate the swelling and shrinking process of the clay, so the single value needed to be set is the layer spacing of the dehydrate clay, which was taken from the experimental result of Berend [44], as shown in Table 3-1. After equilibration we can obtain a new value of the layer spacing, which was taken as the initial layer spacing value for the following simulation. The difference between swelling and shrinking processes is adding water molecules for swelling and reducing water molecules for shrinking.

### 3.2.2. Simulation details of swelling simulations under the effect of temperature

The initial configurations of each montmorillonite at 1-, 2- and 3-layer hydrated state are taken from our preceding simulation results which were performed at 300K. Each simulation series is composed by two processes, warming and cooling, in total 17 simulations. The temperature of the system increases from 300K with a step of 20K to reach 400K where we inset a special point, 373K, the 100 degree Centigrade. Then the system is cooled down with the same step to reach 260K just below 273K, the 0 degree Centigrade. The temperature of the clay system returns to 300K, as the initial state, to form a complete warming-cooling circle. The initial configuration of each simulation comes from its preceding simulation result.

The simulations are performed with the procedure presented in section 2.4.2. With the increasing of the number of molecules and the temperature, the equilibration of the clay system becomes difficult to obtain that the third step is repeated till that the variations of potential energy and then the z-dimension value of the cell tend to constant.

## 3.3. Swelling and shrinking of montmorillonite at 300K

### 3.3.1. Choice of the water model

We performed firstly the simulations of Li- and Na-Wyoming montmorillonite. We test the swelling and shrinking of these two clays with MCY, TIP4P and SPC/E types of water model and potential model.

Simulated and experimental swelling curves for Li-montmorillonite are presented in Figure 3-2, where (a), (b) and (c) show our simulation results using MCY, TIP4P, SPC/E potential models respectively compared with experimental swelling and shrinking values presented by Berend [44] and (b), and additionally, compared with the simulation swelling curve of Boek et al. [31] who studied the same type of montmorillonite and used the TIP4P type potential. Whereas with the different parameters from that of Chang et al. [16] used in our simulations.

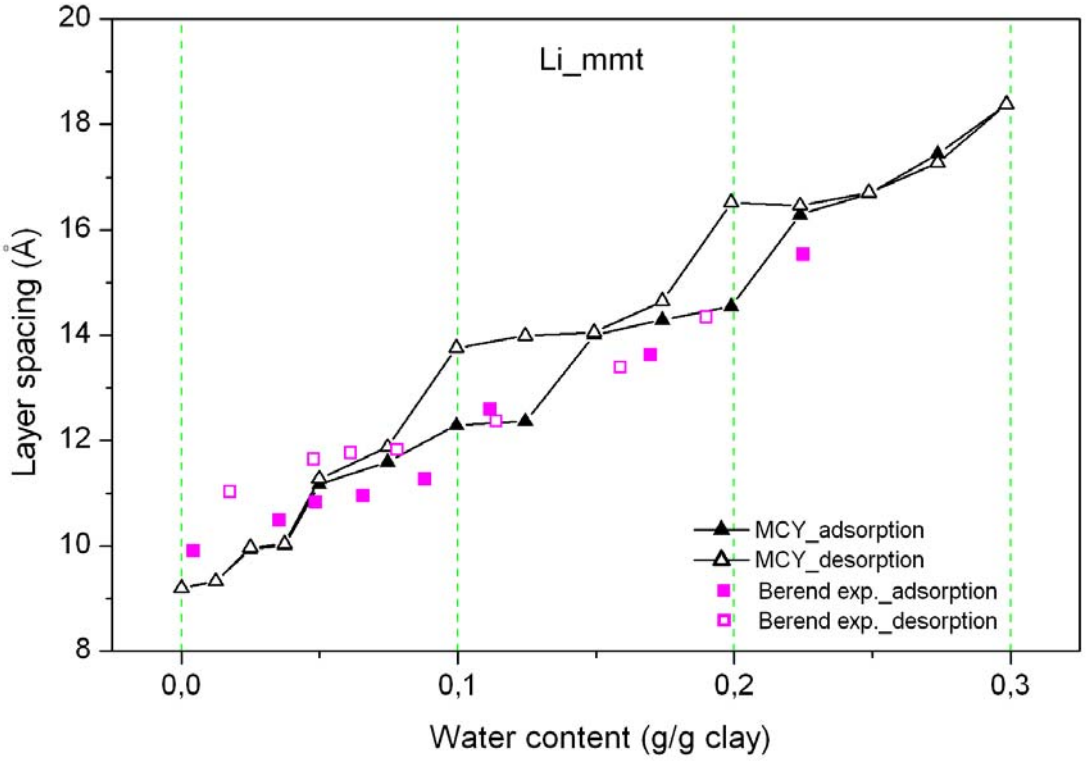


(a)

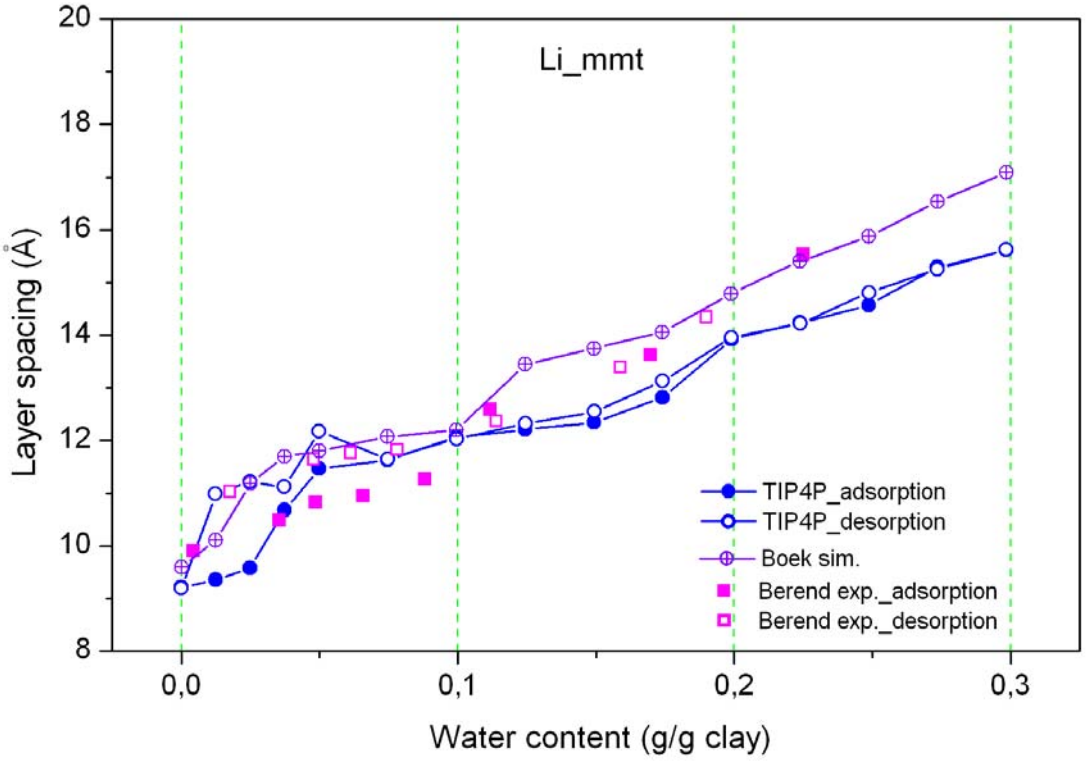


(b)

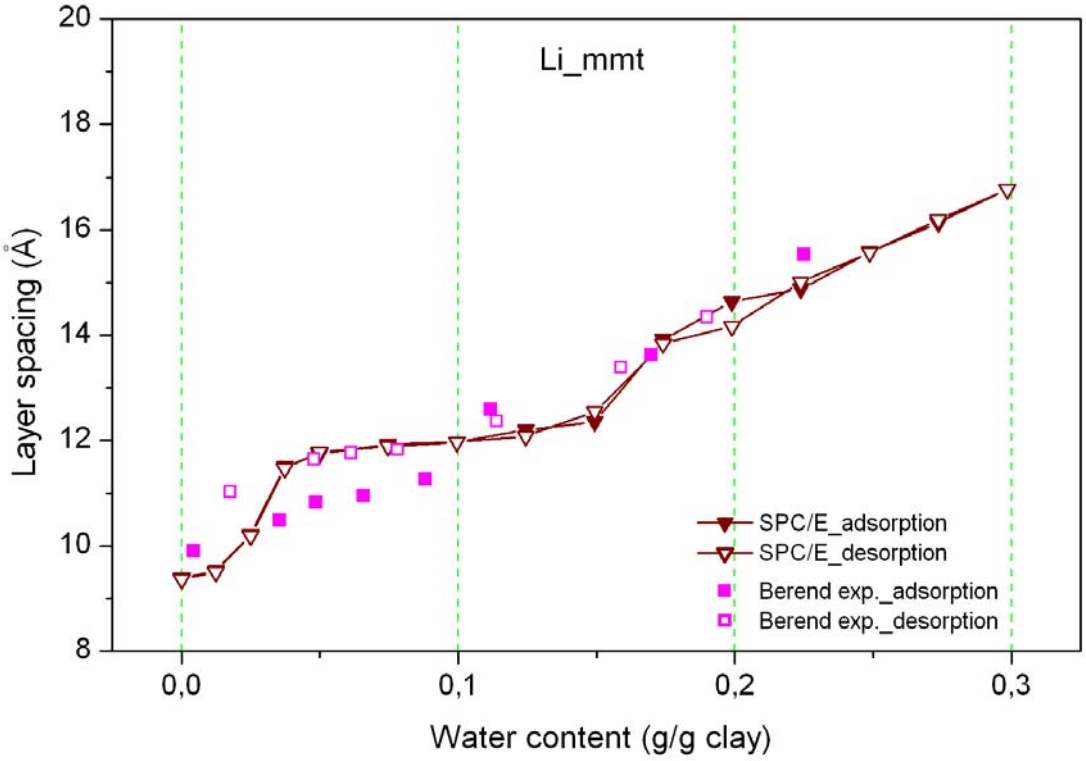


(c)

Figure 3-2: Simulated and experimental layer spacing (Å) of Li-Wyoming montmorillonite as a function of water content (g/g clay). The vertical dashed-lines indicate dehydrated and hydrated 1-, 2-, 3-layer respectively: (a)Our simulation result using MCY potential model (filled triangles for swelling, open triangles for shrinking); experimental values of Berend [44] (filled squares for swelling, open squares for shrinking). (b) Our simulation result using TIP4P potential model (filled circles for swelling, open circles for shrinking); simulation swelling curve of Boek et al. [31] (crossed circles); experiment values of Berend [44]. (c) Our simulation result using SPC/E potential model (filled down triangles for swelling, open down triangles for shrinking); experiment values of Berend [44].

From Berend's experimental points we can find a hysteresis occurring between 0 and 0.1 water content where shrinking curve is upon the swelling one. After that, the difference between swelling and shrinking is not evident. Boek et al. present a variation of layer spacing as a function of increasing water content without specifying swelling or shrinking process. Compared with the experimental curves, it fits better the shrinking curves.

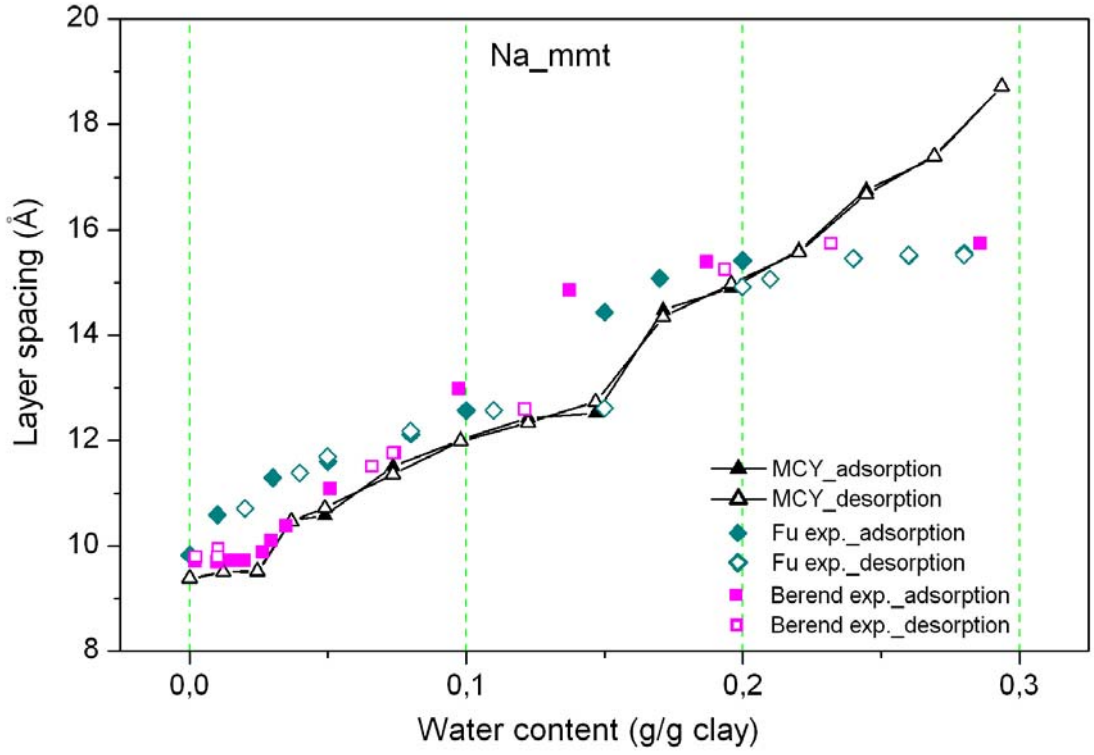


(a)

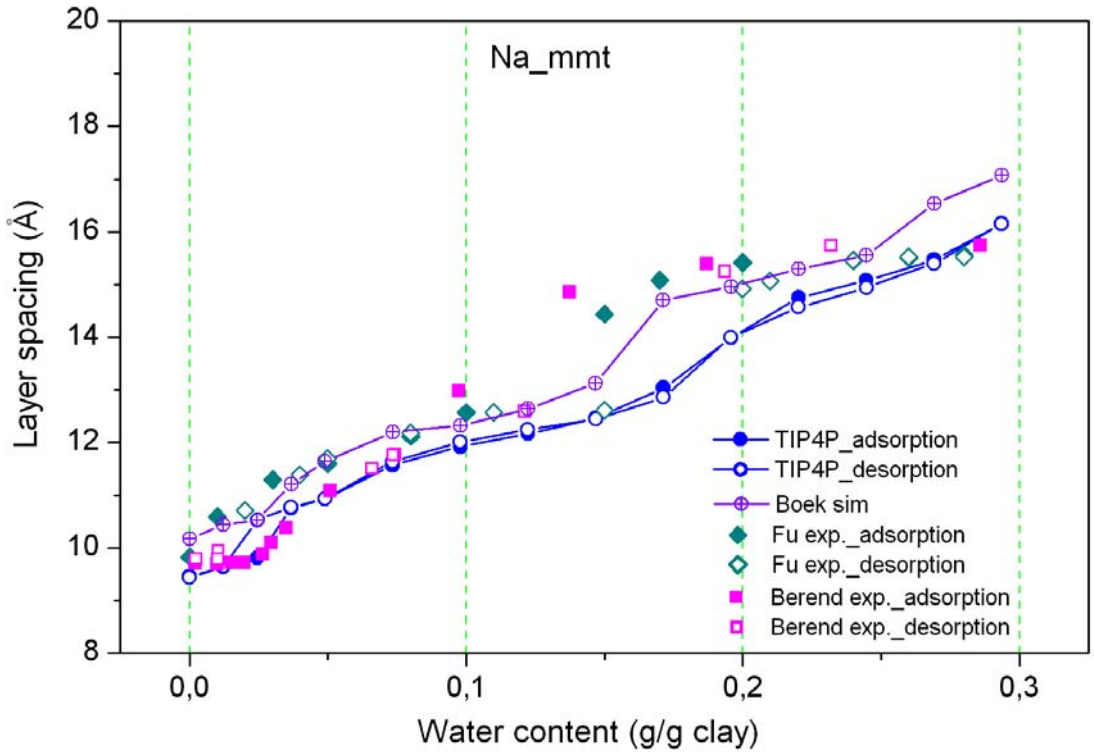


(b)

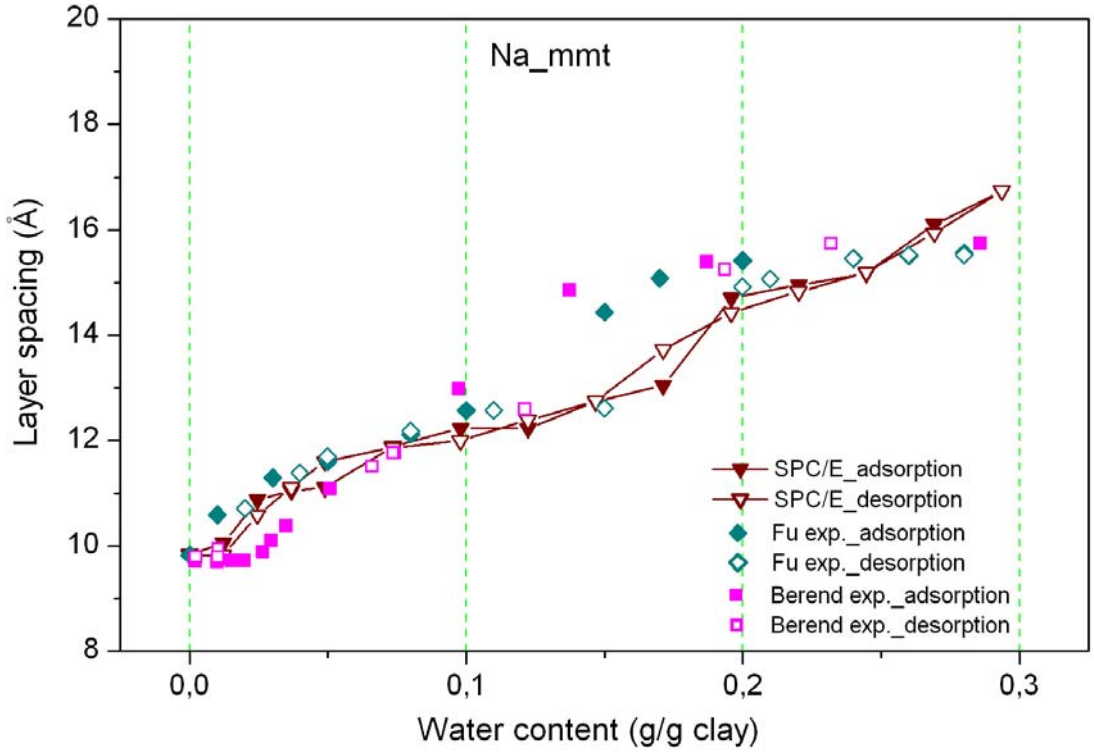


(c)

Figure 3-3: Simulated and experimental layer spacing (Å) of Na-Wyoming montmorillonite as a function of increasing water content (g/g clay). The vertical dash-lines indicate dehydrate, 1-, 2-, 3-layer hydrated respectively. (a)Our simulation result using MCY potential model (filled triangle for swelling and open triangle for shrinking); experiment values of Berend [44] (filled square for swelling, open square for shrinking); experiment results of Fu et al. [45] (filled diamond for swelling, open diamond for shrinking). (b) Our simulation result using TIP4P potential model (filled circles for swelling, open circles for shrinking); simulation result of Boek et al. [31] (crossed circles); compared with experiment values of Berend and Fu. (c) Our simulation result using SPC/E potental model (filled down triangle for swelling, open down triangle for shrinking); compare with experiment values of Berend and Fu.

Our three simulation curves show good agreement in the overall swelling pattern and in the values of layer spacing over the whole range of crystalline swelling (up to ~19 Å). The MCY simulation curves show a hysteresis between one and two hydrated layers; while the TIP4P ones show a hysteresis fitting well the experiment. The latter ones show also a few hysteresis between one and two hydrated layers. The SPC/E simulation pattern shows a negligible hysteresis between one and two

hydrated layers. The swelling and shrinking curves overlap at lower and higher hydrate, where we can see that the simulation curves at lower hydration fit first the experimental swelling values and then jump to fit the experimental shrinking values till one hydrated layer.

Figure 3-3 shows the swelling and shrinking curves of Na-montmorillonite. This clay has been widely studied both experimentally and theoretically. Here the experimental results of Fu et al. [45] and Berend [44] are presented in (a), (b) and (c), together with the simulations of Boek et al. [31] shown in (b). Both of the two experiments about Na-montmorillonite show a hysteresis between one and two hydrated layer, rather than between 0 and 0.1 water content, with the swelling process upon the shrinking one. There is a small difference between Fu and Berend experiment results but the pattern and the tendency are the same, which is maybe related to different clay sample and experiment conditions. Boek's simulation curve is enclosed in the experimental hysteresis.

Our MCY, TIP4P and SPC/E type simulations fit well with the experimental data especially the shrinking ones. The hysteresis obtained from MCY and TIP4P type simulations is negligible; whereas SPC/E simulations show a weak hysteresis although it is smaller than the experimental one.

In general, all the three type water and potential models work well in the simulations of swelling and shrinking processes of Li- and Na-montmorillonite, especially at low hydrated state where water content is less than 0.15. When the hydration increases, the MCY simulation variations are above the experimental ones while in the case of the TIP4P simulation the variations are below the experimental lines. Compared with the two previous simulations, the SPC/E results are closer to the experimental ones. Moreover, the parameters needed in this kind of potential model depend on the element rather than the site pairs so that it is easy to introduce new element into the clay system. For these reasons, this model will be chosen as potential model to be used for all remaining simulations in this work.

### 3.3.2. Montmorillonite with monovalent counterions

The swelling and shrinking processes of K-, Rb- and Cs-montmorillonite are shown in Figure 3-4 to Figure 3-6 respectively, together with experimental data obtained by Berend [44]. Since the relative pressure is less than 0.95, Berend's experiments end at the monolayer stage. Hysteresis here is not obvious compared

with the case of Li- and Na-montmorillonite. We may see that the Rb- and Cs-curves fit perfectly with experimental data in the region of 0 to 0.1 of water content. Although the K-curves fit no so well in this zone, the layer spacing value at monolayer hydrated is consistent with experiment one.

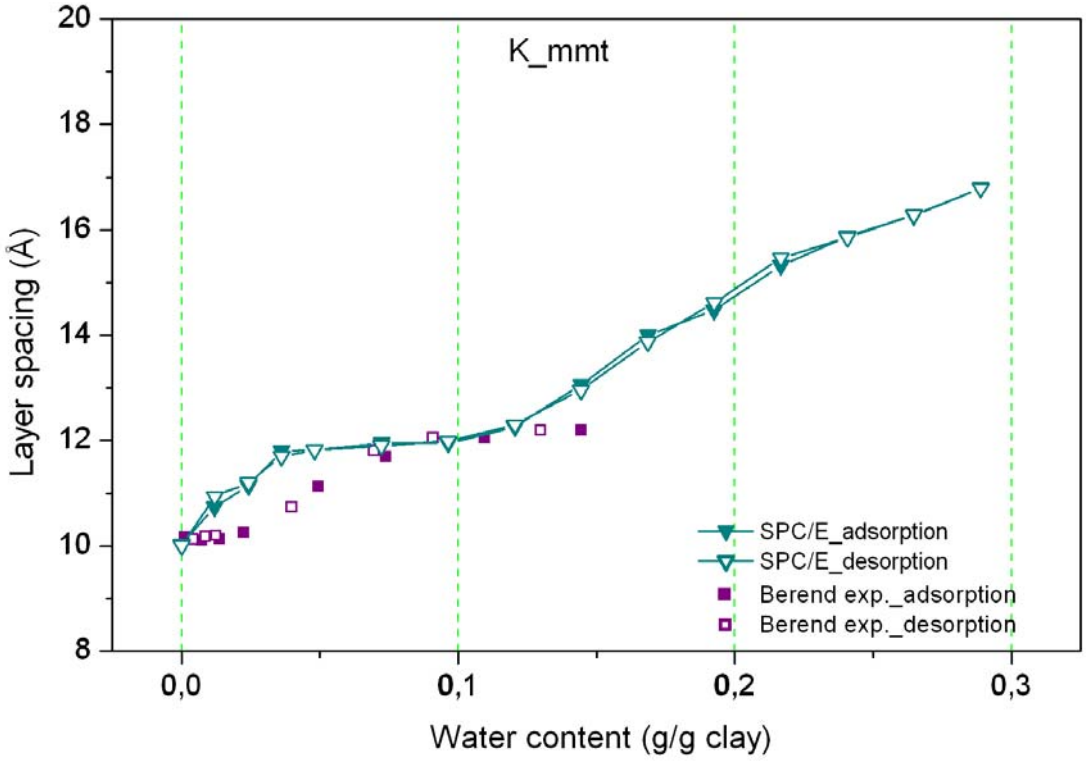


Figure 3-4: Simulated and experimental layer spacing (Å) of K-Wyoming montmorillonite as a function of increasing water content (g/g clay). The vertical dash-lines indicate dehydrated, 1-, 2-, 3-layer hydrated respectively. Our simulation results using SPC/E potential model (filled down triangle for swelling, open down triangle for shrinking), compared with experimental values of Berend [44] (filled square for swelling, open square for shrinking).

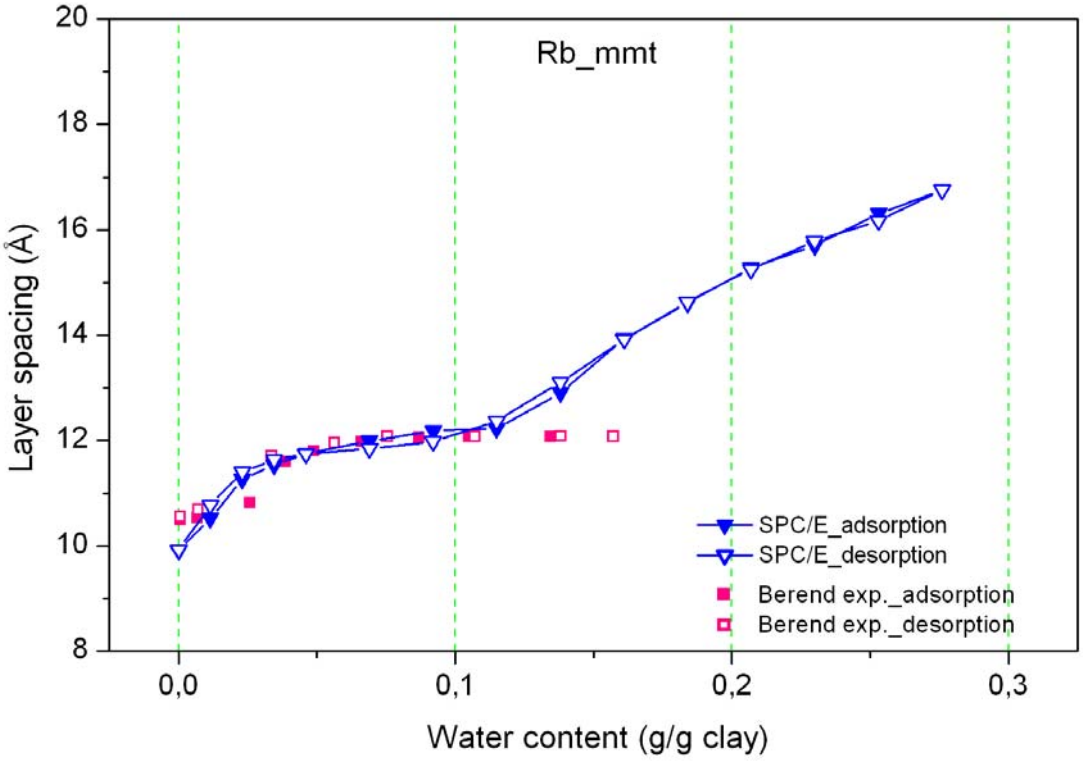


Figure 3-5: Simulated and experimental layer spacing (Å) of Rb-Wyoming montmorillonite as a function of increasing water content (g/g clay). The vertical dash-lines indicate dehydrated, 1-, 2-, 3-layer hydrated respectively. Our results using SPC/E water model (filled down triangle for swelling, open down triangle for shrinking), compared with experimental data of Berend [44] (filled square for swelling, open square for shrinking).

### 3.3.3. Montmorillonite with divalent counterions

The same simulations were performed to montmorillonite including divalent cations, $Ca^{2+}$ for example. Figure 3-7 presents the simulated and experimental swelling curves of Ca-montmorillonite. The experimental curves of Berend [44] reveal an important hysteresis in the region of 0 to ~0.15 water content, and after that the swelling and shrinking curves are overlap. The obtained swelling and shrinking patterns have the same tendency as the experimental ones.

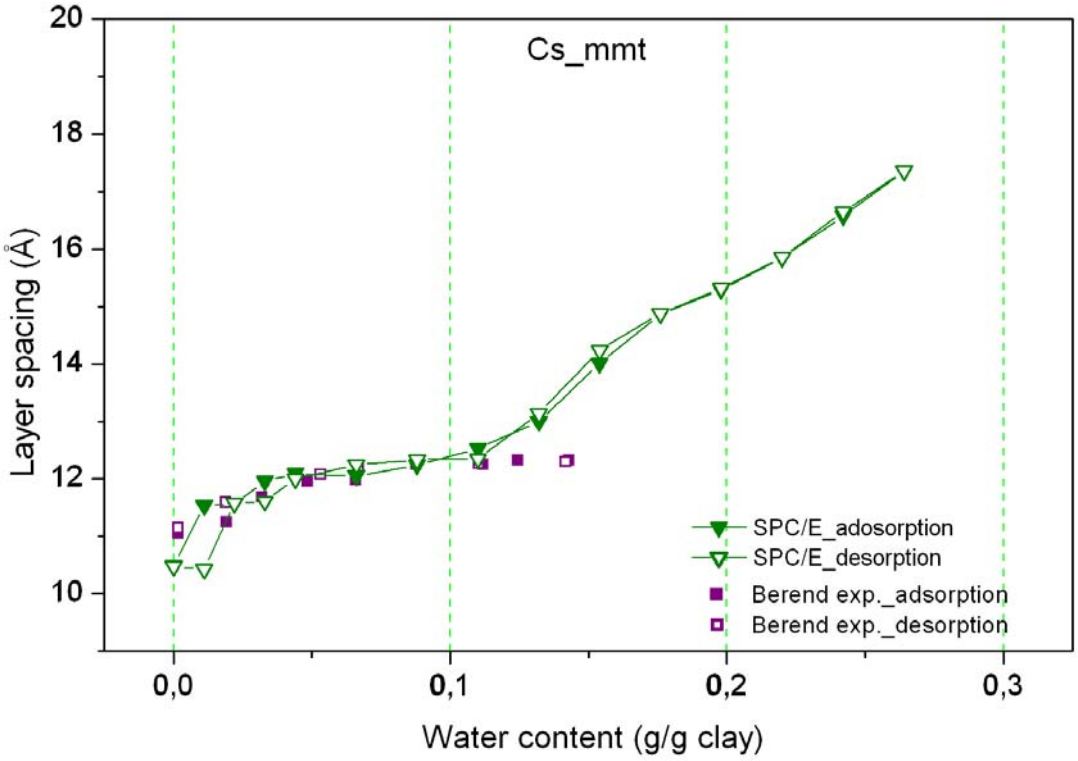


Figure 3-6: Simulated and experimental layer spacing (Å) of Cs-Wyoming montmorillonite as a function of increasing water content (g/g clay). The vertical dash-lines indicate dehydrated, 1-, 2-, 3-layer hydrated respectively. Our results using SPC/E water model (filled down triangle for swelling, open down triangle for shrinking), compared with experimental values of Berend [44] (filled square for swelling, open square for shrinking).

From the comparison of our simulation results and the experimental values, we may conclude that our simulation methods and the water model chosen are coherent. This potential model should be successful in comparable systems, which justify widely further studies in the present work concerning the prediction of swelling and shrinking problems in montmorillonite including some heavy metal ions which appear commonly in pollutant clay, $Ni^{2+}$, $Zn^{2+}$ and $Pb^{2+}$, as presented in Figure 3-8 to Figure 3-10.

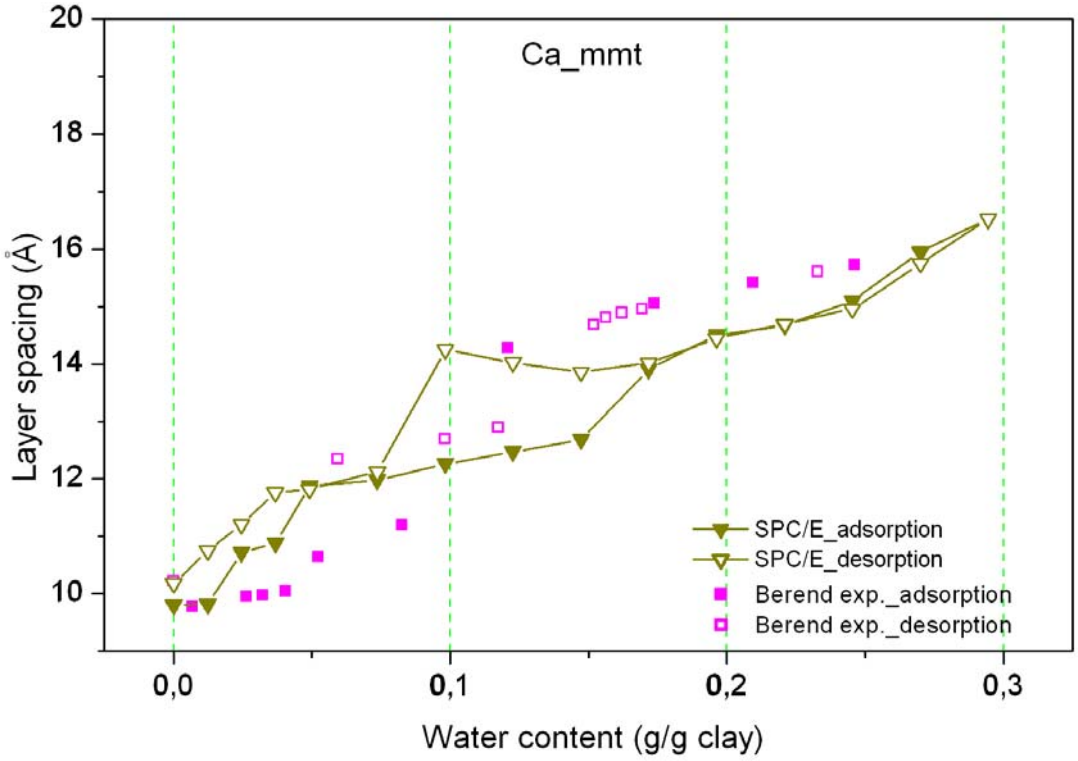


Figure 3-7: Simulated and experimental layer spacing (Å) of Ca-Wyoming montmorillonite as a function of increasing water content (g/g clay). The vertical dash-lines indicate dehydrated, 1-, 2-, 3-layer hydrated respectively. Our simulation result using SPC/E water model (filled down triangle for swelling, open down triangle for shrinking); experiment values of Berend [44] (filled square for swelling, open square for shrinking).

We may clearly see the important hysteresis in the case of both Ni and Zn which corresponds well with the tendency occurring in Ca-montmorillonite. However the swelling and shrinking pattern of Pb-montmorillonite doesn't show a clear hysteresis and its tendency is more close to Rb and Cs. To explain this phenomenon, we review the curves in the series of montmorillonite containing monovalent cations. The patterns of experiments show hysteresis in Li- and Na-montmorillonite curves, whereas this hysteresis phenomenon becomes less obvious in montmorillonite including bigger cations such as $K^+$, $Rb^+$ and $Cs^+$. This tendency may explain the phenomenon occurring in Pb-montmorillonite. That is to say, the magnitude of hysteresis between swelling and shrinking of montmorillonite may depend on the size of contained cations in the interlayer space.

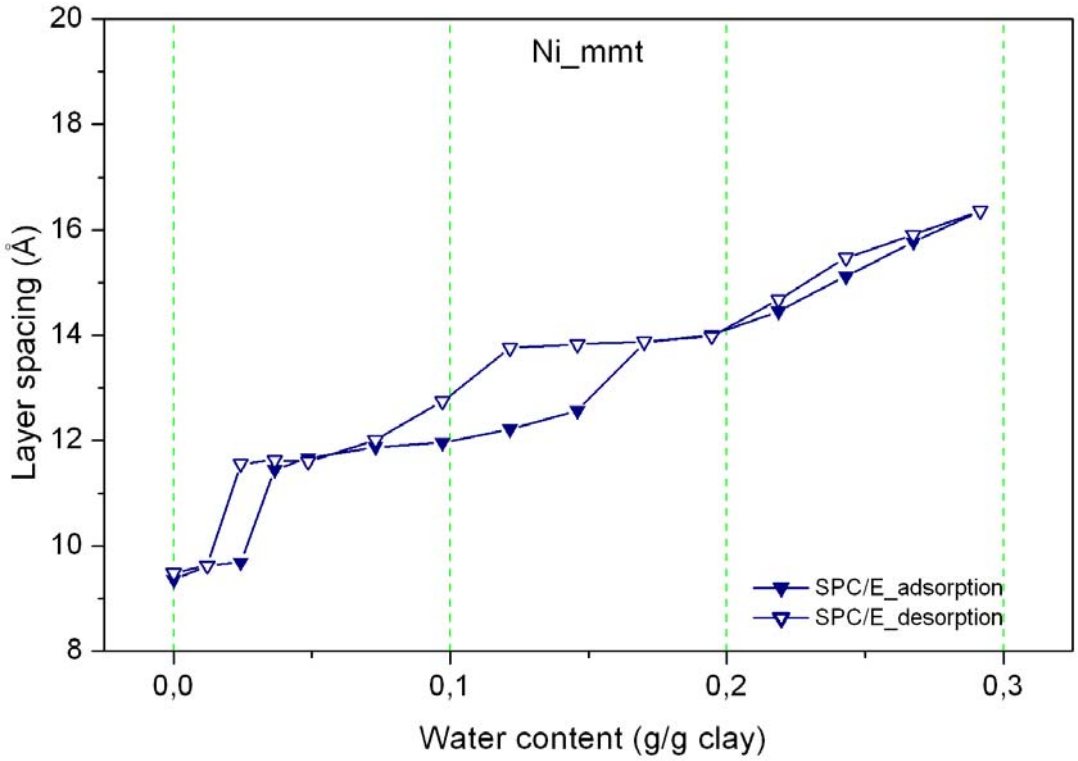


Figure 3-8: Simulated and experimental layer spacing (Å) of Ni-Wyoming montmorillonite as a function of increasing water content (g/g clay). The vertical dash-lines indicate dehydrated, 1-, 2-, 3-layer hydrated respectively. Our simulation results using SPC/E potential model (filled down triangle for swelling, open down triangle for shrinking).

### 3.3.4. Discussion

The data of interlayer spacing of montmorillonite at different hydrations and different counterions, compared with other simulation and experimental values are presented in Table 3-1 to Table 3-4, corresponding to dehydrated, monolayer hydrated, two-layer hydrated and three-layer hydrated state. The most important deduction here is the expected increase of the layer from one-layer hydrated to two-layer and so on, and the small variation of the layer spacing with the counterions.

The difference between the process of absorbing and desorbing water which is performed in the figures is the hysteretic curve. We found that, for monovalent ions, such as $Li^+$, $Na^+$, $K^+$, $Rb^+$, $Cs^+$, the hysteresis phenomena are not so obvious. While for the double valent cation such as $Ca^{2+}$, our computed curve performs a clear hysteretic, which agrees well with the experiment. The same occurs in our simulation

performed on montmorillonite including $Ni^{2+}$ and $Zn^{2+}$, as a prediction. Although Pb-montmorillonite doesn't follow this tendency, as explained in Section 3.3.3, which is believed to be due to the influence of the cation's size, the hysteresis between swelling and shrinking of divalent montmorillonite is important.

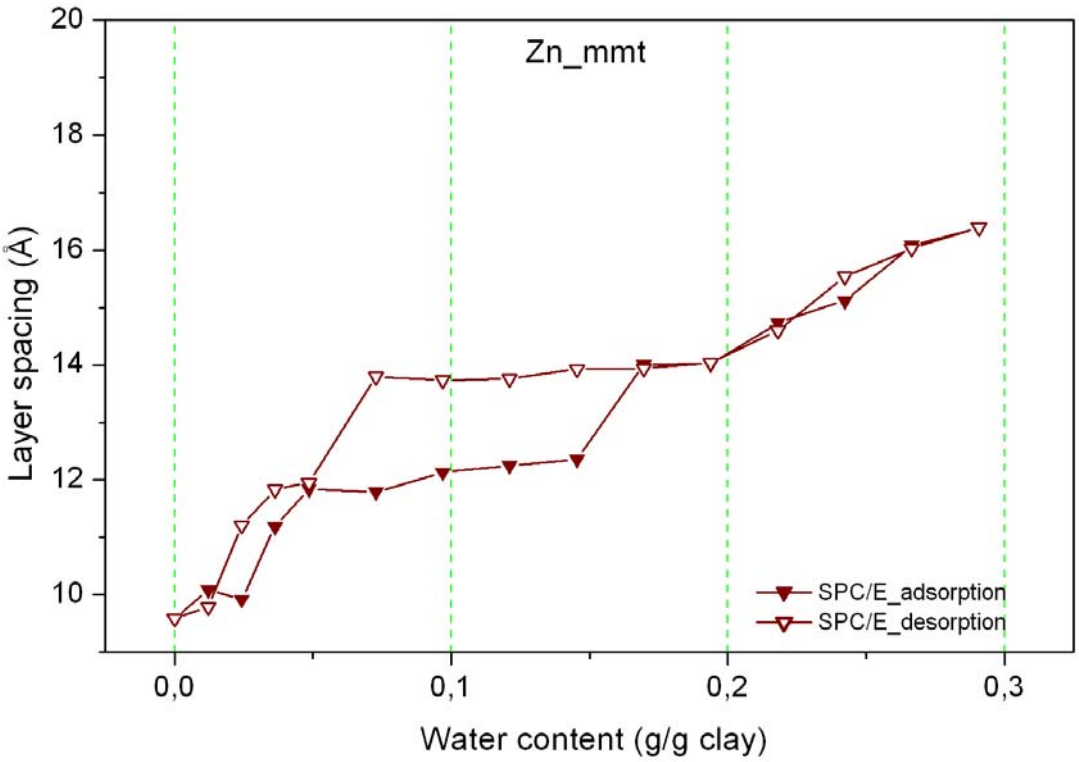


Figure 3-9: Simulated and experimental layer spacing (Å) of Zn-Wyoming montmorillonite as a function of increasing water content (g/g clay). The vertical dash-lines indicate dehydrated, 1-, 2-, 3-layer hydrated respectively. Our simulation results using SPC/E potential model (filled down triangle for swelling, open down triangle for shrinking).

The swelling hysteresis is due to the increase/decrease of water molecules in a given space. For energetic equilibrium of the system the water molecules induces the breaking of hydrogen bonds between water layers on each side of the clay layers and new hydrogen bonds within each layer are predominantly formed. The breaking of these bonds causes fluctuations in the internal pressure of the clay, which modifies obviously the energetic stability of the system. Looking for more comfortable positions, the system will rearrange itself the orientations of molecules according to the water content, the layer spacing and, of course, the counter ions, which could be present in that system. These ions influence the internal pressure as well, since they

are related to their different positions in the interlayer and their coordination with water molecules.

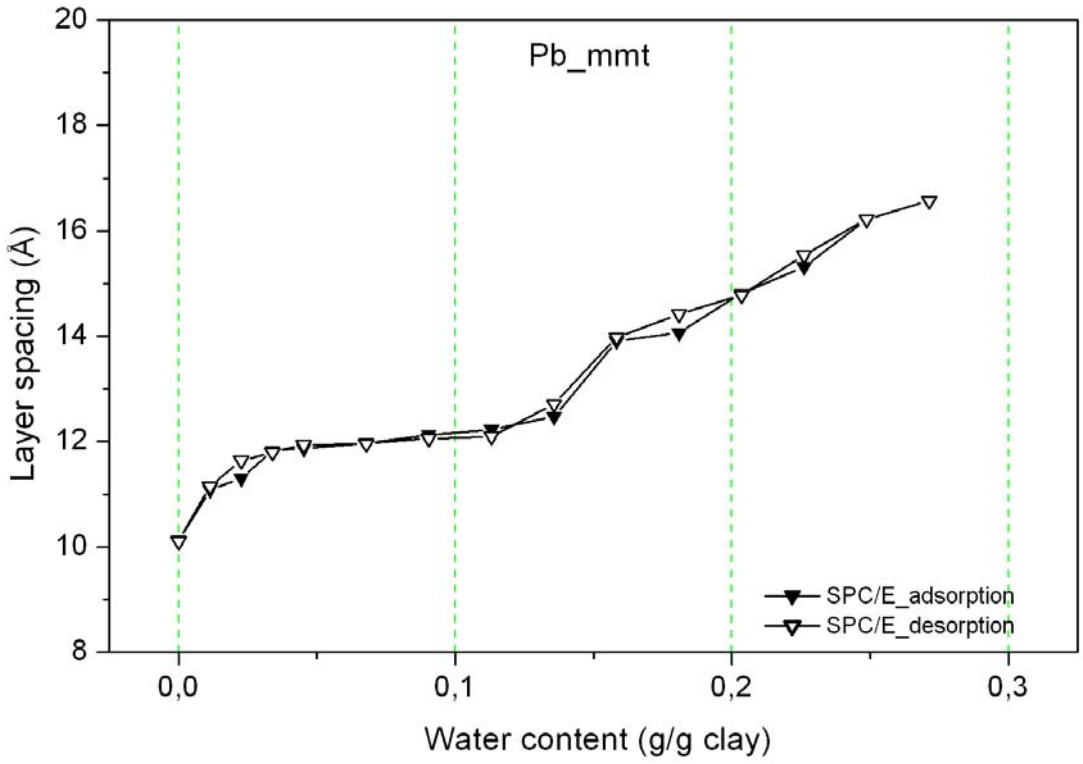


Figure 3-10: Simulated and experimental layer spacing (Å) of Pb-Wyoming montmorillonite as a function of increasing water content (g/g clay). The vertical dash-lines indicate dehydrated, 1-, 2-, 3-layer hydrated respectively. Our simulation results using SPC/E potential model (filled down triangle for swelling, open down triangle for shrinking).

With the two hydrated layer as a starting point, a decrease in water content induces desorption of water molecules from the interlayer space, followed by a relatively small decrease of basal spacing and small rearrangement of the counter ions and water molecules. However, the reverse pathway requires that hydrogen bonds between the molecules in each water layer need to be broken, and new bonds need to be formed between the two layers of water molecules. This can only be accomplished by desorption of water molecules from the system, and therefore hysteresis occurs. Once critical water content is reached, the system can shrink to the one hydrated layer. Our predictions point to mechanism in which an extra step is taken during the transition from a two to one hydrated layer. Depending on their size

and hydration, counter ions can move to the mid-plane of the clay mineral at a basal spacing, thereby stabilizing a one-and a half state.

**Table 3-1: Layer spacing of montmorillonite without water (Å).**

| | | absorption | desorption | experiment |
|---|---|---|---|---|
| Li-mmt | MCY | 9.21±0.04 | 9.20±0.04 | 9.59-10[a] |
| | TIP4P | 9.22±0.03 | 9.20±0.04 | |
| | SPC/E | 9.39±0.04 | 9.37±0.03 | |
| | Boek sim. | 9.60±0.04 | | |
| Na_mmt | MCY | 9.37±0.05 | 9.39±0.06 | 9.55[a]<br>9.83[b] |
| | TIP4P | 9.46±0.06 | 9.44±0.03 | |
| | SPC/E | 9.84±0.05 | 9.83±0.05 | |
| | Boek sim. | 10.17±0.06 | | |
| K_mmt | MCY | 10.44±0.08 | 10.87±0.09 | 9.96[a] |
| | SPC/E | 10.03±0.06 | 10.00±0.06 | |
| | Boek sim. | 9.86±0.04 | | |
| Rb_mmt | SPC/E | 9.92±0.05 | 9.93±0.05 | 10.25-10.56[a] |
| Cs_mmt | SPC/E | 10.49±0.06 | 10.48±0.08 | 10.7-11.5[a] |
| Ca_mmt | SPC/E | 9.81±0.05 | 10.18±0.05 | 9.55[a] |
| Ni_mmt | SPC/E | 9.36±0.03 | 9.49±0.03 | - |
| Zn_mmt | SPC/E | 9.59±0.03 | 9.59±0.04 | - |
| Pb_mmt | SPC/E | 10.13±0.06 | 10.11±0.07 | - |

[a]Berend experiment [44], [b]Fu experiment[45].

**Table 3-2: Layer spacing of one-layer hydrated montmorillonite (Å)**

| | | absorption | desorption | experiment |
|---|---|---|---|---|
| Li-mmt | MCY | 12.29±0.07 | 13.76±0.13 | 12-12.21[a] |
| | TIP4P | 12.07±0.07 | 14.03±0.04 | |
| | SPC/E | 11.97±0.06 | 11.97±0.06 | |
| | Boek sim. | 12.20±0.07 | | |
| Na_mmt | MCY | 12.01±0.06 | 11.99±0.08 | 12.49[a]<br>12.57[b] |
| | TIP4P | 11.92±0.08 | 12.01±0.08 | |
| | SPC/E | 12.23±0.10 | 12.00±0.06 | |
| | Boek sim. | 12.32±0.09 | | |
| K_mmt | MCY | 12.46±0.11 | 12.5±0.10 | 12.5[a] |
| | SPC/E | 11.95±0.07 | 11.99±0.07 | |
| | Boek sim. | 11.77±0.05 | | |
| Rb_mmt | SPC/E | 12.18±0.09 | 11.98±0.07 | 12.5[a] |
| Cs_mmt | SPC/E | 12.24±0.08 | 12.33±0.08 | 12.4[a] |
| Ca_mmt | SPC/E | 12.26±0.08 | 14.25±0.11 | 12.07-12.5[a] |
| Ni_mmt | SPC/E | 11.96±0.04 | 12.75±0.16 | - |
| Zn_mmt | SPC/E | 12.13±0.07 | 13.74±0.10 | - |
| Pb_mmt | SPC/E | 12.12±0.08 | 12.06±0.07 | - |

[a]Berend experiment [44], [b]Fu experiment[45].

**Table 3-3: Layer spacing of two-layer hydrated montmorillonite (Å).**

| | | absorption | desorption | experiment |
|---|---|---|---|---|
| Li-mmt | MCY | 14.55±0.12 | 16.52±0.18 | 15.62[a] |
| | TIP4P | 13.92±0.08 | 13.96±0.05 | |
| | SPC/E | 14.64±0.12 | 14.17±0.13 | |
| | Boek sim. | 14.79±0.10 | | |
| Na_mmt | MCY | 14.9±0.15 | 14.97±0.13 | 15.55[a] |
| | TIP4P | 13.99±0.05 | 14.00±0.04 | |
| | SPC/E | 14.71±0.12 | 14.43±0.10 | |
| | Boek sim. | 14.96±0.09 | | |
| K_mmt | MCY | 16.20±0.27 | 16.63±0.16 | 16.01[a] |
| | SPC/E | 14.48±0.10 | 14.62±0.14 | |
| | Boek sim. | 13.67±0.08 | | |
| Rb_mmt | SPC/E | 14.61±0.16 | 14.63±0.11 | - |
| Cs_mmt | SPC/E | 14.87±0.13 | 14.88±0.14 | - |
| Ca_mmt | SPC/E | 14.5±0.10 | 14.45±0.10 | 15.15-15.6[a] |
| Ni_mmt | SPC/E | 14.01±0.05 | 13.98±0.06 | - |
| Zn_mmt | SPC/E | 14.02±0.08 | 14.04±0.07 | - |
| Pb_mmt | SPC/E | 14.07±0.09 | 14.42±0.12 | - |

[a]Berend experiment [44], [b]Fu experiment[45].

**Table 3-4: Layer spacing of three-layer hydrated montmorillonite (Å).**

| | | absorption | experiment |
|---|---|---|---|
| Li-mmt | MCY | 18.38±0.19 | 18[c] |
| | TIP4P | 15.62±0.12 | |
| | SPC/E | 16.77±0.12 | |
| | Boek sim. | 17.09±0.13 | |
| Na_mmt | MCY | 18.72±0.19 | 18[c] |
| | TIP4P | 16.15±0.14 | |
| | SPC/E | 16.74±0.09 | |
| | Boek sim. | 17.07±0.14 | |
| K_mmt | MCY | 19.59±0.27 | 18[c] |
| | SPC/E | 16.79±0.09 | |
| | Boek sim. | 15.54±0.09 | |
| Rb_mmt | SPC/E | 16.76±0.10 | - |
| Cs_mmt | SPC/E | 17.36±0.16 | - |
| Ca_mmt | SPC/E | 16.52±0.10 | - |
| Ni_mmt | SPC/E | 16.36±0.10 | - |
| Zn_mmt | SPC/E | 16.39±0.14 | - |
| Pb_mmt | SPC/E | 16.57±0.13 | - |

[c]Mooney experiment [49]

## 3.4. Swelling behaviour of hydrated montmorillonite under the temperature effect

Our simulations are divided into two groups. One consists of montmorillonite including monovalent cations, covering Li-, Na-, K-, Rb- and Cs-Wyoming

montmorillonite. The other involves the clay with divalent cations, the Ca-, Ni-, Zn- and Pb-Wyoming montmorillonite.

To study the warming and cooling process of the clay, the interlayer spacing has been treated as a function of temperature. The curves of 1-, 2- and 3-layer hydrated of each montmorillonite are presented in Figure 3-11 to Figure 3-19 respectively. In total, 17 points along each curve have been calculated, yielding a detailed picture of the evolution behaviour of the interlayer space. The variation range of the basal spacing of the nine type montmorillonite is summarized in Table 3-5.

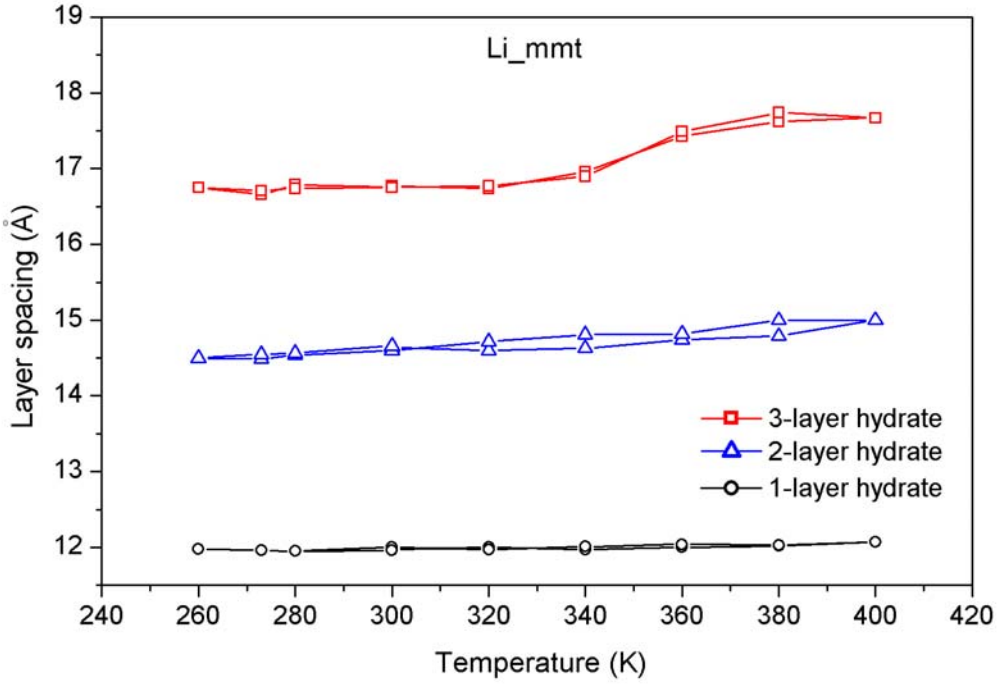


Figure 3-11: Evolution of interlayer space of 1_layer, 2_layer and 3_layer hydrated Li-montmorillonite as a function of temperature.

From the last figures we notice that the layer spacing of three-layer hydrated clay varies with more fluctuation than that of two-, and one-layer hydrated when the temperature changes. The variation range of the two-layer hydrated curve is between that of one- and three-layer hydrated. The fluctuation of the 1-layer hydrated curves is negligible, so we can conclude that the temperature's influence on low hydrated clay is weak.

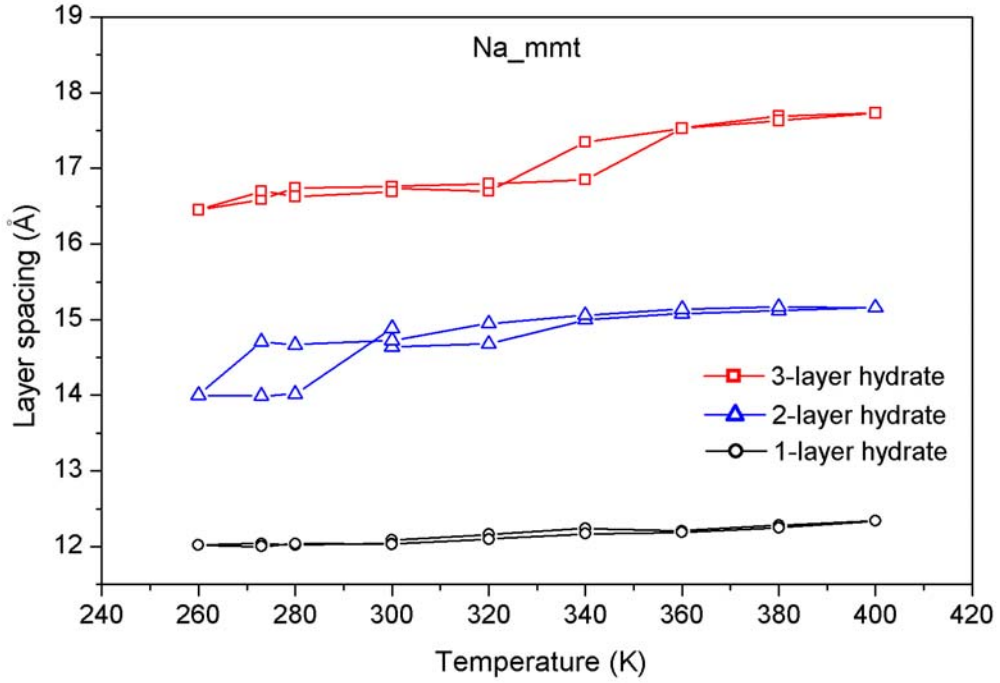


Figure 3-12: Evolution of interlayer space of 1_layer, 2_layer and 3_layer hydrated Na-montmorillonite as a function of temperature.

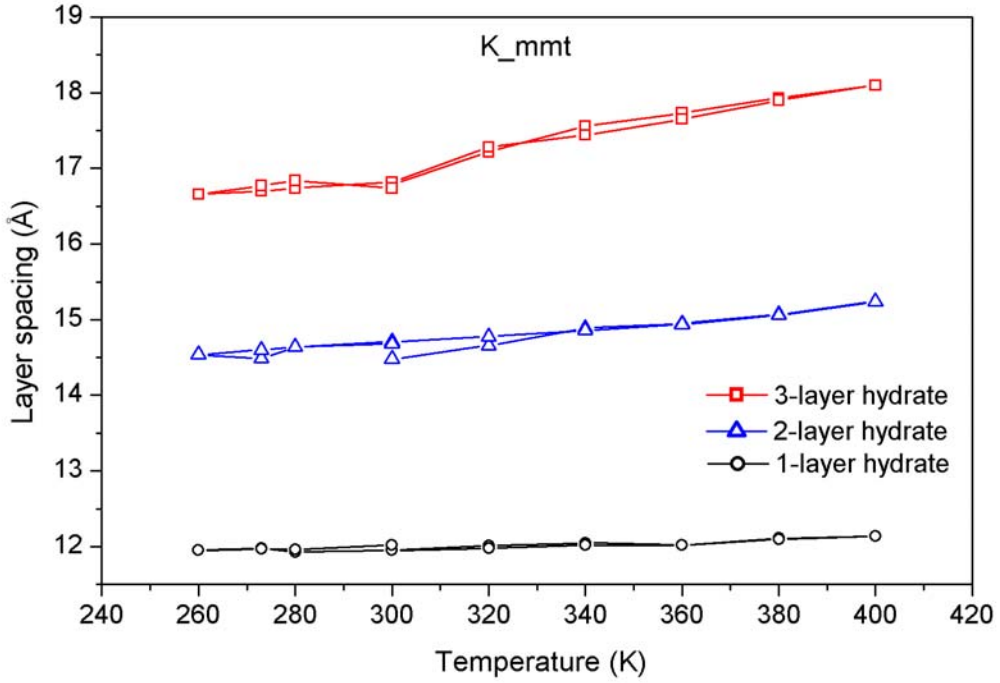


Figure 3-13: Evolution of interlayer space of 1_layer, 2_layer and 3_layer hydrated K-montmorillonite as a function of temperature.

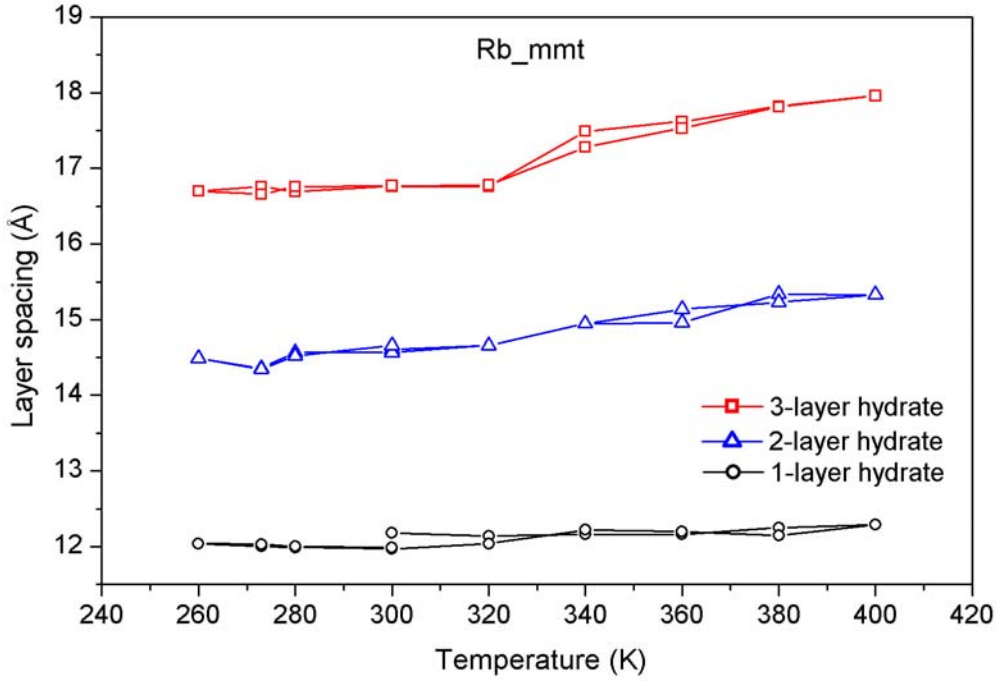


Figure 3-14: Evolution of interlayer space of 1_layer, 2_layer and 3_layer hydrated Rb-montmorillonite as a function of temperature.

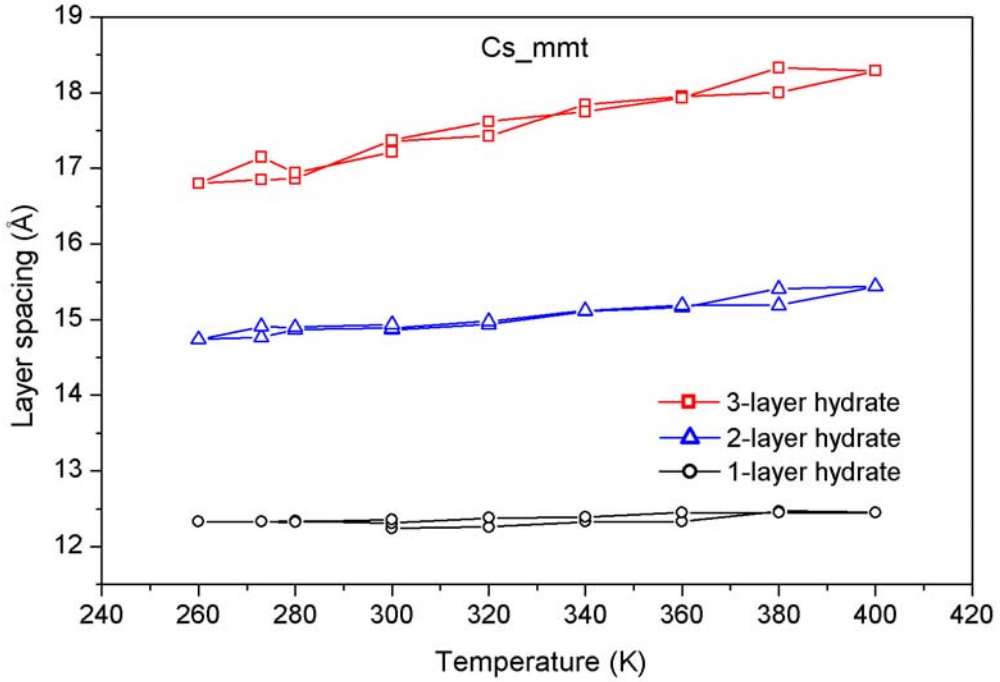


Figure 3-15: Evolution of interlayer space of 1_layer, 2_layer and 3_layer hydrated Cs-montmorillonite as a function of temperature.

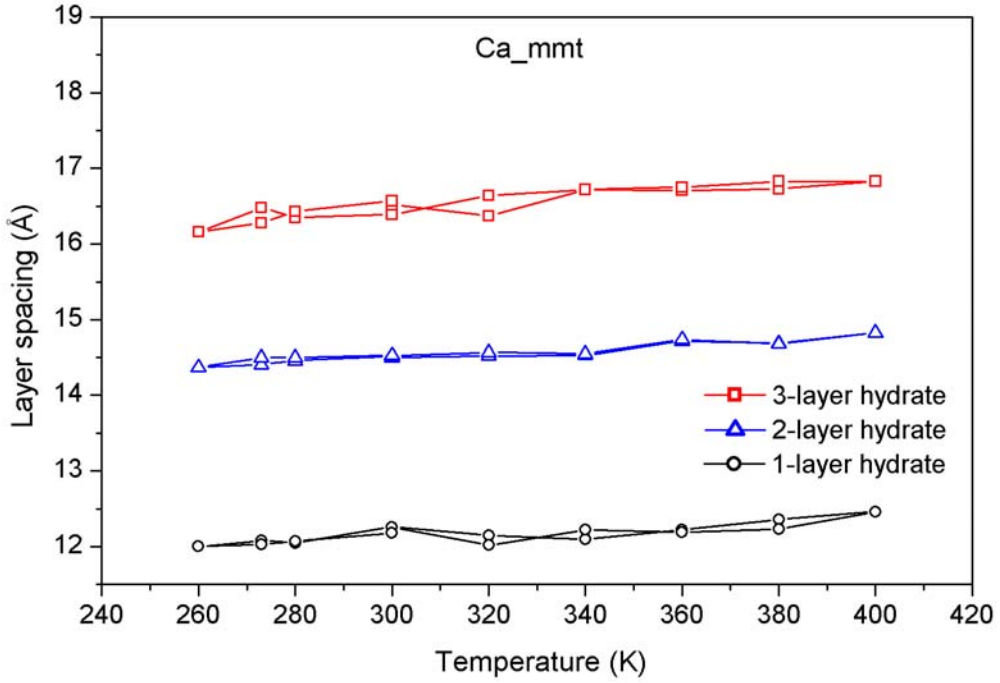


Figure 3-16: Evolution of interlayer space of 1_layer, 2_layer and 3_layer hydrated Ca-Wyoming montmorillonites as a function of temperature.

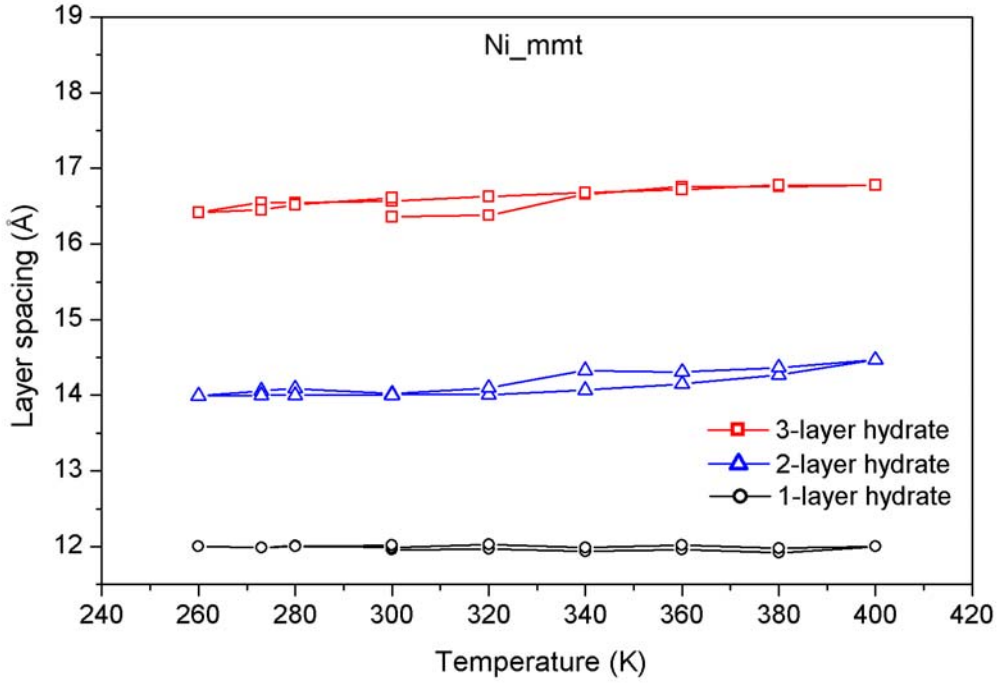


Figure 3-17: Evolution of interlayer space of 1_layer, 2_layer and 3_layer hydrated Ni-Wyoming montmorillonite as a function of temperature.

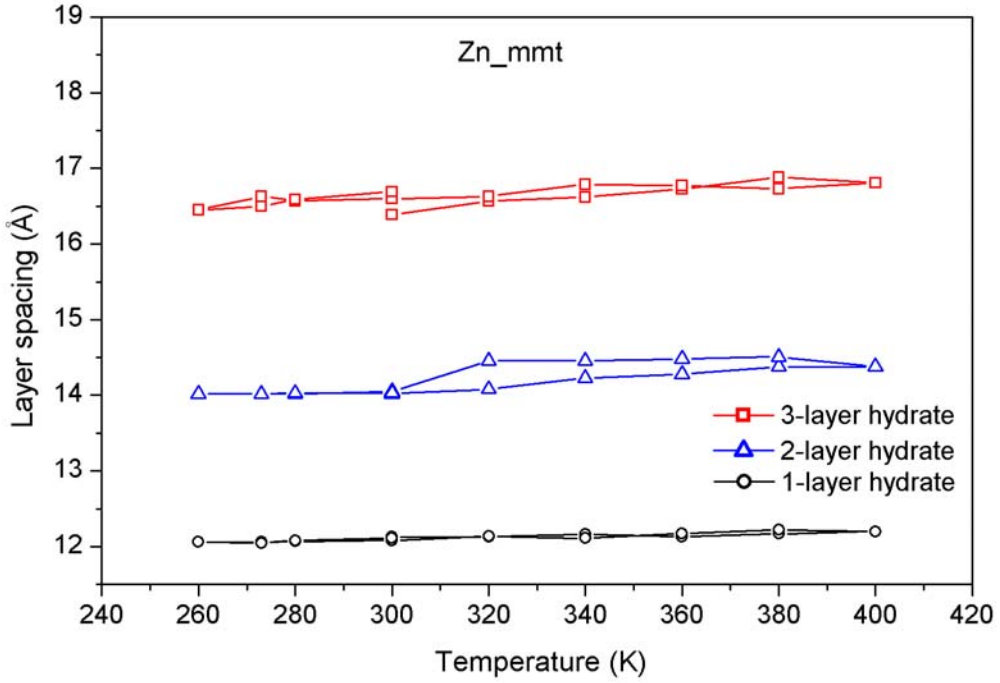


Figure 3-18: Evolution of interlayer space of 1_layer, 2_layer and 3_layer hydrated Zn-Wyoming montmorillonite as a function of temperature.

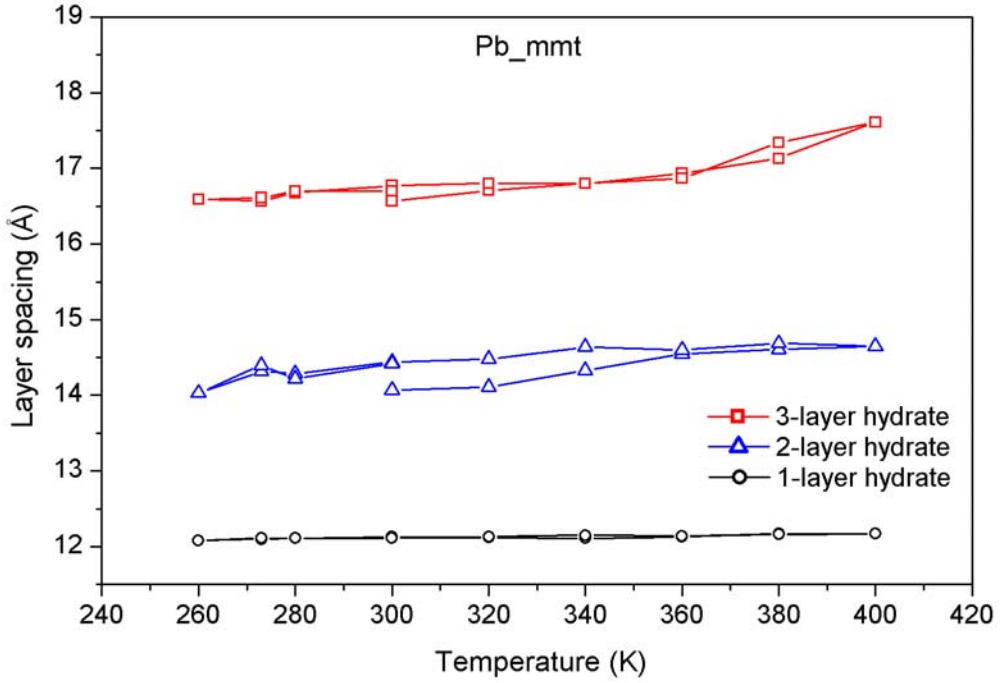


Figure 3-19: Evolution of interlayer space of 1_layer, 2_layer and 3_layer hydrated Pb-Wyoming montmorillonite as a function of temperature.

**Table 3-5: The range and change rate of the interlayer space (Å) of montmorillonite under temperature between 260K and 400K**

| hydrate | one-layer | | two-layer | | three-layer | |
|---|---|---|---|---|---|---|
| Li-mmt | 0.12 | 1.00% | 0.51 | 3.48% | 1.08 | 6.44% |
| Na-mmt | 0.34 | 2.81% | 1.18 | 8.06% | 1.28 | 7.65% |
| K-mmt | 0.21 | 1.76% | 0.76 | 5.25% | 1.44 | 8.58% |
| Rb-mmt | 0.32 | 2.63% | 0.99 | 6.78% | 1.3 | 7.76% |
| Cs-mmt | 0.23 | 1.88% | 0.7 | 4.71% | 1.53 | 8.81% |
| Ca-mmt | 0.46 | 3.75% | 0.46 | 3.17% | 0.67 | 4.06% |
| Ni-mmt | 0.11 | 0.92% | 0.38 | 2.71% | 0.42 | 2.57% |
| Zn-mmt | 0.17 | 1.40% | 0.49 | 3.50% | 0.49 | 2.99% |
| Pb-mmt | 0.09 | 0.74% | 0.66 | 4.69% | 1.04 | 6.28% |

- The change rate is obtained by dividing the range by the layer spacing value at initial 300K.

Temperature factor plays different role in the warming/cooling process of different hydrated montmorillonite with different counterions, as indicated in Table 3-5. Variations of basal spacing of 2-layer hydrated clay are about three times greater than that of 1-layer hydrated clay including no matter monovalent or divalent cations except Ca- and Pb-montmorillonite. The fluctuation of layer space of 3-layer hydrated montmorillonite including monovalent counterions is evident in contrast with its 2-layer hydrated state. However this phenomenon is not very obvious in divalent cations included in the clay except for Pb-montmorillonite.

While the temperature increases, the vibration of the water molecules and counterions locating in the interlayer space of clay will be more and more violent. This will bring to pressure on the clay lattice which will push the neighbouring clay layers apart. This force breaks the balance of the interactions between the clay layers, molecules and counterions, so the clay-water system needs to vary in order to reach its new equilibrium. The compensated force generated by the influence of temperature depends greatly on the quantity of water molecules included in the interlayer space of clay. Hence, the layer spacing vibration of 3-layer hydrated clay is greater than 2-layer hydrate and the latter is greater than 1-layer hydrate.

For all these nine montmorillonites, we note that the variation behaviour of basal space of Ca-montmorillonite is distinct from the others. The fluctuation of the layer under the change of temperature is almost the same for Ca-MMT at different hydrated states. We may then conclude that the existence of $Ca^{2+}$ is the most important factor in the swelling behaviour of hydrated montmorillonite under the influence of temperature.

Among the other special cases, we can notice the role of $Pb^{2+}$ in this warming/cooling process of clay. In 1-layer hydrated Pb-MMT, the vibration of the basal spacing of clay is the smallest in all these montmorillonite. While in 2- and 3-layer hydrated state, the fluctuation of interlayer space is much bigger than the other clay including divalent cations. This phenomenon can be explained by the fact that $Pb^{2+}$ is much larger and heavier than the other considered cations, so it needs much important force to move.

In general, at low hydrated state, the quantity of water molecules is small and the force generated by the vibration of molecules under temperature is not great enough to let it move. With the number of water molecules increases, the quantity of the vibration force rises. Once the counterions begin to move, according to their inertia, the cations will keep moving. This vibration of counterions together with that of water molecules leads to greater variation of layer spacing of montmorillonite.

Details information are presented in Figure 3-20 to Figure 3-23 from which we can clearly see what happens with the basal spacing of different hydrated clay under the change of temperature.

Figure 3-20 shows the evolution of interlayer space of 1-layer hydrated Na-montmorillonite with temperature effect. Although the variation range of layer spacing is very small (about 0.35Å), the difference between warming and cooling process is clear indicating the hysteresis process. In the interval of 300K and 400K, the warming curve is over the cooling one, whereas in the interval of 260K to 300K, the difference between warming and cooling is not obvious.

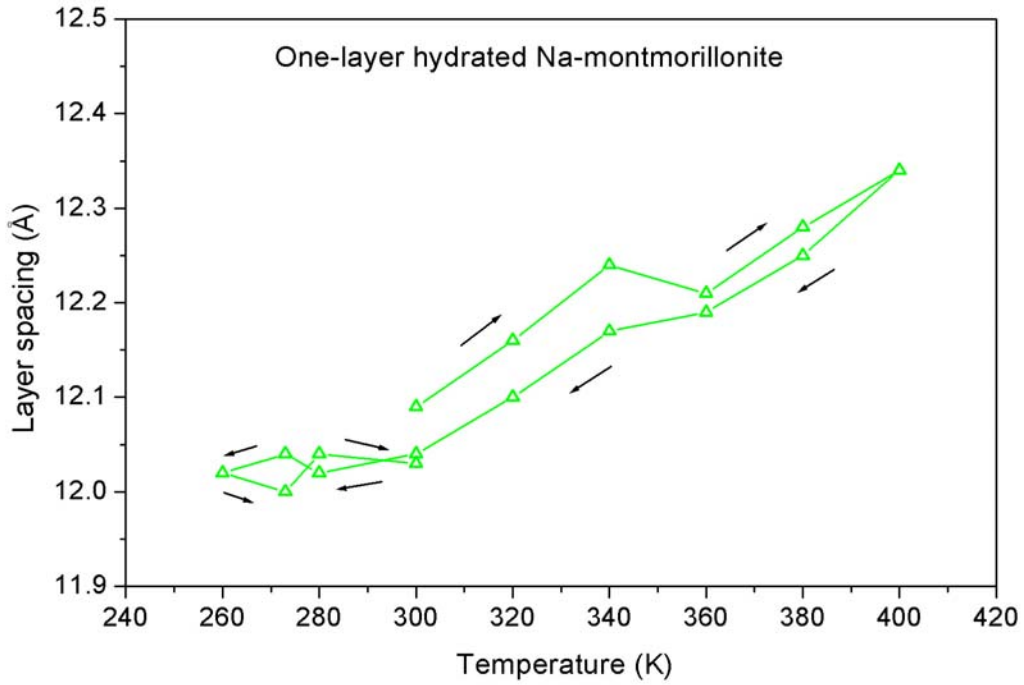


Figure 3-20: Evolution of interlayer space of 1_layer hydrated Na-montmorillonite as a function of temperature.

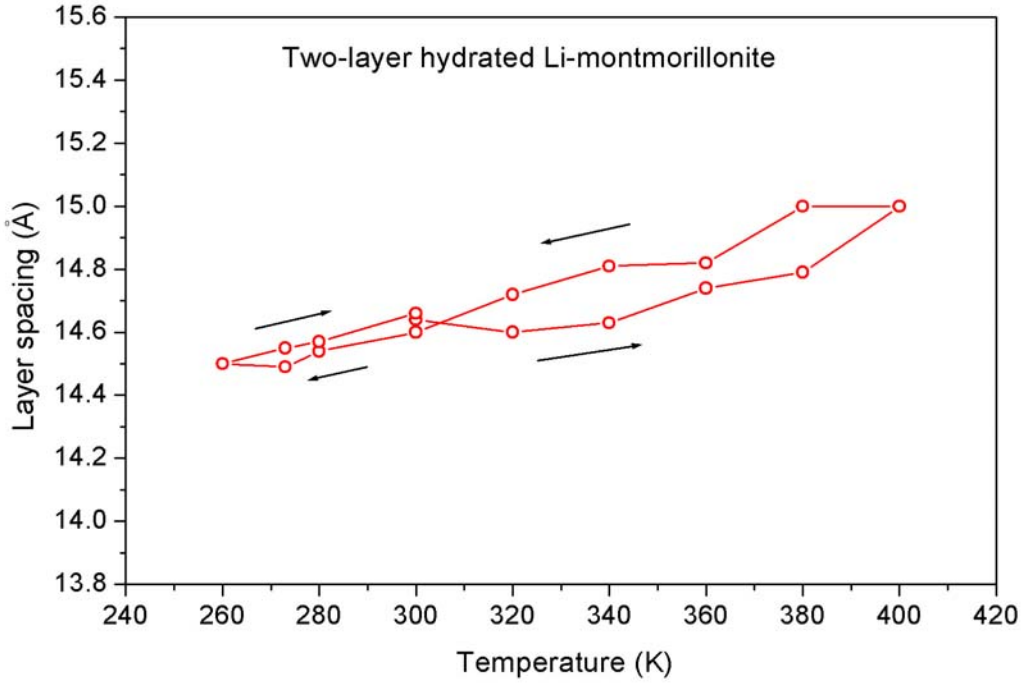


Figure 3-21: Evolution of interlayer space of 2_layer hydrated Li-montmorillonite as a function of temperature.

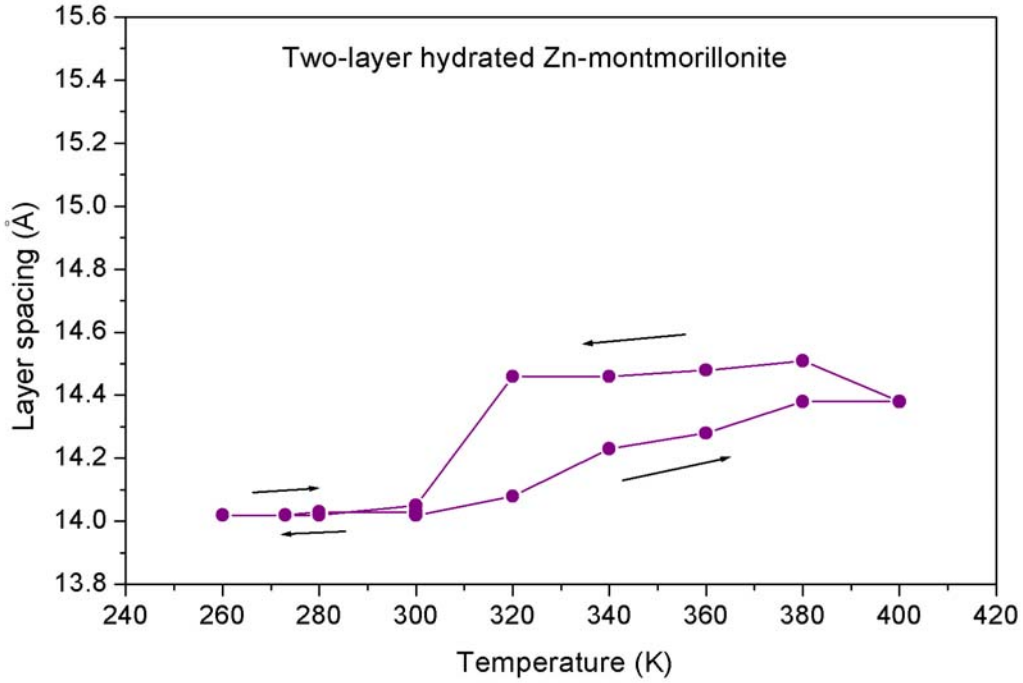


Figure 3-22: Evolution of interlayer space of 2_layer hydrated Zn-Wyoming montmorillonite as a function of temperature.

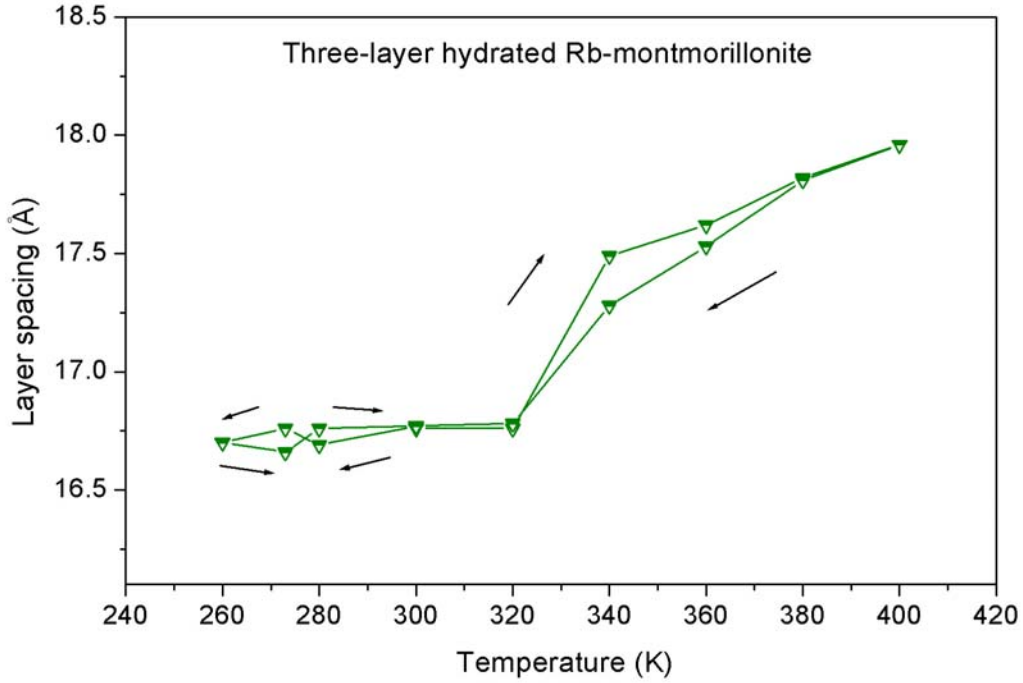


Figure 3-23: Evolution of interlayer space of 3_layer hydrated Rb-montmorillonite as a function of temperature.

Examples for 2-layer hydrated clay are shown in Figure 3-21 and Figure 3-22. In both of the figures, hysteresis phenomenon can be found between 300K and 400K, with a small fluctuation between 260K and 300K, just as what we found in 1-layer hydrated Na-MMT. However, we note that the hysteresis in these two figures is different from Figure 3-20 since the warming curve is below the cooling one.

For 3-layer hydrated clay, Rb-montmorillonite is taken as an example shown in Figure 3-23 where the hysteresis is similar to 1-layer hydrated Na-MMT in the interval of 320K to 400K and Negligible vibration in the range of 260K to 320K.

Above all, the hysteresis phenomenon generally exists in the warming/cooling process of hydrated montmorillonite especially at high temperature. The increase of temperature will lead to important vibration of the interlayer molecules and cations. This force brings to pressure on the clay lattice, so that the clay layer will move to reach its stable state. The clay lattice moves as an entity and it has greater inertia than the interlayer particles. According to the definition of inertia, the clay lattice endeavours to stay in its present state. Therefore, while temperature begins to decrease, clay layer couldn't change immediately which cause the phenomenon of hysteresis.

## 3.5. Conclusion

We have investigated, by means of Monte Carlo simulations, the swelling and shrinking processes in the hydrated Wyoming montmorillonite clay including different monovalent and divalent cations [60]. The best potential model was fixed from the comparison of our simulation with available experiment and preceding theoretical works. We have then extended our study to the clay with some other cations which have never been studied, especially heavy metal ions such as $Ni^{2+}$, $Zn^{2+}$ and $Pb^{2+}$.

We found that the phenomenon of hysteresis which claims the different behaviour of swelling and shrinking is easily realisable in double valent counterions than the monovalent ions in the interspacing of montmorillonite. This difference is evident in montmorillonite including small counterions than big ones. We have shown that stable hydrated layers depend on the type of counterion and the water content. The type of counterion influences the swelling process.

The analysis of the results mainly shows that during the swelling, hydrogen bonds between two water layers are broken, and new hydrogen bond in each layer is formed. The favourable agreement between our results and available experimental and/or preceding theoretical works on the matter supports widely the predicted findings regarding, especially, the clay including pollutants. This gives a predictive idea on the swelling and shrinking behaviours of Wyoming montmorillonite clay under specific environmental conditions.

Simulations on the swelling behaviours of different hydrated montmorillonite under the effect of temperature [61] show that the influence of temperature is much more important at higher hydrated state than at the lower one. To balance the same negative charge in montmorillonite, the number of divalent cations is half of the monovalent ones. The different size and mass of the ions leads to different solvation characteristics. So we may conclude that the influence of temperature on the swelling behaviour of montmorillonite depends on the quantity of counterions together with their solvation characteristics and their attraction capacities.

At the same condition, the counterions play different role on the swelling behaviour of the clay. Comparing the warming/cooling curves, we find the phenomenon of Hysteresis which exists generally in hydrated montmorillonite especially at high temperature. On the other hand, the vibration of the basal spacing at low temperature is negligible. Moreover, the obtained results show that the effect of temperature on the monovalent counterions is much important than that on the divalent counterions.

# Chapter 4

# Diffusion of water and counterions in hydrated montmorillonite

## 4.1. Introduction

Swelling clays is always used for retaining water and contaminants due to their property of low permeability. To understand the diffusive transport of solutes and water in clays is important for the disposal of radioactive waste. Several theoretical and experimental studies have been devoted to describe the behaviour of diffusion of water and some cations in smectite clay [15, 16, 62-71].

Molecular dynamic simulation methods have been employed to study the diffusion behaviour of counterions and water molecules in smectite clay. Chang, F.-R.C et al have addressed the self-diffusion coefficient of $Li^+$ [16], $Na^+$ [15], $K^+$ [68] and water in hydrated montmorillonite at 300K. Rebecca Sutton et al. [70] have presented the transport of $Cs^+$ and water in Cs-smectite at 300K. Greathouse et al. have studied the diffusion of water in Mg-smectite [17] at 300K and 400K, and have shown a much greater diffusion of water at 400K than at 300K. These simulations were performed with MCY water model. The different results of coefficient diffusion under different temperature stimulate the idea to extend these studies to a large variety of cations and to investigate the evolution of diffusion behaviour of water and counterions under the influence of temperature.

This part of the thesis is a continuity of our preceding work developed in chapter 3 where SPC/E water model has been employed in the Monte Carlo simulations of

swelling and shrinking process of montmorillonites. The SPC/E water model has been proved to work well in the swelling simulations. With the configurations of different hydrated montmorillonites obtained by Monte Carlo simulations, which can be directly introduced into DL_POLY, Molecular Dynamic simulation research can be followed on the diffusion behaviour of water and counterions.

In this work, we will study, first, the diffusion behaviour of water molecules and different counterions including in 1-, 2- and 3-layer hydrated montmorillonite at 300K. We look for the influence of water content on the diffusion of interlayer particles. Moreover, the effect of the presence of different monovalent ($Li^+$, $Na^+$, $K^+$, $Rb^+$ and $Cs^+$) and divalent counterions especially some heavy metal cations ($Ca^{2+}$, $Ni^{2+}$, $Zn^{2+}$ and $Pb^{2+}$) on the translational diffusion of water in certain hydrated clay is important to investigate.

Thereafter, the diffusion behaviours under the variation of temperature will be investigated. We extend the simulations to 300K in a range between 260 and 400K in order to find the evolution of diffusion property of water molecules and cations in different hydrated clay under the influence of temperature. We will also consider the effect of temperature and the presence of different monovalent and divalent counterions especially the heavy metal ions on the translational diffusion of water in the clay.

## 4.2. Simulation methods

Our Molecular Dynamics (MD) simulations were performed using the computer program DL_POLY [72-74]. Van der Waals interactions are treated within an all-image regime [29], with a cut-off radius of 9 Å. Long-range electrostatic interactions are calculated by using the Ewald sum method [29] in conjunction with three-dimensional periodic boundary conditions [31].

The initial configurations of 1-, 2- and 3-layer hydrated montmorillonite concerning nine different counterions are taken from the equilibrium configurations obtained by Monte Carlo simulations presented in Chapter 3. Since the object of this study is the diffusion behaviour of interlayer particles, the atoms in the clay framework are frozen here to simplify the calculations. Our simulations are performed in the microcanonical (NVE) ensemble, which is the most appropriate to calculate dynamic quantities as diffusion coefficients [71]. The leapfrog integration algorithm[29]

with a time step of 1.0 fs was used to integrate the equations of motion. Each system was equilibrated over 400ps. Production runs consisted of a further 400 000 time step (400ps) after equilibration. Intermediate configurations were saved every 100 steps in order to calculate self-diffusion coefficients of water molecules or counterions. The pressure is fixed at 1 bar during the simulation, and the temperature is fixed at 300K in the first part of simulations. Whereas, it extends to a range of 260K to 400K with a step of 20K, where the freezing point, 273K and the boiling point, 373K were considered as the special cases.

A three-dimensional Einstein relation was used to calculate self-diffusion coefficients of cations and water molecules:

$$D = \frac{1}{6}\frac{d}{dt}\left\langle r(t)^2 \right\rangle \tag{5.1}$$

Where $\left\langle r(t)^2 \right\rangle$ is the mean-square displacement of the particle defined by

$$r(t) = R(t) - R(0) \tag{5.2}$$

$R(t)$ is the particle position at time $t$.

## 4.3. Diffusion of water and cations in montmorillonite at 300K

### 4.3.1. Choice of ensemble

As mentioned above the NVE ensemble is widely used to simulate the diffusion behaviour of interlayer particles in smectite clay [70, 71]. However, NVT ensemble is also employed in the simulation of cations diffusing in aqueous solutions [34]. We were curious to test these two ensembles on Na-montmorillonite in order to see which one works better in this diffusion simulation. Our simulation results together with available experiment and other simulation results are presented in Table 4-1.

Our simulations in NVT and NVE ensembles gave different results for the diffusion coefficient of both water molecules and counterions in 1-, 2- and 3-layer hydrated montmorillonite. It is clear that the simulation results of water diffusion in NVE ensemble are about three times greater than that in NVT. Whereas the diffusion coefficients of $Na^+$ in NVE are about three times smaller than that in NVE ensemble. Comparing our simulation results with available experimental values, the results

obtained from NVE simulations agree better with experiment than NVT ones. Then it is proved once again that the NVE ensemble is appropriate to calculate the diffusion coefficient. This ensemble is employed to the rest of our simulations.

**Table 4-1: Simulation results of diffusion coefficient of water and $Na^+$ in different hydrated montmorillonite with NVT and NVE ensembles compared with other calculated results and experiment data.**

| hydrate | $D_{water}$ ($10^{-10}m^2/s$) | | | | | $D_{Na^+}$ ($10^{-10}m^2/s$) | | | | |
|---|---|---|---|---|---|---|---|---|---|---|
| | Our results | | Other simulation results | | Exp. | Our results | | Other simulation results | | Exp. [75] |
| | NVT | NVE | | | | NVT | NVE | | | |
| 1-layer | 0.51 | 2.25 | 2.50[15] | 1.0[16] | 4.00[64] | 0.12 | 0.04 | 0.39[15] | 0.15[16] | 0.01 |
| 2-layer | 3.22 | 9.41 | 14.00[15] | 7.9[16] | 10.00[62] | 3.16 | 1.63 | 5.10[15] | 2.53[16] | 1.00 |
| 3-layer | 4.95 | 11.02 | 13.00[15] | 7.2[16] | 10.00[64] | 5.22 | 0.92 | 1.80[15] | 1.1[16] | 2.00 |
| Bulk water | | | | | 15.0[65] | | | | | 9.0 |

**Table 4-2: Simulation results of diffusion coefficient of water and $Li^+$ in different hydrated montmorillonite with NVE ensemble compared with other calculated results and experiment values.**

| hydrate | $D_{water}$ ($10^{-10}m^2/s$) | | | $D_{Li^+}$ ($10^{-10}m^2/s$) | | |
|---|---|---|---|---|---|---|
| | Our results | Other simulation results[16] | Experiment [62, 64, 67] | Our results | Other simulation results[16] | Experiment [75] |
| 1-layer | 4.24 | 1.3 | 0.5 to 4 | 0.34 | 0.11 | |
| 2-layer | 7.33 | 4.5 | 2.6 to 7 | 3.05 | 0.67 | |
| 3-layer | 11.18 | 14 | 10 | 1.42 | 4.3 | |
| Bulk water | | | 23 [65] | | | 10 |

Our NVE simulation results of Na- and Li-montmorillonite compared with those of Chang et al. [15, 16], which is based on MCY water model are presented in Table 4-1 and Table 4-2 respectively. We may see that our simulation results agree better with the experimental values than the latter ones. Hence, the SPC/E water model used in

our clay-water system can well simulate the diffusion behavior of interlayer particles in the clay.

### 4.3.2. Mean square displacement (MSD)

The computed values of diffusion coefficient were taken from the sixth of the slope of the Mean Square Displacement (MSD) curve. We present, as an example, the MSD of water in three-hydrated Na-montmorillonite in Figure 4-1. From just above zero to about 175 ps the MSD is well fitted by a straight line. But at longer times the gradient of the MSD slightly decreases at around 175 ps and 170 $Å^2$. This shape of MSD is similar to what Greathouse et al. have found in the MSD for water molecules in Mg-beidellite [17]. The decrease of gradient in the MSD is due to the free diffusion of water in a zone about 170 $Å^2$, but the diffusion over larger distances is hindered.

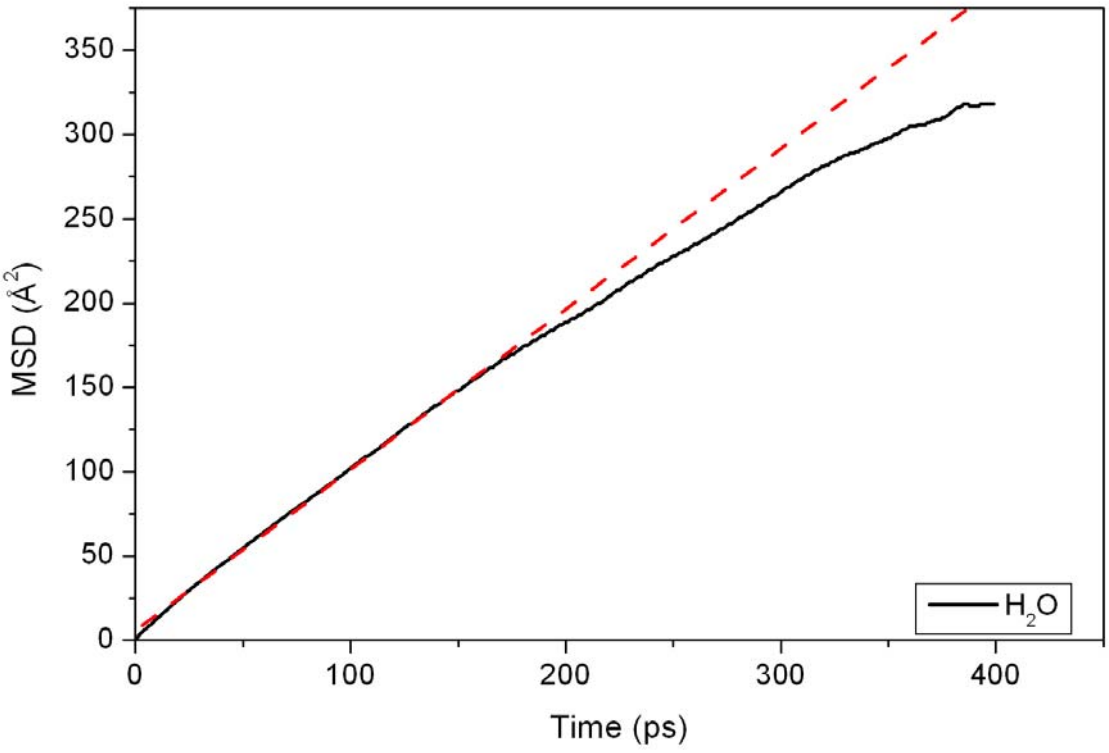


Figure 4-1: Mean-square displacement of water molecules in three-layer hydrated Na-montmorillonite versus time.

The slope of MSD curve decreases which means that the calculated diffusion coefficient decreases versus time. So it is important to apply a suitable length of

simulation time to obtain a reasonable value. If the simulation time is not long enough, the calculated results will be significantly greater than experimental value. That is why there are different results for the diffusion coefficients of water and $Na^+$ in Na-montmorillonite presented by Chang et al. in 1995 [15] and 1997 [16] where the MD simulation time was set as 205 ps for the former and 405ps for the latter one. On the other hand, whereas the simulation time may be the longer the better, it is unwise to perform a simulation in an infinite period. From the plot in Figure 4-1, we found that the slope of the MSD curve began to decrease from about 175 ps. The magnitude of gradient reduced versus time and at about 400 ps, the difference of diffusion coefficient is less than $0.01\times10^{-10}$ $m^2/s$. Therefore we may conclude that the simulation time of 400 ps is enough to simulate the long-time diffusion behavior of interlayer particles in clay.

### 4.3.3. Results and discussions

The same simulation method is performed to predict the diffusion behavior of water and different counterions especially some heavy metal pollutant cations in montmorillonite. The diffusion coefficients of water and monovalent cations in montmorillonite are shown in Table 4-3 and those of the divalent cations are shown in Table 4-4.

**Table 4-3: Simulation results of diffusion coefficient of water and monovalent cations in different hydrated montmorillonite.**

D : $10^{-10}$ ($m^2/s$)

| hydrate | Li_mmt | | Na_mmt | | K_mmt | | Rb_mmt | | Cs_mmt | |
|---|---|---|---|---|---|---|---|---|---|---|
| | $H_2O$ | $Li^+$ | $H_2O$ | $Na^+$ | $H_2O$ | $K^+$ | $H_2O$ | $Rb^+$ | $H_2O$ | $Cs^+$ |
| 1-layer | 4.24 | 0.34 | 2.25 | 0.04 | 2.38 | 0.53 | 2.04 | 0.029 | 4.41 | 0.083 |
| 2-layer | 7.33 | 3.05 | 9.41 | 1.63 | 4.73 | 0.54 | 9.96 | 0.63 | 13.11 | 0.578 |
| 3-layer | 11.18 | 1.42 | 11.02 | 0.92 | 15.17 | 5.05 | 12.95 | 5.127 | 18.91 | 3.655 |

Since there are no many corresponding experimental results to make comparison, we have found some other simulation results, such as the diffusion coefficients of water and counterions in 1-, 2- and 3-layer hydrated K-montmorillonite

presented by Chang et al. [68], and the diffusion coefficients of interlayer water in Cs-smectite reported by Sutton [70]. Although our simulations results don't correspond exactly to the latter simulations, our calculated values are of the same order of magnitude. The difference is maybe due to the employed water and clay model, and the employed simulation condition.

**Table 4-4: Simulation results of diffusion coefficient of water and divalent cations in different hydrated montmorillonite.**

D: $10^{-10}$ ($m^2/s$)

| hydrate | Ca_mmt | | Ni_mmt | | Zn_mmt | | Pb_mmt | |
|---|---|---|---|---|---|---|---|---|
| | $H_2O$ | $Ca^{2+}$ | $H_2O$ | $N^{i2+}$ | $H_2O$ | $Zn^{2+}$ | $H_2O$ | $Pb^{2+}$ |
| 1-layer | 2.950 | 0.031 | 4.519 | 0.020 | 3.490 | 0.005 | 2.352 | 0.002 |
| 2-layer | 7.524 | 0.429 | 5.271 | 0.167 | 3.774 | 0.141 | 4.318 | 0.025 |
| 3-layer | 11.037 | 6.358 | 13.713 | 0.759 | 7.555 | 0.145 | 17.374 | 0.684 |

The diffusion of water molecules in all montmorillonites at 1-, 2- and 3-layer hydrated state, it increases versus the quantity of water content. Similarly phenomenon occurs for the diffusion of counterions in different hydrated clay. Only an exception can be found in Li- and Na-montmorillonite where the transport of $Li^+$ and $Na^+$ in 3-layer hydrated clay is slower than that in 2-layer hydrated ones. Obviously, the quantity of water content in the clay plays an important role on the diffusion behavior of water molecule and counterions. Whether the monovalent or divalent, the cations together with water molecules diffuse slowly in low hydrated clay, and relatively rapidly in higher hydrated one.

At low hydrated states, the diffusion of water is less affected by the cation type. However, the diffusion of monovalent cations is generally greater than that of divalent ones because the quantity of monovalent cations is twice of divalent ones in unit clay.

The quantity of water molecules affect the force generated by the vibration of water molecules and this force, as the interactions between water and counterions, will be applied on the counterions. At low hydrated state, water quantity is small and the force applied on the cations is weak. Then the weight of cation has great influence on its movement. For example, in Table 4-4, it is evident that the diffusion of divalent cations in 1- and 2-layer hydrated clay decreases when the cation's weight increases. In other words, the heavy cations diffuse more difficultly than the

lighter ones.

However, at high hydrated state, the problem is not so simple. The interlayer spacing of high hydrated montmorillonite is large enough which permits the counterions to be completely hydrated. The hydrated cations consist of the counterions surrounded by attracted water molecules, which move as a large molecule in the interlayer solution. So the diffusion of counterions in high hydrated clay depends not only on the cations' size and weight but also on their capacity of attracting water molecules. This may explain the exception behavior of diffusion of $Li^+$ and $Na^+$ in 3-layer hydrated clay. Both $Li^+$ and $Na^+$ have strong hydrate capacity which means that their hydrated cations consist of more water molecules and the whole size of this hydration is large; furthermore, the quantity of free water molecules decreases. As a consequence, the diffusion of these cations together with the water molecules is slowed down.

On the other hand, the heavy metal cations have large size, and due to their size, their capacity of attracting water molecules is not very strong. This causes therefore the great degree of free water so that water and these heavy cations can diffuse much more easily than expected in the clay.

## 4.4. Effect of temperature on the diffusion behaviour of water and counterions in montmorillonite

The 1-, 2- and 3-layer hydrated montmorillonite containing the nine types of counterions have been simulated respectively. These thermodynamic simulations start with the configurations at 300K which are taken from our previous simulation results.

### 4.4.1. Diffusion of water

The evolution of diffusion coefficient of water in 1-, 2- and 3-layer hydrated montmorillonite versus temperature is shown in Figure 4-2 to Figure 4-7.

Figure 4-1 shows the diffusion of water in 1-layer hydrated montmorillonite including monovalent counterions. A fitting curve has been employed to present the tendency of diffusion evolution under the change of temperature in each montmorillonite. It is clear that the diffusion of water in this 1-layer hydrated clay rises when temperature increases; whereas, this raising behaviour is different depending on the interlayer counterions included in the montmorillonite.

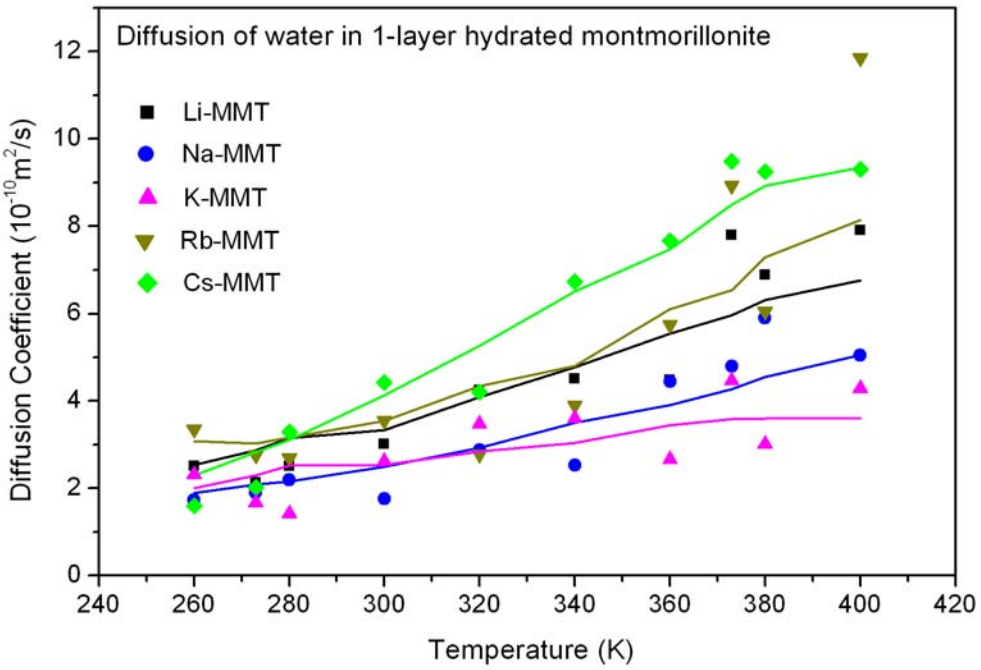


Figure 4-2: Evolution of self-diffusion coefficient of water in one-layer hydrated montmorillonite including monovalent counterions with the change of temperature.

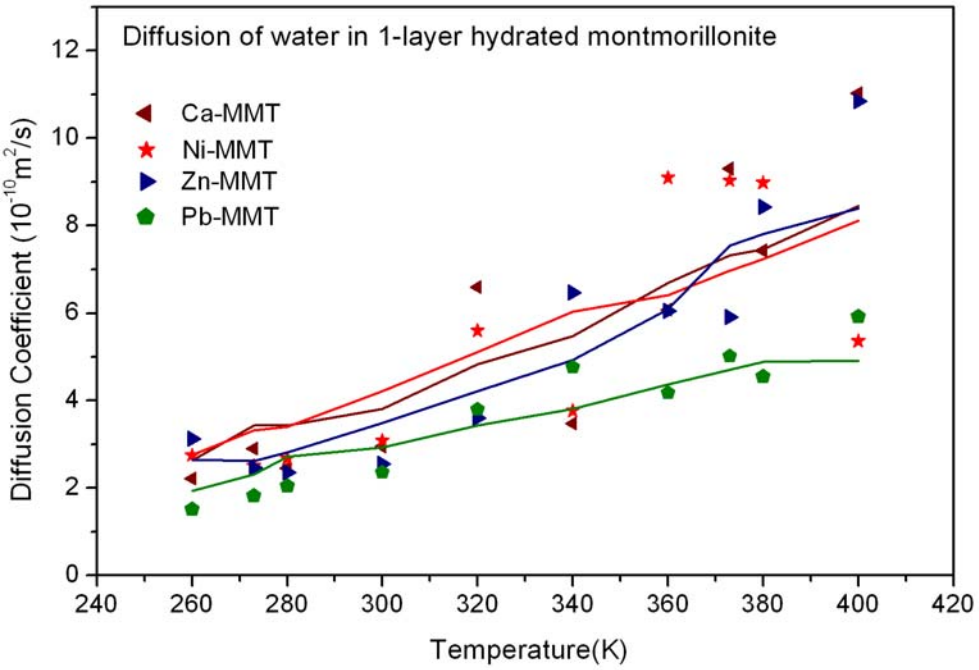


Figure 4-3: Evolution of self-diffusion coefficient of water in one-layer hydrated montmorillonite including divalent counterions with the change of temperature.

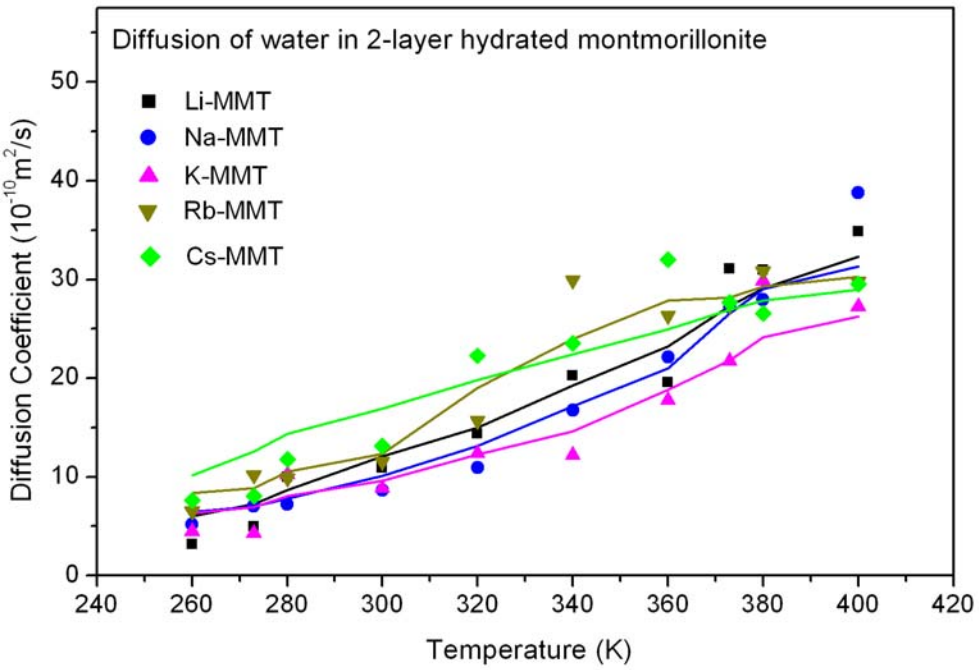


Figure 4-4: Evolution of self-diffusion coefficient of water in two-layer hydrated montmorillonite including monovalent counterions with the change of temperature.

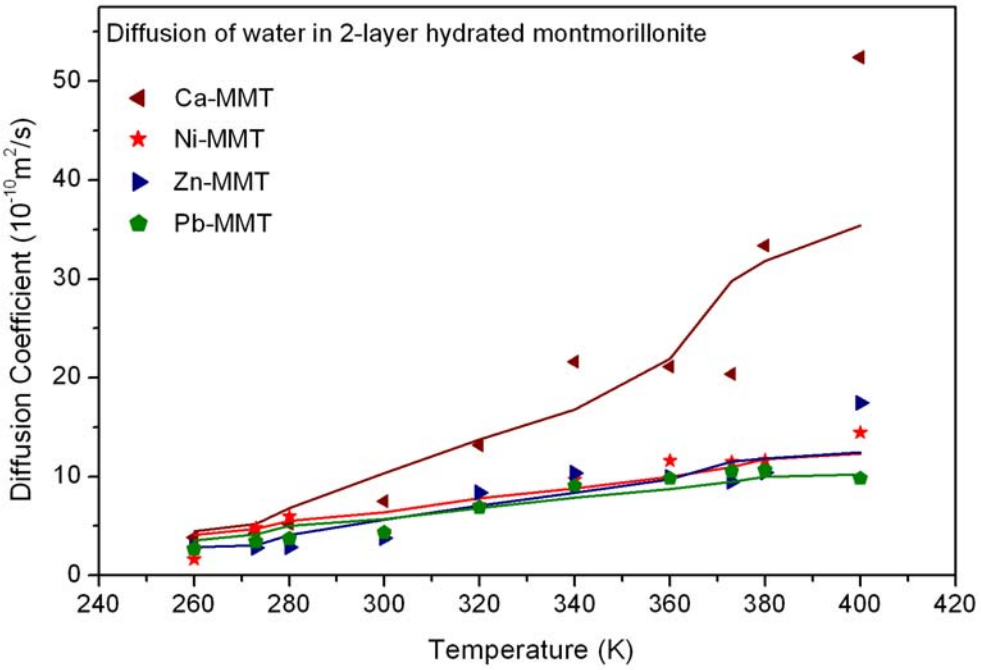


Figure 4-5: Evolution of self-diffusion coefficient of water in two-layer hydrated montmorillonite including divalent counterions with the change of temperature.

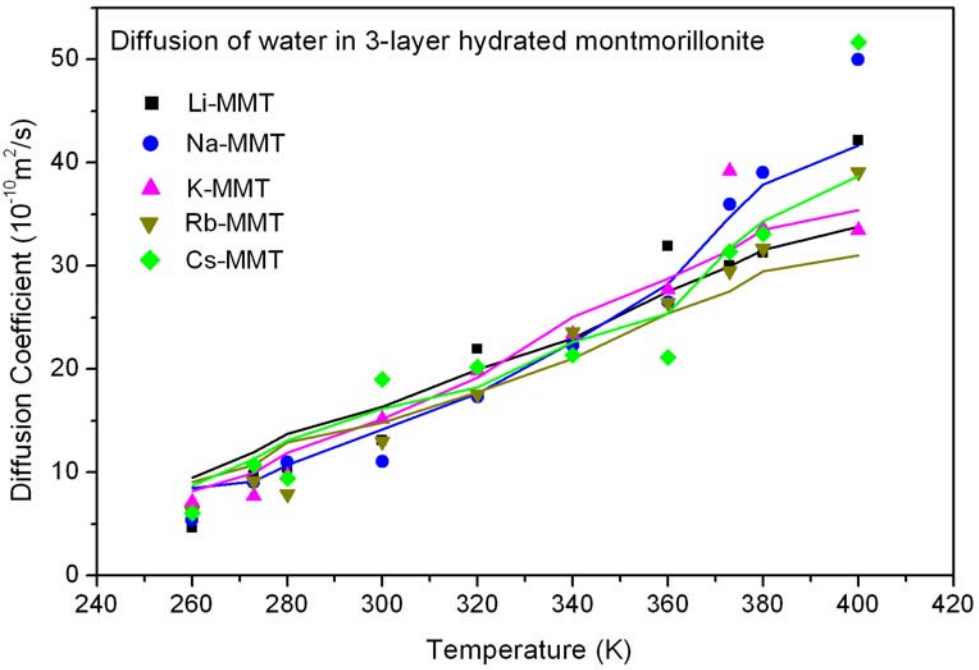


Figure 4-6: Evolution of self-diffusion coefficient of water in three-layer hydrated montmorillonite including monovalent counterions with the change of temperature.

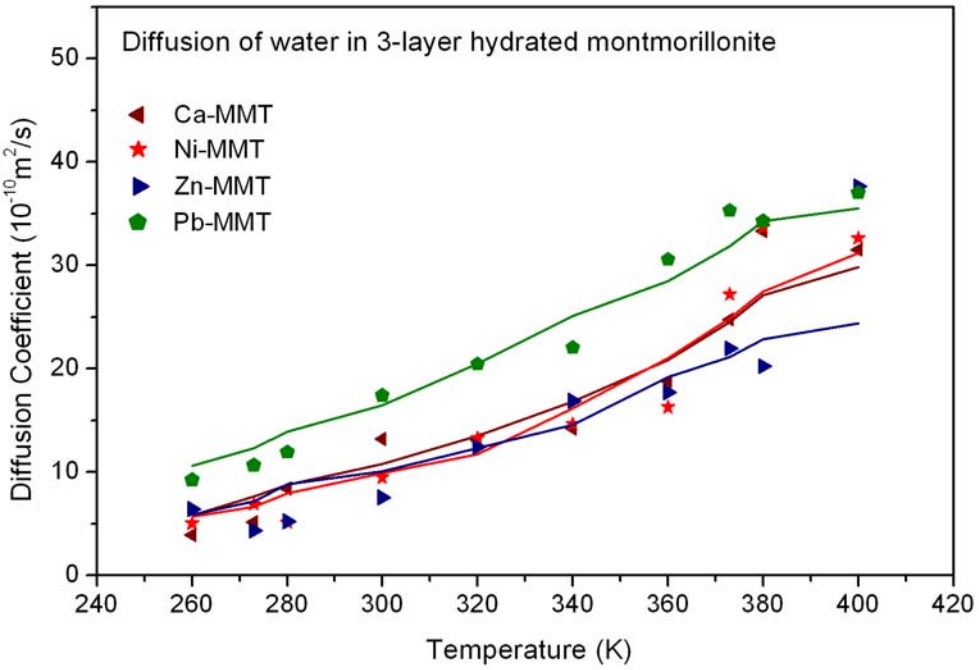


Figure 4-7: Evolution of self-diffusion coefficient of water in three-layer hydrated montmorillonite including divalent counterions with the change of temperature.

For comparison, the diffusion of water in divalent cations containing montmorillonite is presented in Figure 4-3. We can see that the diffusion curves of water in Ca-, Ni- and Zn-montmorillonite are similar to each other whereas the slope of diffusion curve of Pb-clay is smaller than the others. The same scale in y-axis is preformed in Figure 4-1 and Figure 4-2 to make it easy to compare the diffusion behaviour of water in monovalent and divalent counterions included in the clay. We can see clearly the effect of cations on the diffusion of water in 1-layer hydrated montmorillonite.

Figure 4-4 and Figure 4-5 show the diffusion of water in 2-layer hydrated montmorillonite including monovalent and divalent counterions respectively. The tendency is quite similar in all cases presented in Figure 4-4. In Figure 4-5, the diffusion behaviour of water in Ni-, Zn- and Pb-MMT is very similar to each other, whereas the curve of Ca-clay has a more important slope than the others, which means that the diffusion of water in 2-layer hydrated Ca-montmorillonite is highly affected by the temperature.

The diffusion of water in 3-layer hydrated montmorillonite under the influence of temperature is shown in Figure 4-6 and Figure 4-7 respectively. These variation have almost the same tendency and they show a process of a quasi linear variation to a non-linear variation divided by the boiling point. At high hydrated clay, the influence of existing counterions on the diffusion behaviour of water is negligible.

### 4.4.2. Diffusion of counterions

The diffusion of counterions in corresponding hydrated montmorillonite is shown in Figure 4-8 to Figure 4-13, respectively. It is quite evident that the diffusion of monovalent cations is much greater than divalent ones in hydrated montmorillonite. The monovalent cations diffuse roughly when the temperature rise, while the diffusion of divalent cations remains almost constant near zero. Moreover, at 3-layer hydrated state, the diffusion of divalent cations begins to increase versus the temperature.

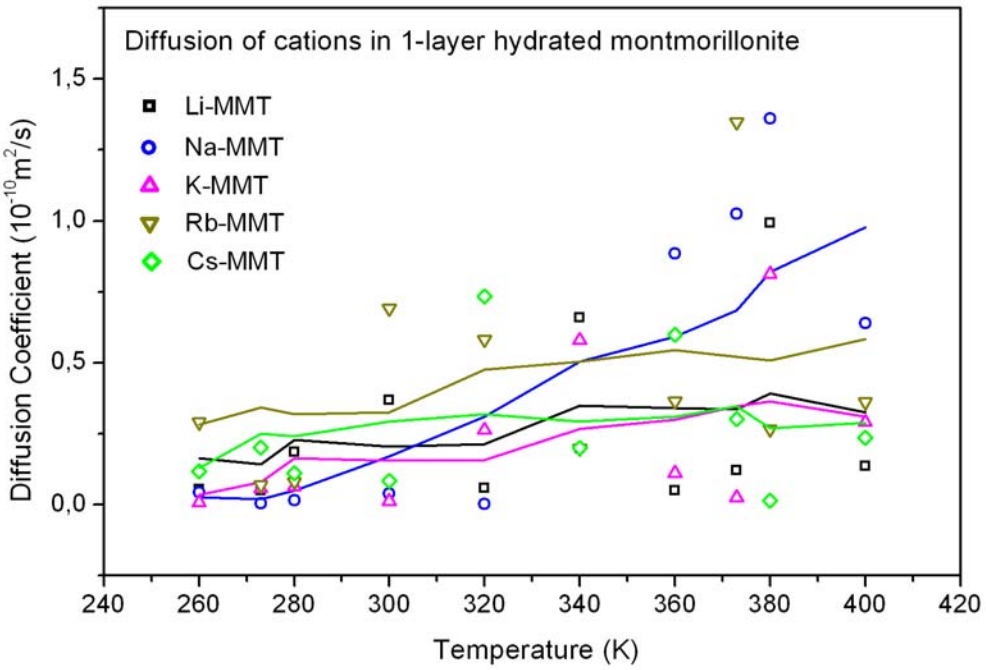


Figure 4-8: Evolution of self-diffusion coefficient of monovalent counterions in one-layer hydrated montmorillonite with the change of temperature.

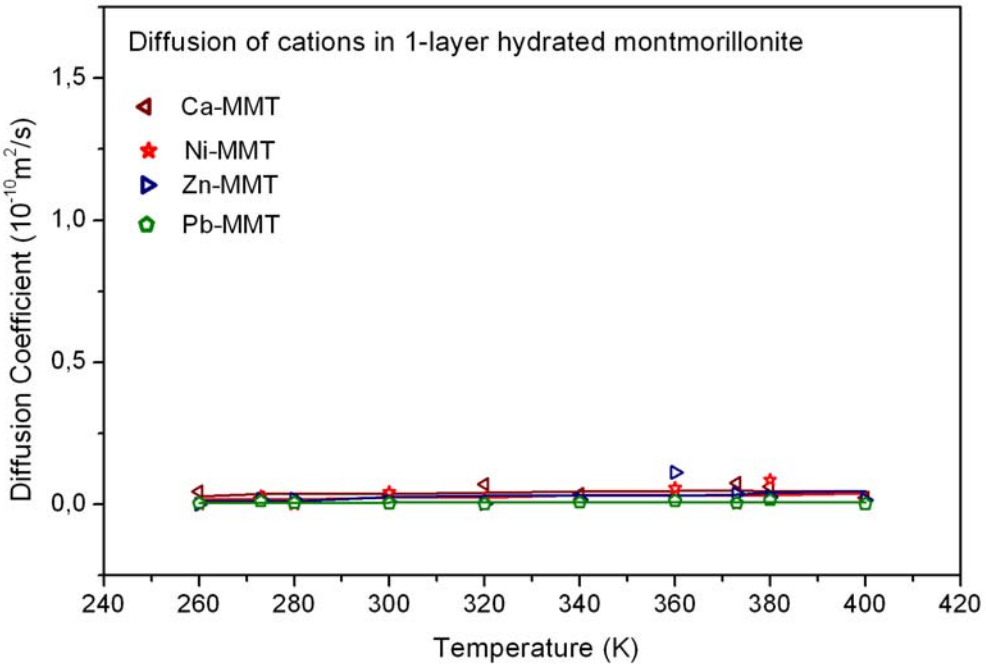


Figure 4-9: Evolution of self-diffusion coefficient of divalent counterions in one-layer hydrated montmorillonite with the change of temperature.

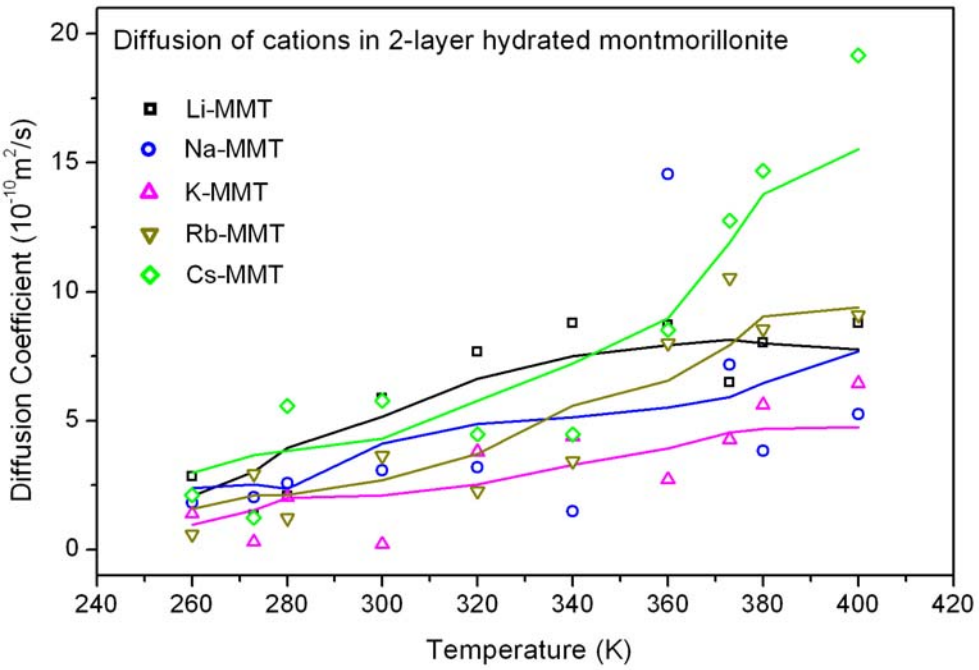


Figure 4-10: Evolution of self-diffusion coefficient of monovalent counterions in two-layer hydrated montmorillonite with the change of temperature.

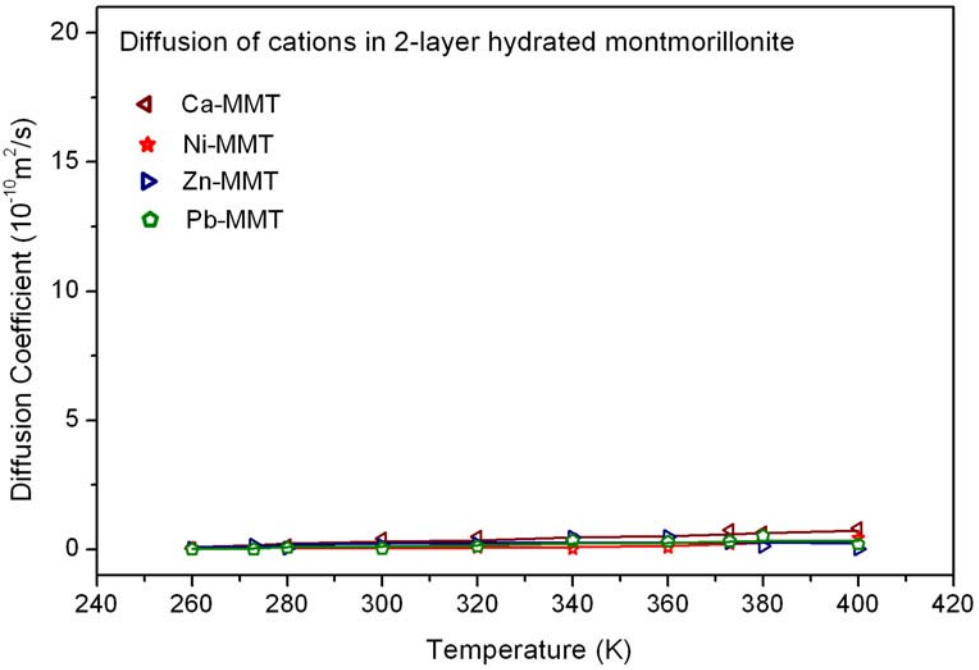


Figure 4-11: Evolution of self-diffusion coefficient of divalent counterions in two-layer hydrated montmorillonite with the change of temperature.

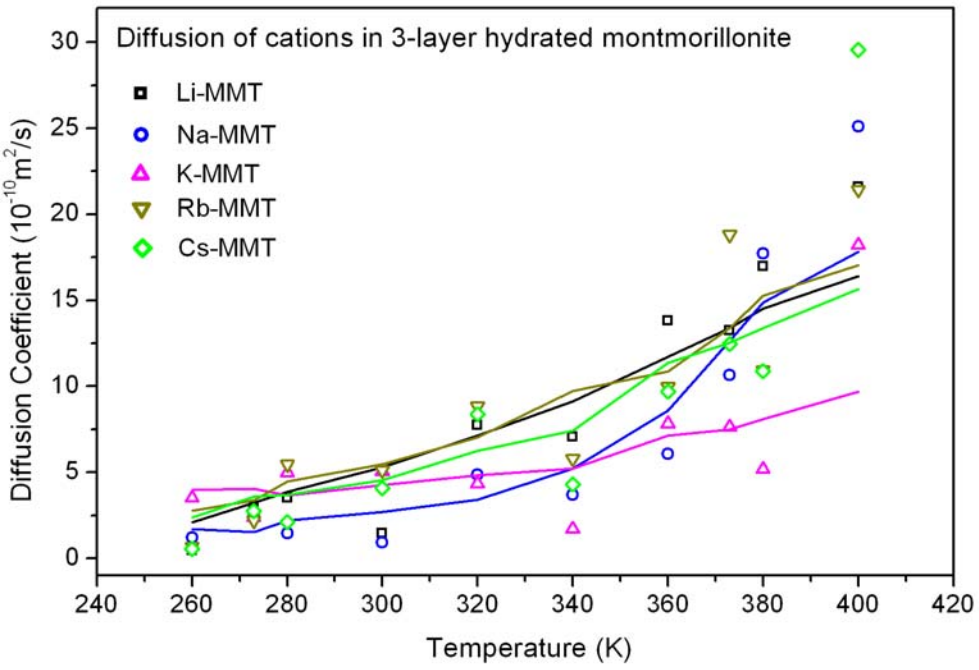


Figure 4-12: Evolution of self-diffusion coefficient of monovalent counterions in three-layer hydrated montmorillonite with the change of temperature.

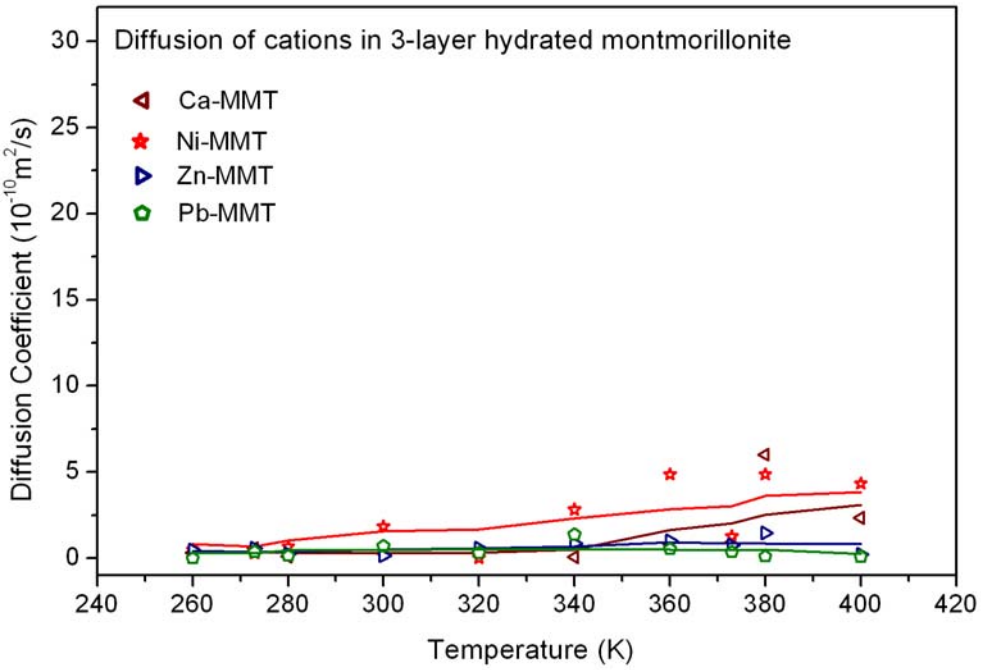


Figure 4-13: Evolution of self-diffusion coefficient of divalent counterions in three-layer hydrated montmorillonite with the change of temperature.

### 4.4.3. Effect of hydration

The diffusion of water and counterions in three different hydrated montmorillonite is collected together according to the counterions' type, shown in Figure 4-14 to Figure 4-22 respectively. In each figure, the solid lines represent the diffusion of water and the dashed lines correspond to the diffusion of counterions. Three different colours of curves represent the diffusion behaviour at different hydrated degree. The same colour for the curve of water and cation at the same hydrated degree helps us to find the difference between them.

From all the nine figures we can see that the distance between the curves of water and cations widens with the raise of temperature. The increase of water curve of 1-layer hydrated clay is much slower than that of higher hydrate, so the distance between the 1 and the 2, 3 curves increase. However, the diffusion behaviour of water in 2 and 3-layer hydrated clay is not always the same. We can see that, in Rb-, Cs- and Ca-MMT, the variations in 2 and 3-layer hydrate approach to each other. In contrast, those variations in Li-, Na-, Ni-, Zn- and Pb-MMT split which means that the diffusion of water is greatly influenced by the hydration of the clay.

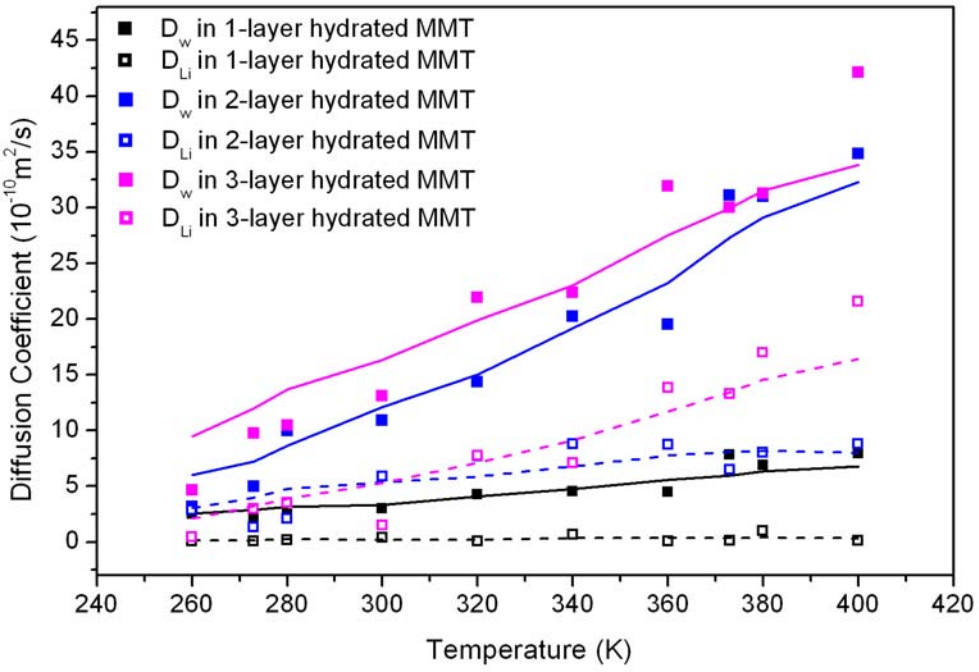


Figure 4-14: Evolution of self-diffusion coefficient of water and $Li^+$ in 1-, 2- and 3-layer hydrated montmorillonite with the change of temperature.

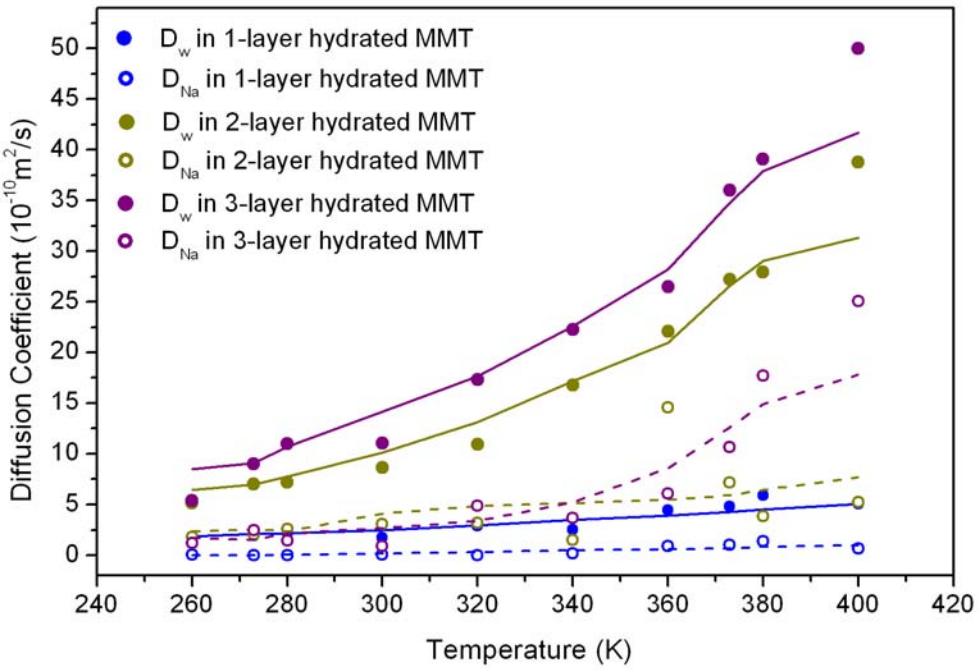


Figure 4-15: Evolution of self-diffusion coefficient of water and $Na^+$ in 1-, 2- and 3- layer hydrated montmorillonite with the change of temperature.

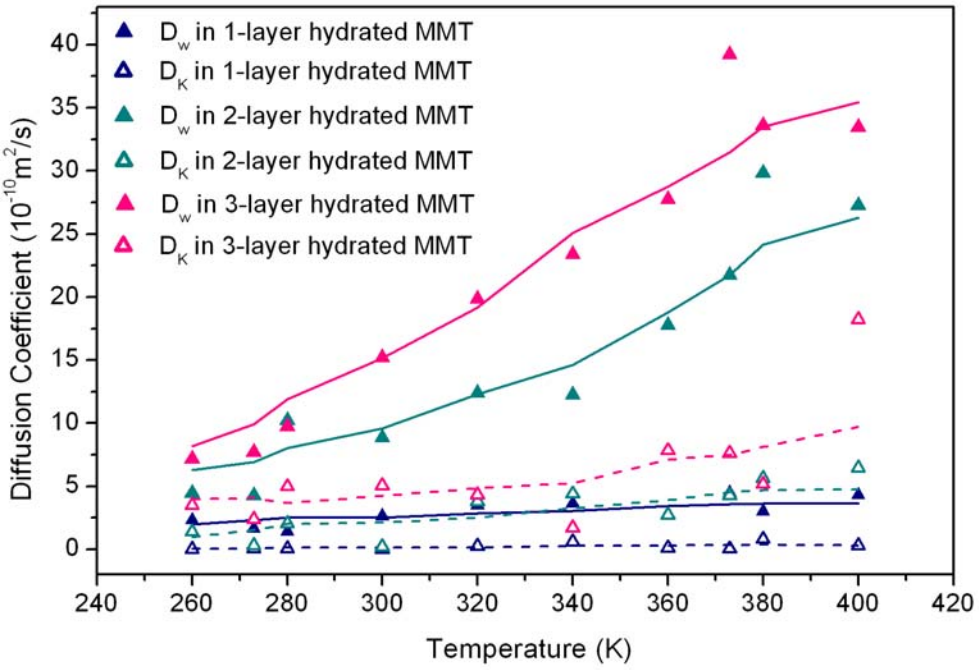


Figure 4-16: Evolution of self-diffusion coefficient of water and $K^+$ in 1-, 2- and 3- layer hydrated montmorillonite with the change of temperature.

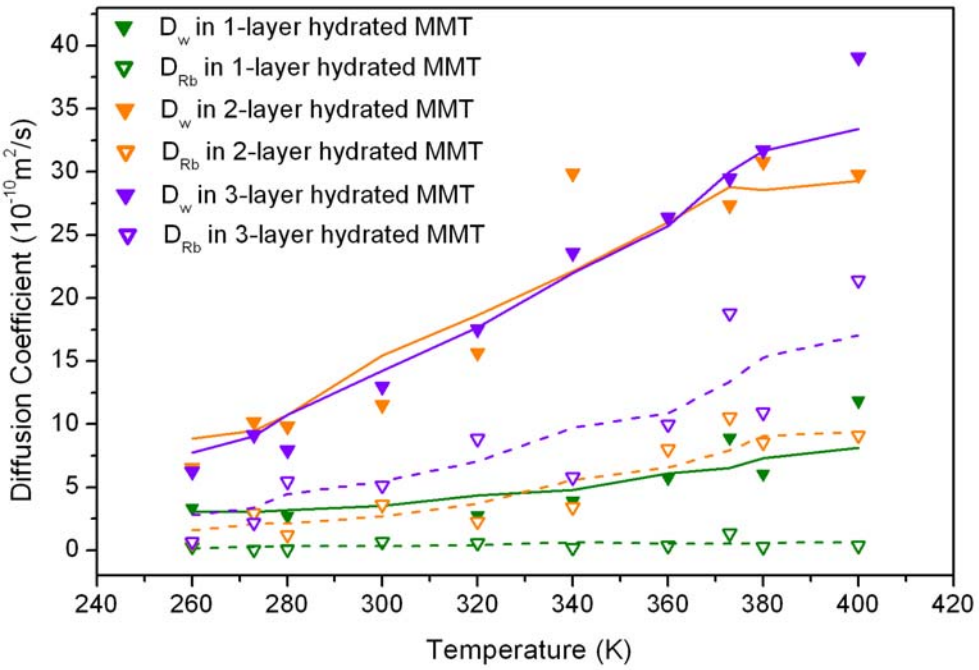


Figure 4-17: Evolution of self-diffusion coefficient of water and $Rb^+$ in 1-, 2- and 3- layer hydrated montmorillonite with the change of temperature.

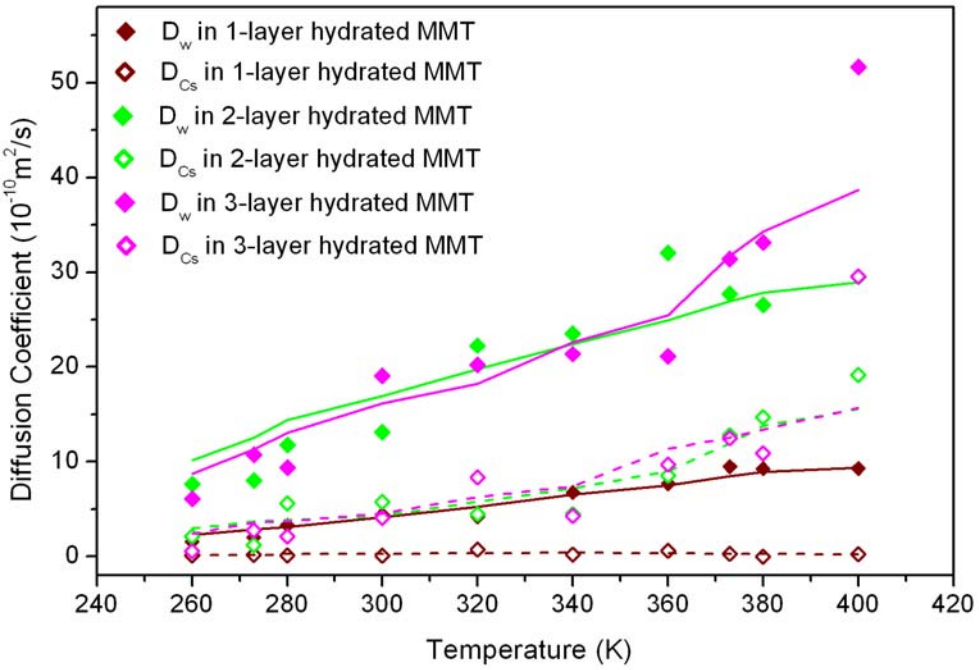


Figure 4-18: Evolution of self-diffusion coefficient of water and $Cs^+$ in 1-, 2- and 3- layer hydrated montmorillonite with the change of temperature.

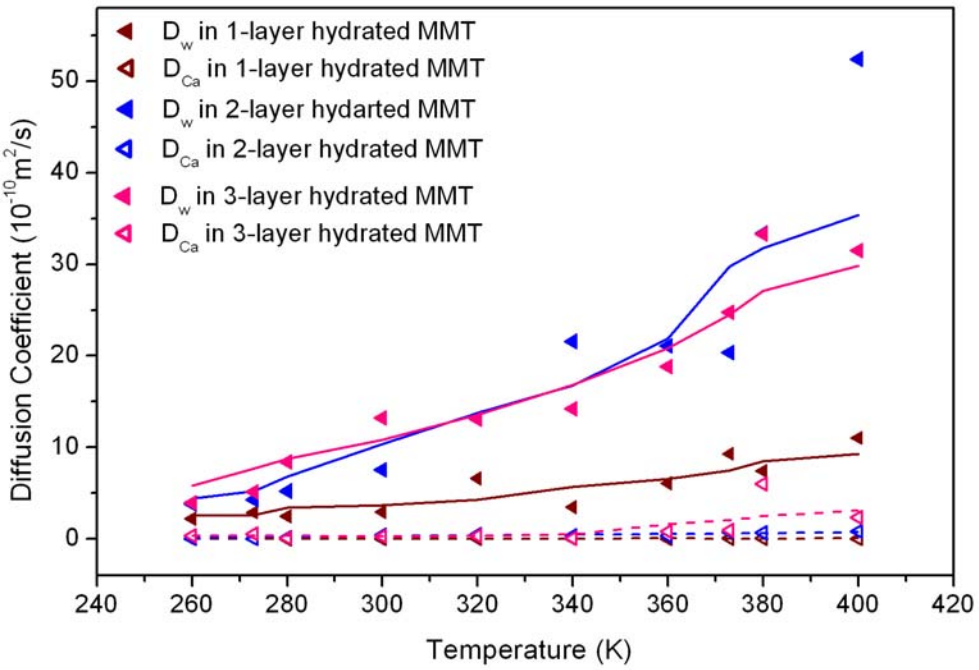


Figure 4-19: Evolution of self-diffusion coefficient of water and $Ca^{2+}$ in 1-, 2- and 3- layer hydrated montmorillonite with the change of temperature.

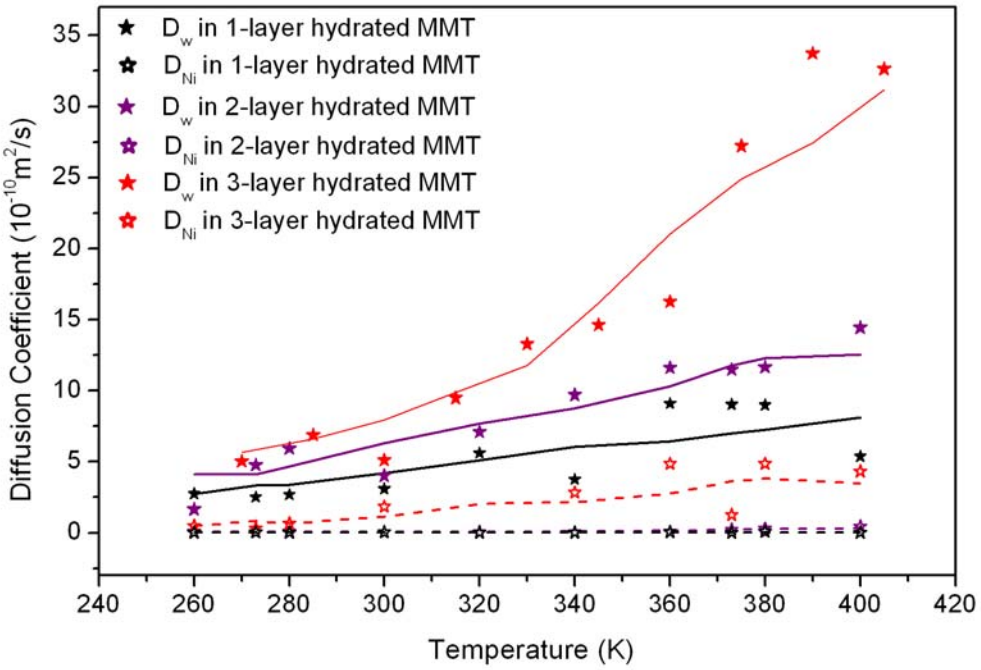


Figure 4-20: Evolution of self-diffusion coefficient of water and $Ni^{2+}$ in 1-, 2- and 3- layer hydrated montmorillonite with the change of temperature.

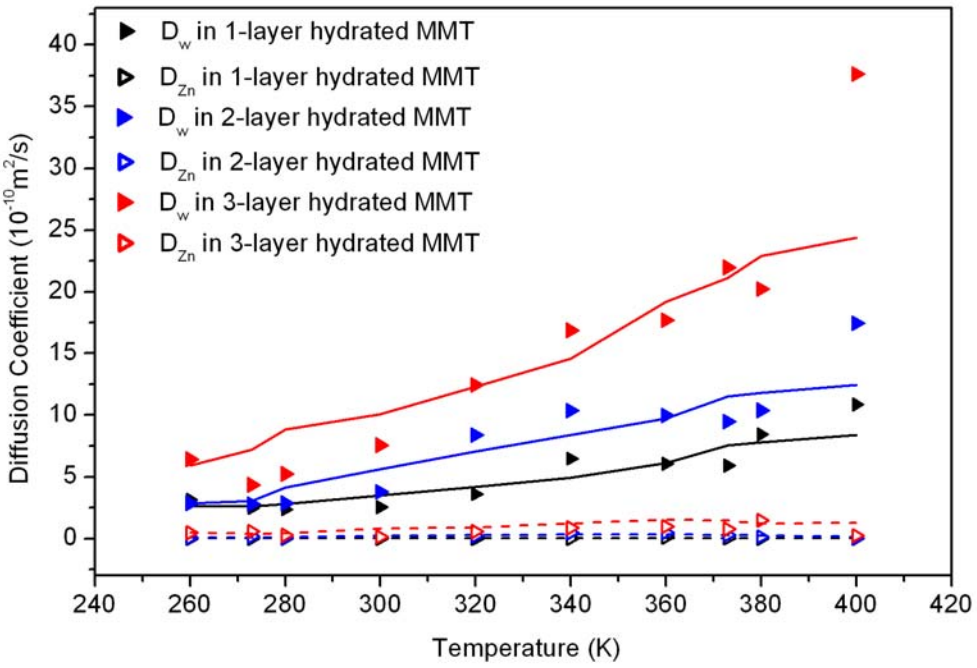


Figure 4-21: Evolution of self-diffusion coefficient of water and $Zn^{2+}$ in 1-, 2- and 3- layer hydrated montmorillonite with the change of temperature.

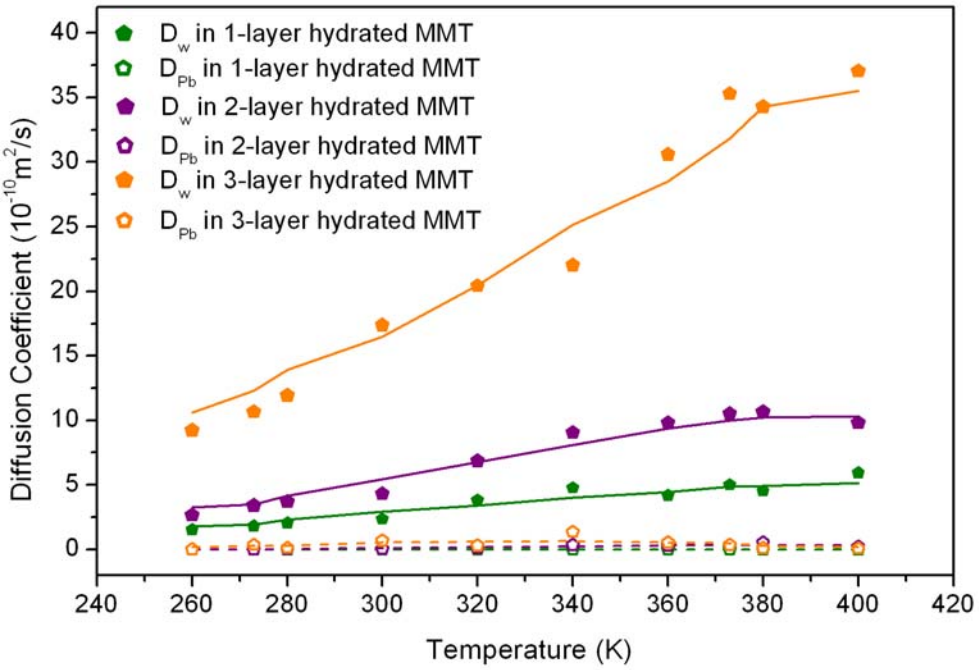


Figure 4-22: Evolution of self-diffusion coefficient of water and $Pb^{2+}$ in 1-, 2- and 3- layer hydrated montmorillonite with the change of temperature.

The curves of cation at 1-layer hydrated montmorillonite are always located at the bottom of the figures which means that the diffusion of cation at low hydrated clay is difficult even if the temperature increases. The diffusion curves of monovalent cations in 2- and 3-layer hydrated clay rise. In contrast, the divalent cations diffuse always not easily even in 2- or 3-layer hydrated clay. Although the raise of hydrated degree gives some increase to the diffusion of divalent cations, these diffusions trend to zero while the weight of cations rises.

### 4.4.4. Radial distribution function (RDF) studies

We have studied the RDF curves of all atom pairs in the systems at 300K and 400K. As prototype example, we show the RDF of $Li^+$-$O_w$, $O_w$-$O_w$ and $O_w$-Hw in three-layer hydrated montmorillonite in Figure 4-23 to Figure 4-25 respectively.

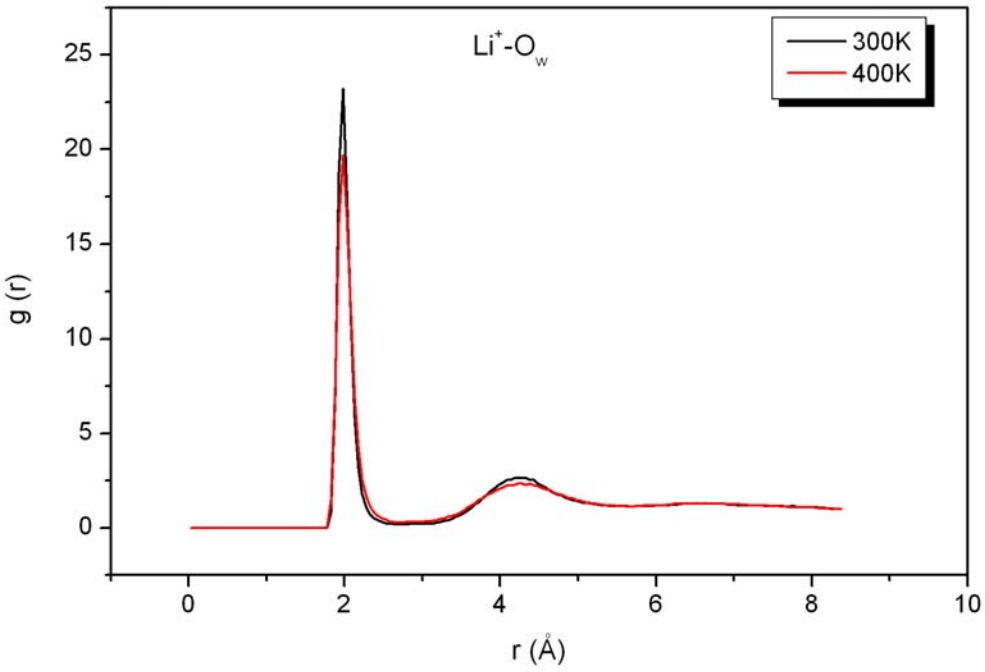


Figure 4-23: RDF of $Li^+$ and O of water in 3-layer hydrated Li-montmorillonite at temperature of 300K and 400K.

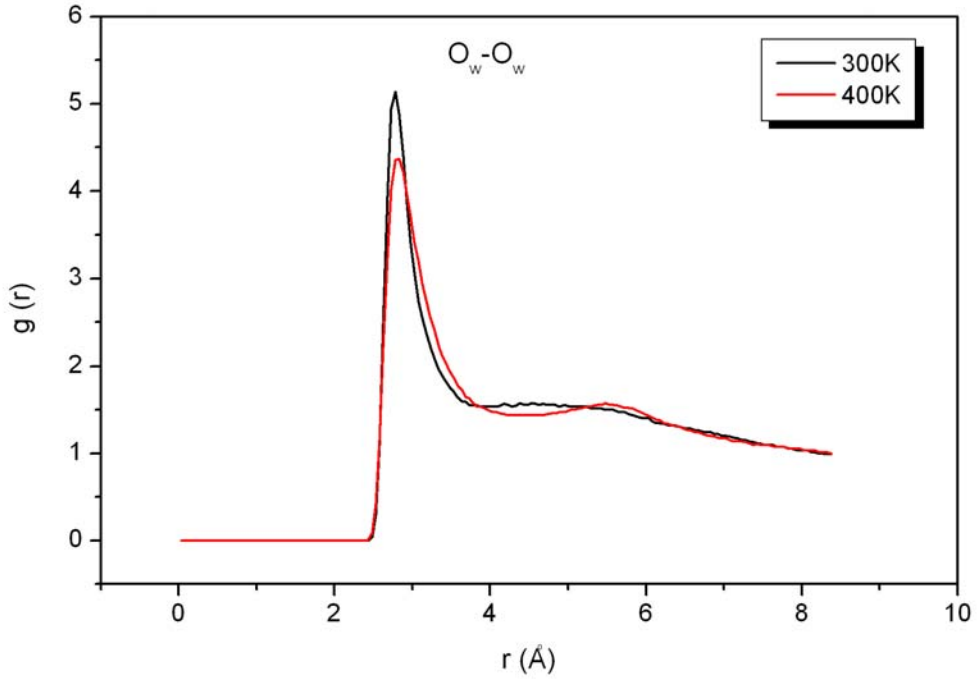


Figure 4-24: RDF of O in water in 3-layer hydrated Li-montmorillonite at temperature of 300K and 400K.

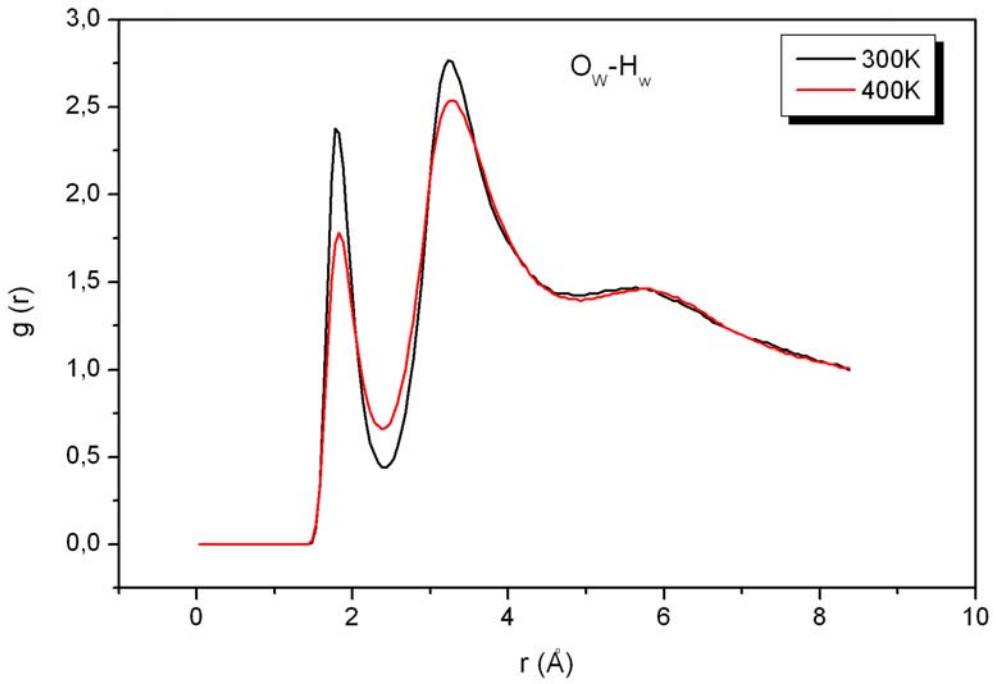


Figure 4-25: RDF of H and O in water in 3-layer hydrated Li-montmorillonite at temperature of 300K and 400K.

**Table 4-5: The coordinates of the first peak in RDF curves of three-layer hydrated Li-montmorillonite**

| Li_mmt r (Å) | 1-layer hydrate | | 2-layer hydrate | | 3-layer hydrate | |
|---|---|---|---|---|---|---|
| | 300K | 400K | 300K | 400K | 300K | 400K |
| $Li^+$-$O_W$ | 1,96 | 1,96 | 1,98 | 1,98 | 1,98 | 1,98 |
| $O_W$-$O_W$ | 2,83 | 2,88 | 2,78 | 2,83 | 2,78 | 2,83 |
| $O_W$-$H_W$ | 1,82 | 1,87 | 1,78 | 1,83 | 1,78 | 1,83 |

We find that the peaks' positions in the curve of 300K and 400K have only a little difference. The detail data were presented in Table 4-5, from which we can clearly see the variation of RDF value in one-, two- and three-layer hydrated Li-montmorillonite. It is evident that the distance between $Li^+$ and oxygen of water doesn't change while the temperature and the hydration degree rise. However, the distance between oxygen-oxygen and oxygen-hydrogen in water has a little increase when temperature rises. We find that these distances at low hydrated clay are a little bigger than that at the higher ones. Generally, RDF study shows no phase transition of hydrated clay at a temperature of 400K.

## 4.5. Conclusion

We have investigated the diffusion of water and the counterions in Li-, Na-, K-, Rb-, Cs-, Ca-, Ni-, Zn- and Pb-montmorillonite at one-, two- and three-hydrated states by means of Molecular Dynamics Simulations. Simulations were performed first at 300K [76]; thereafter extend to a range of 260K to 400K [77].

We have compared our simulation results of Na-montmorillonite with available experimental values together with other simulation results, and find that the SPC/E water model works better than MCY model and the NVE ensemble works better than NVT to simulate the diffusion properties.

According to our simulation results and analysis, we found that the hydrated degree has great influence on the diffusion of both water and counterions in montmorillonite that their diffusion coefficients increase versus the quantity of water content. At low hydrated state, the diffusion of water is weakly affected by the type of counterions presented in the clay, but the monovalent cations diffuse more than the

divalent ones. At high hydrated state, the type of counterions plays an important role in the diffusion of both water molecule and cations themselves. Their size, weight and capacity of attracting water molecule affect water's diffusion behaviour. The presence of heavy metal cations will increase the diffusion of water. So we can conclude that the existence of heavy metal pollutants will dry the clay and it is not easy to eliminate them because of their low activity.

While investigating the influence of temperature on the diffusion behaviour of interlayer particles in the clay, we found that the influence of temperature on the diffusion of water is much important than the one of cations. The diffusion behaviour of interlayer particles becomes generally violent with the increasing of hydration of the clay. At high hydrated state, the diffusion curves of water versus temperature tend to a linear variation below the boiling point and they become no-linear while the temperature increases above the boiling point. The diffusion of monovalent cations is always greater than that of divalent ones. In addition, the effect of temperature is not obvious concerning the diffusion of heavy metal ions, even if the hydrated degree of clay increases. The RDF study shows that the temperature of 400K will not cause a phase transition in the hydrated clay.

# Chapter 5

# The Bulk Modulus and Phase Transition Pressure of Hydrated Montmorillonite

## 5.1. Introduction

As mentioned previously, swelling and hydration of smectite clay minerals impact a wide variety of environmental and engineering processes. The mechanical properties of clay mineral are required to be studied especially for engineering. Many researches have been performed by experiments [78, 79], theoretical approximations [80] and DFT simulations [81-83].

In spite of the numerous papers on clay systems, only few of them were devoted to the montmorillonite including pollutants. Similar remarks can be done for the study of the rigidity of these hydrated clays. To the best to our knowledge, there is no experimental or theoretical study addressing these problems.

It is the purpose of this part of the thesis to give a detailed study on the hydrated montmorillonite including different counterions especially some heavy metal cations, to shed light on the rigidity and the effects of the nature of pollutant on this quantity.

As for the preceding chapter, the counterions including in montmorillonite considered are monovalent cations such as $Li^+$, $Na^+$, $K^+$, $Rb^+$, $Cs^+$, and divalent cations such as $Ca^{2+}$, $Ni^{2+}$, $Zn^{2+}$, $Pb^{2+}$. Simulations have been performed on these montmorillonites at 1-, 2-, 3-layer hydrated and dehydrated states respectively. In these simulations, the pressure of the clay-water system increases from 1 atmosphere pressure to about 20 GPa and the volumes of clay system

corresponding to each pressure have been collected to form a pressure-volume curve.

The bulk modulus of a system at pressure zero can be defined by Murnaghan equation of state, where the pressure P is a function of volume V:

$$P(V) = \frac{B_0}{B'_0}\left(\left(\frac{V_0}{V}\right)^{B'_0} - 1\right) \tag{5.1}$$

Where $B_0$ is the bulk modulus at pressure zero; $V_0$ is the volume of the system at pressure zero; $B'_0$ represents the bulk modulus pressure derivative, $B'_0 = \frac{\partial B}{\partial P}$.

The bulk modulus at different pressure can be formally defined by the equation:

$$B = -V\frac{\partial P}{\partial V} \tag{5.2}$$

Where P is pressure, V is volume, and $\frac{\partial P}{\partial V}$ denotes the partial derivative of pressure with respect to volume.

According to the definition of bulk modulus, we can obtain the evolution curve of the bulk modulus of clay versus pressure. Comparing these curves we can find the effect of hydration on the bulk modulus of clay. Moreover, the influence of existing counterions on this quantity can be achieved. Both the Monte Carlo and Molecular Dynamic methods have been employed to perform the simulations to study the mechanical properties of montmorillonite.

## 5.2. Simulation details

The simulation conditions of Monte Carlo method are the same as those used in Chapter 3. The procedure of each simulation has been described in section 2.4.2.

We use the same simulation conditions presented in Chapter 4 to perform our Molecular Dynamics (MD) simulations. However, in order to well simulate the compressing process of the hydrated clay, the atoms in the clay layers are not frozen that CLAYFF [84] force field is employed to describe the interactions in the clay system. The leapfrog integration algorithm[29] with a time step of 1.0 fs served to integrate the equations of motion. Each system was equilibrated over 40ps. Production runs consisted of a further 40 000 time step (40ps) after equilibration.

Intermediate configurations were saved every 100 steps. The temperature is fixed at 300K.

Our MC and MD simulations were performed in the isothermal-isobaric (NPT) ensemble. The volume of the system is allowed to vary, and the simulation will predict the layer spacing and then the volume. The initial configurations of each montmorillonite at 0-, 1-, 2- and 3-layer hydrate state are taken from our proceeding simulation results presented in Chapter 3 which were performed at $10^5$ Pa. Then the pressure of clay system increases up to maximum 20GPa.

## 5.3. Results and discussions

### 5.3.1. Pressure-volume variation

The pressure-volume curves of dehydrated Li-montmorillonite by means of MC and MD simulation methods are shown in Figure 5-1 (a) and (b) respectively. We can find clearly that the volume of the clay system decreases when the pressure increases. The curve in Figure 5-1 (a) is very smooth which means that with the MC method the evolution of clay's volume under increasing pressure is continuous. In contrast, the curve obtained by MD method presented in Figure 5-1 (b) is not perfectly smooth as the former. Some points of inflexion can be found in the curve.

However, in the pressure-volume curves of hydrated clay, both MC and MD simulations show the inflexion phenomenon. We illustrate the curves of 1-layer hydrated montmorillonite obtained by means of both MC and MD simulations in Figure 5-2 (a) and (b). The variation obtained by MD simulation method is much smoother than the MC one but the inflexion is clear.

### 5.3.2. Bulk modulus at pressure zero

Analyzing the variation of pressure-volume of different hydrated clay, the bulk modulus of the clay at pressure zero can be obtained by using the Murnaghan equation of state. The $B_0$ values of different hydrated montmorillonite including $Li^+$ and $Na^+$ are collected in Table 5-1, where the results of Monte Carlo and Molecular Dynamic simulations are both shown in the table.

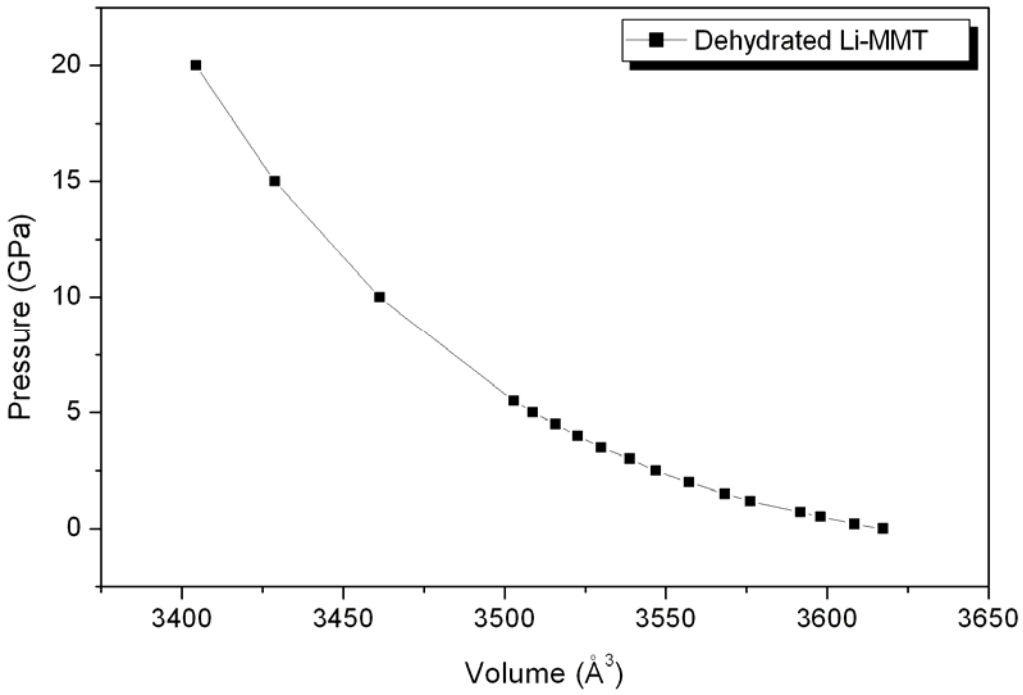


(a) MC simulation

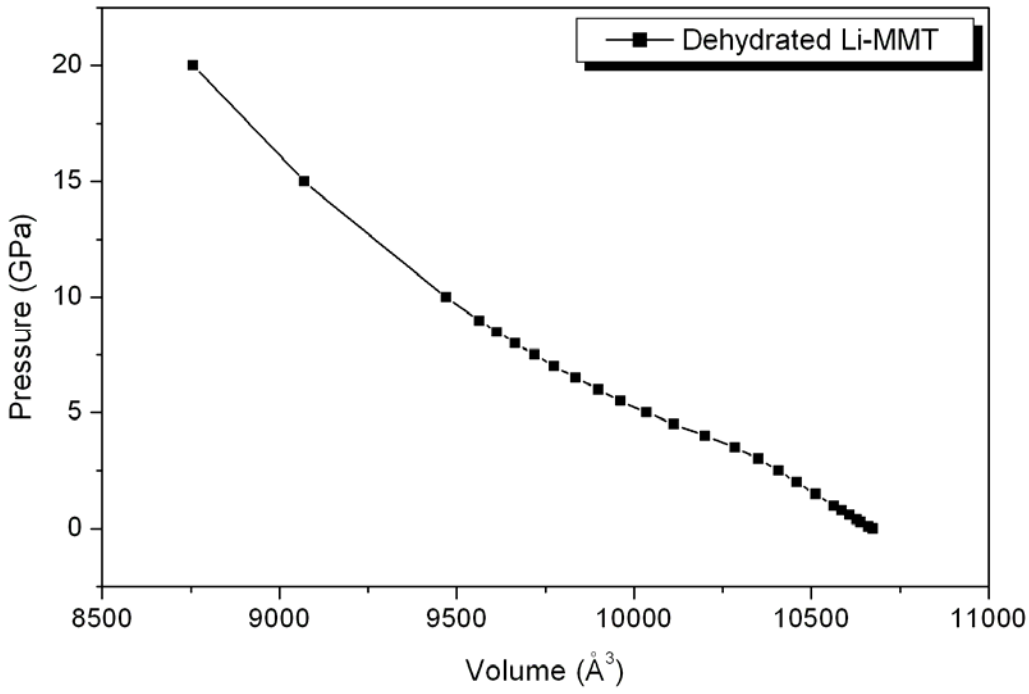


(b) MD simulation

Figure 5-1: Pressure –Volume variation of dehydrated Li-montmorillonite.

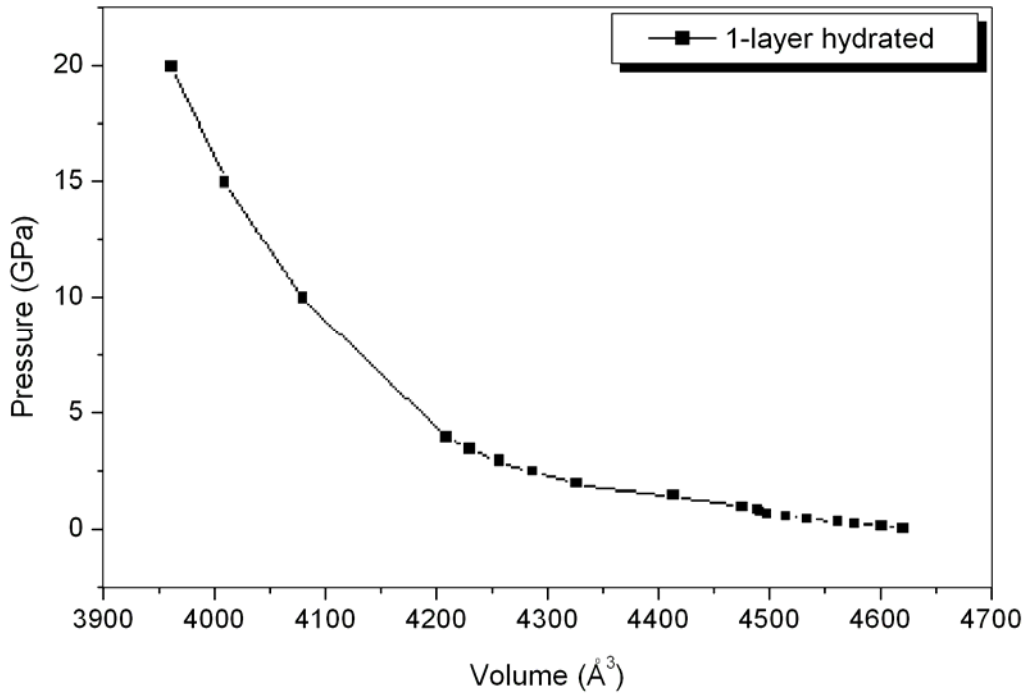


(a) MC simulation

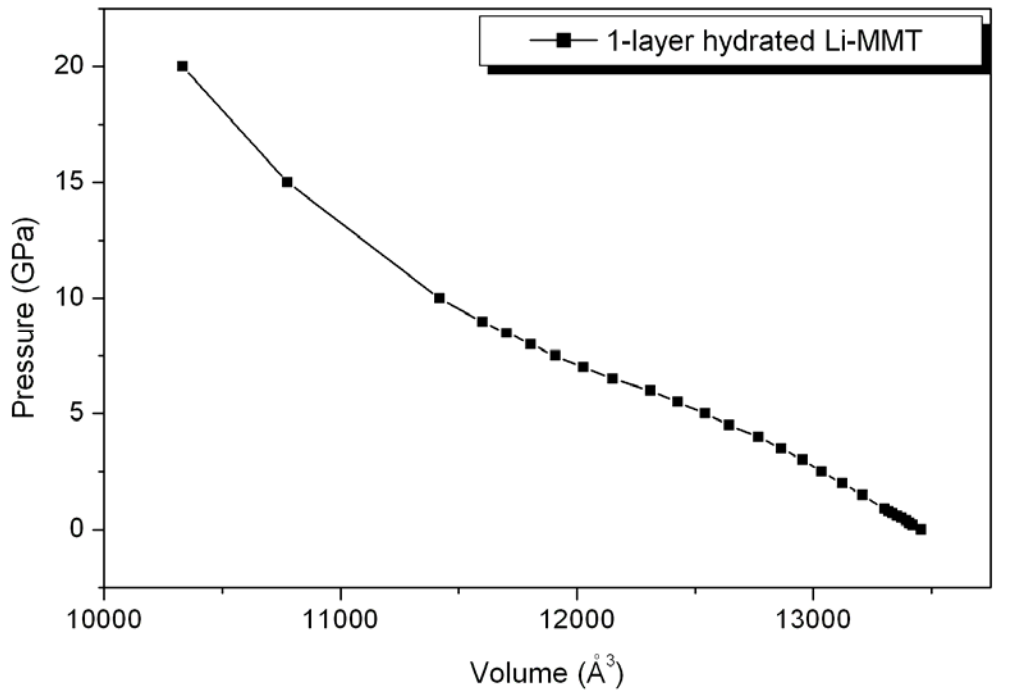


(b) MD simulation

Figure 5-2: Pressure –Volume variation of 1-layer hydrated Li-montmorillonite.

**Table 5-1: Bulk Modulus at pressure zero ($B_0$) of different hydrated Li-, Na-montmorillonite.**

**(GPa)**

| Hydrate | Li-mmt | | Na-mmt | |
|---|---|---|---|---|
| | MC | MD | MC | MD |
| 0-layer | 81.7 | 94.7 | 25.3* | 101.2 |
| 1-layer | 20.6 | 59.6 | 20.2 | 81.6 |
| 2-layer | 8.7 | 55.6 | 4.5 | 62.6 |
| 3-layer | 5.6 | 53.9 | 4.4 | 53.6 |

**13* (DFT simulation result [85])

The values of bulk modulus obtained by Monte Carlo simulations are much less than that of Molecular Dynamic simulations especially in hydrated clay. The bulk modulus of dehydrated Na-montmorillonite with Monte Carlo simulation is comparable with DFT simulation results proposed by Berghout et al. [85]. To the best of our knowledge, the bulk modulus of Monte Carlo simulation results seems more reasonable than that of molecular dynamic simulation results, which means that the frozen in the clay's framework during the simulation seems more representative to study the rigidity of clay.

Table 5-2: **Bulk Modulus at pressure zero ($B_0$) of different hydrated montmorillonite (MC simulation results).**

(GPa)

| hydrate | K-mmt | Rb-mmt | Cs-mmt | Ca-mmt | Ni-mmt | Zn-mmt | Pb-mmt |
|---|---|---|---|---|---|---|---|
| 0-layer | 22 | 29.4 | 21.7 | 21.8** | 89.5 | 55.6 | 21 |
| 1-layer | 18.9 | 16 | 19.4 | 16.8 | 21 | 24.1 | 18.9 |
| 2-layer | 5 | 9.4 | 6.3 | 9.9 | 20 | 13.3 | 10.6 |
| 3-layer | 3.6 | 7 | 4.7 | 5.8 | 3.1 | 4.9 | 3.9 |

**25 (DFT simulation result [85])

Monte Carlo simulation results about the $B_0$ values of different hydrated montmorillonite including other cations are shown in Table 5-2. The value of dehydrated calcium montmorillonite has great agreement with DFT simulation results [85]. From this table we can see clearly that the bulk modulus of clay at pressure zero reduces when the hydrated degree increases.

## 5.3.3. Evolution of bulk modulus with pressure

### 5.3.3.1. MC simulation results

MC simulations have been performed to 0-, 1-, 2- and 3-layer hydrated montmorillonite including monovalent counterions such as $Li^+$, $Na^+$, $K^+$, $Rb^+$, $Cs^+$ and divalent cations such as $Ca^{2+}$, $Ni^{2+}$, $Zn^{2+}$ and $Pb^{2+}$. Based on the pressure-volume variation, the bulk modulus of all these montmorillonites at 0-, 1-, 2- and 3-layer hydrated states can be obtained using equation(5.2). The evolutions of bulk modulus of these montmorillonite at each hydrated state are presented from Figure 5-3 to Figure 5-6.

Comparing these figures we can find that the evolution of bulk modulus versus pressure in dry montmorillonite is quit different with that in hydrated ones. From Figure 5-4 to Figure 5-6, we remark an evolution of the bulk modulus under pressure until a critical value where there is a sudden decrease in the curve. This critical point reflects a maximum of rigidity in the system. Clear peaks exist in all the curves of hydrated clay especially in 1- and 2-layer hydrated ones. These peaks are mostly located in a pressure range between zero and about 1GPa. In 3-layer hydrated montmorillonite, vibrations occur in low pressure and the ‘peak’ of the curves is very weak. However in dry montmorillonite, no obvious peak can be found in the pressure range between zero and 20 GPa.

In contrast to the violent vibrations at low pressure, at the pressure greater than the critical one, the bulk modulus of hydrated clay presents an approximately linear increasing tendency. The decrease following this maximum point could also be an indication of structural phase transition under certain pressure. The pressure corresponding to the peak in the curve can be treated as the transition pressure of the system.

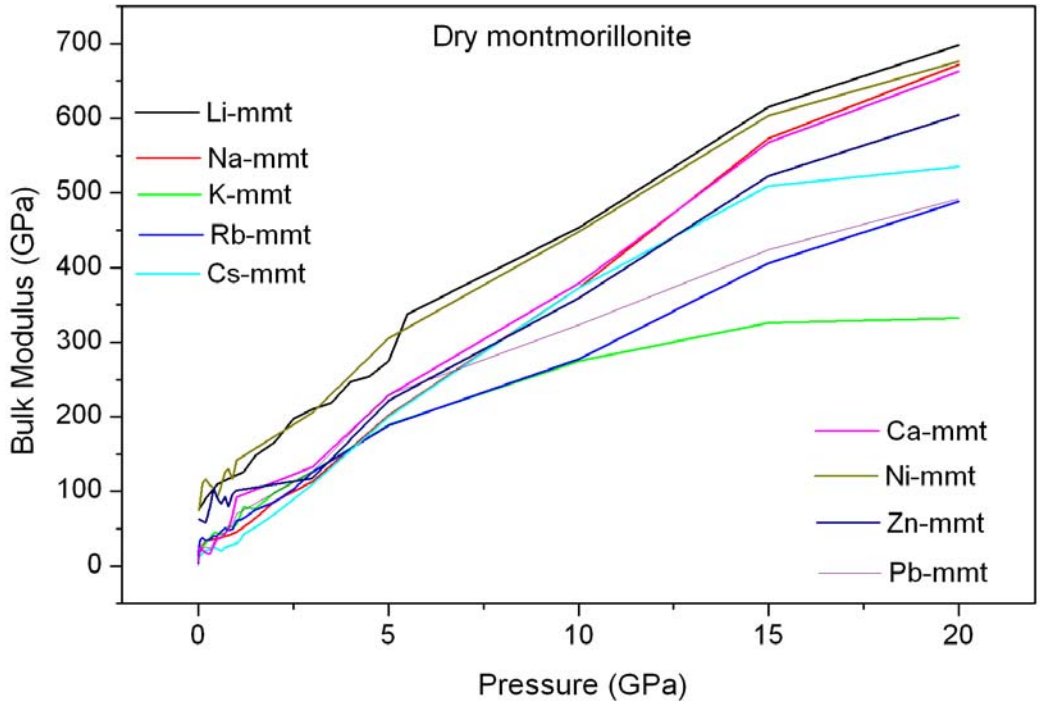


Figure 5-3: Bulk modulus of dry montmorillonite including different counterions.

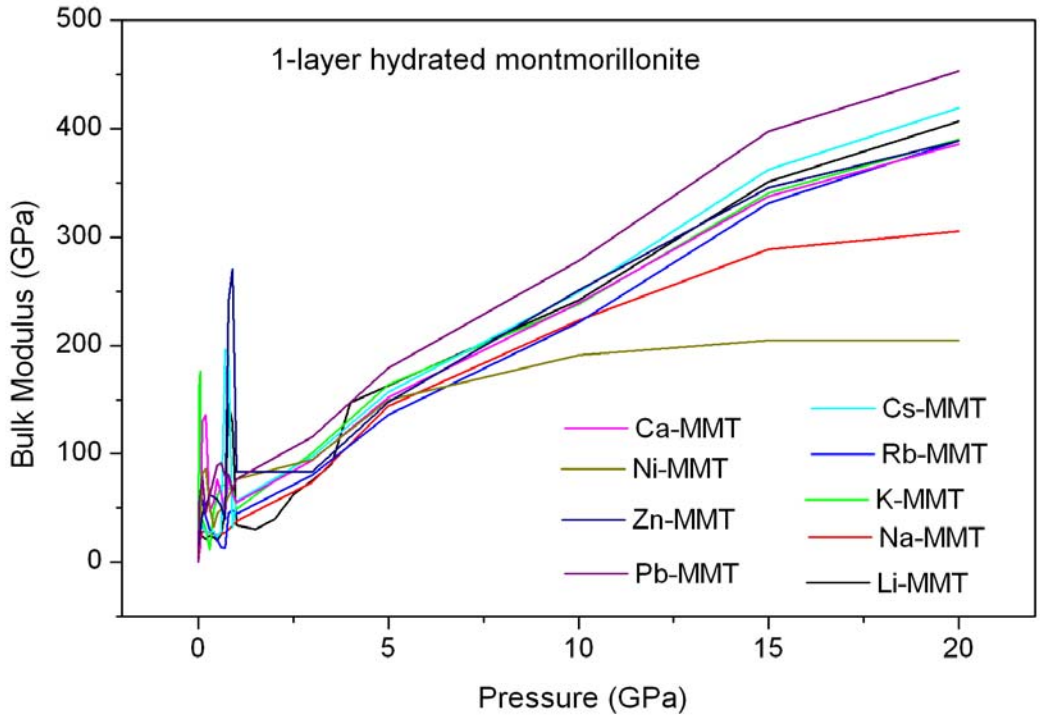


Figure 5-4: Bulk modulus of 1-layer hydrated montmorillonite including different counterions.

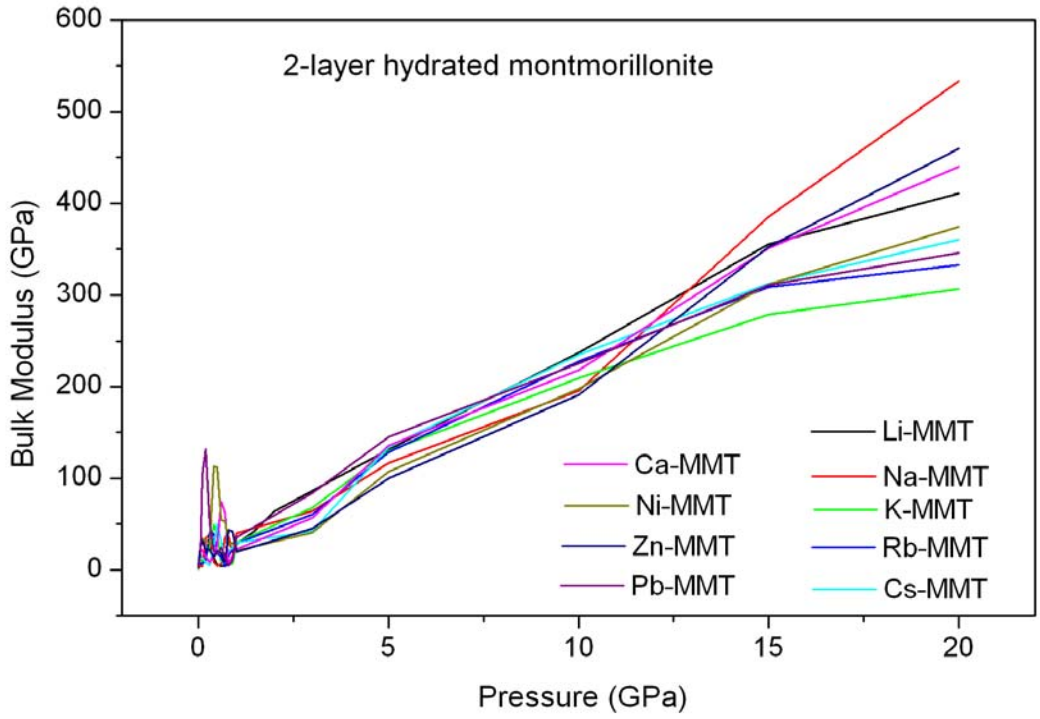


Figure 5-5: Bulk modulus of 2-layer hydrated montmorillonite including different counterions.

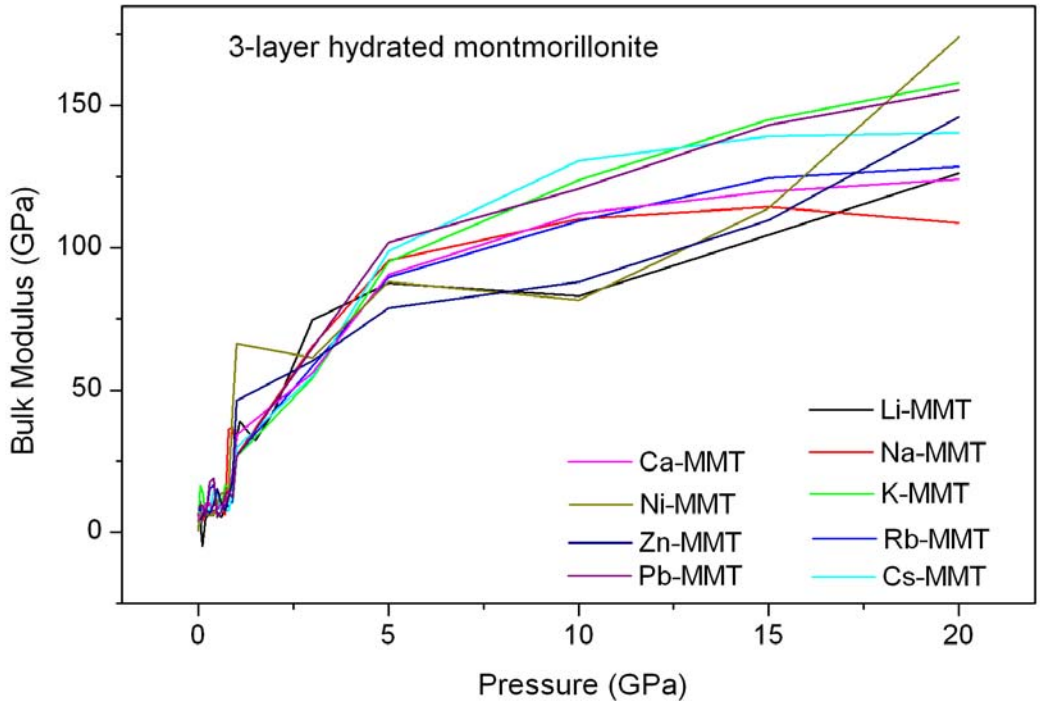


Figure 5-6: Bulk modulus of 3-layer hydrated montmorillonite including different counterions.

**Table 5-3: The Bulk modulus (B) and Transition Pressure ($P_t$) of different hydrated montmorillonite concerning different countions (GPa)**

| MMT | 1-layer hydrate | | 2-layer hydrate | | 3-layer hydrate | |
|---|---|---|---|---|---|---|
| | $P_t$ | B | $P_t$ | B | $P_t$ | B |
| Li-mmt | 0.8 | 146 | 0.3 | 25.6 | 0.08 | 11.3 |
| Na-mmt | 0.3 | 30.3 | 0.3 | 38.8 | 0.4 | 10.7 |
| K-mmt | 0.05 | 176 | 0.05 | 11.9 | 0.05 | 16.3 |
| Rb-mmt | 0.05 | 64.3 | 0.3 | 41.5 | 0.4 | 16.8 |
| Cs-mmt | 0.7 | 196 | 0.05 | 16.8 | 0.4 | 14.9 |
| Ca-mmt | 0.2 | 136 | 0.2 | 15.2 | 0.3 | 10.5 |
| Ni-mmt | 0.2 | 86.9 | 0.4 | 113 | 0.1 | 6.8 |
| Zn-mmt | 0.3 | 61.8 | 0.1 | 32.1 | 0.2 | 7.9 |
| Pb-mmt | 0.1 | 79.6 | 0.2 | 132 | 0.4 | 19.0 |

The values of phase transition pressure and corresponding bulk modulus of different hydrated montmorillonite concerning different counterions are collected in Table 5-3. It is obvious that the phase transition pressures of all these hydrated clay are less than 1GPa. We consider the corresponding value as a definitive bulk modulus for each case. Under pressure the system became denser and consequently more rigid. We consider that the rigidity reflects here a maximum situation of the same system before a transition in which it changes to another one with different properties. It is easily understood that more the clay is compressed more its rigidity would be important. However the real indication of its rigidity is the one where the system reaches its maximum of compressibility in a situation where all its intrinsic properties are saved. Generally, the bulk modulus of the clay system decreases when the hydration of clay increases. We notice an exception for the case of Na-, K-, Ni- and Pb-montmorillonite where the bulk modulus of 2-layer hydrated clay is greater than 1-layer hydrated one.

### 5.3.3.2. MD simulation results

Since the framework of the clay in MC simulations is rigid, only the interlayer space of the clay is compressed. We are curious to find what happen when the

atoms in clay's framework are allowed to move. So the MD simulations are performed with all atoms in the clay's framework flexible. We have simulated the Li-montmorillonite at 0-, 1-, 2- and 3-layer hydrated state respectively.

The evolution of bulk modulus of different hydrated Li-montmorillonite with increasing pressure is shown in Figure 5-7, where (a) presents the MC simulation results and (b) the MD simulation results. The bulk modulus of different hydrated clay rise with pressure and peaking at relatively low pressure. Thereafter the bulk modulus falls to a bottom and then reincreases when pressure continues to rise. This phenomenon may show a possible structural phase transition in the clay.

The most difference between these two figures is that the dry clay presents also a phase transition phenomenon just as hydrated ones by means of MD simulation. Comparing these two figures, we can see that the phase transition phenomenon is more clear with MD simulation than MC one. In Figure 5-7 (b) the 'peak' of the curves locates in the range of pressure not greater than 1GPa for hydrated clay, whereas the 'peak' in dehydrated clay locates a little greater than 1 GPa. The bulk modulus values corresponding to the 'peak' decrease with the hydrated degree.

The crystal structures of 1-layer hydrated Li-montmorillonite are shown in Figure 5-8, where we present the initial structure at 1 bar in (a), the structure of this water-clay system at 'peak point' pressure 0.3 GPa in (b) and at 20GPa in (c), and this structure after relaxing from 20GPa to 1 bar in (d). Comparing (a) and (b), no great difference can be seen between these two configurations. Whereas, from (a) and (c) we can see clearly that both the interlayer space and the framework of the clay are compressed, and the distances between atoms are shortened. The clay structure remains the same but denser. While after relaxation from 20 GPa to atmospheric pressure, the clay system resumes. Both the clay's framework and the interlayer space have relaxed.

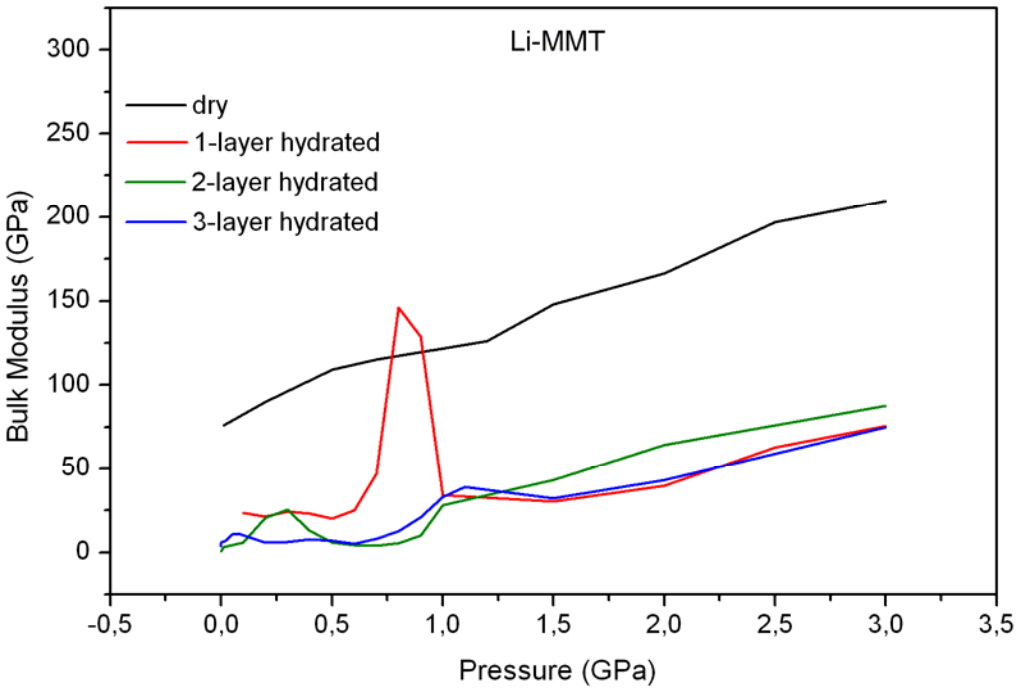


(a) MC simulation

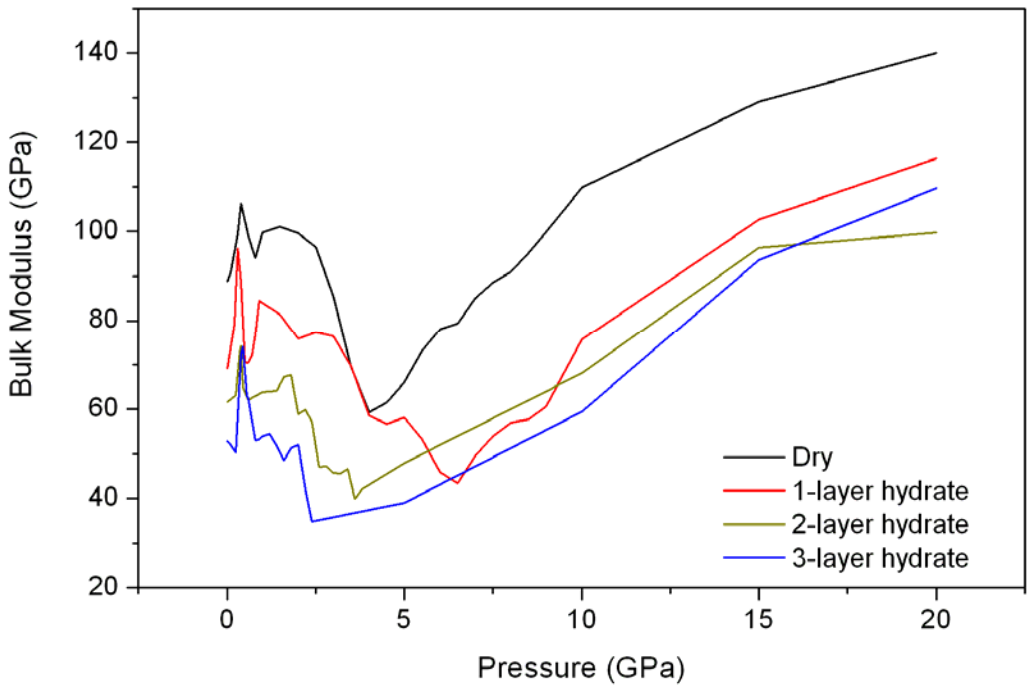


(b) MD simulation

Figure 5-7: Evolution of Bulk Modulus of different hydrated Li-montmorillonite versus pressure.

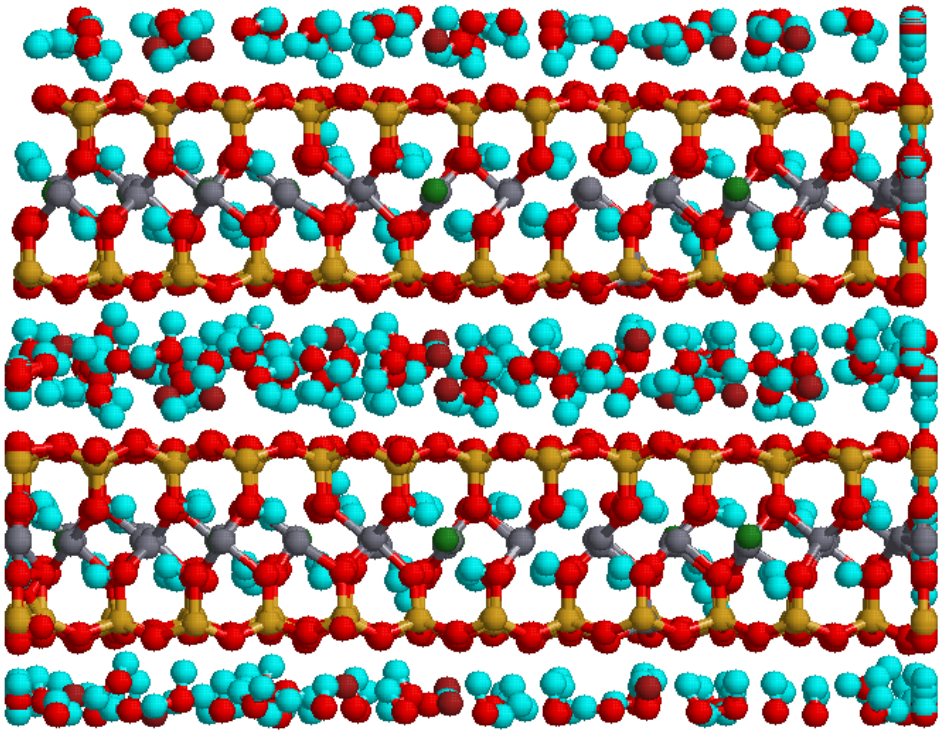

(a) At 1 bar

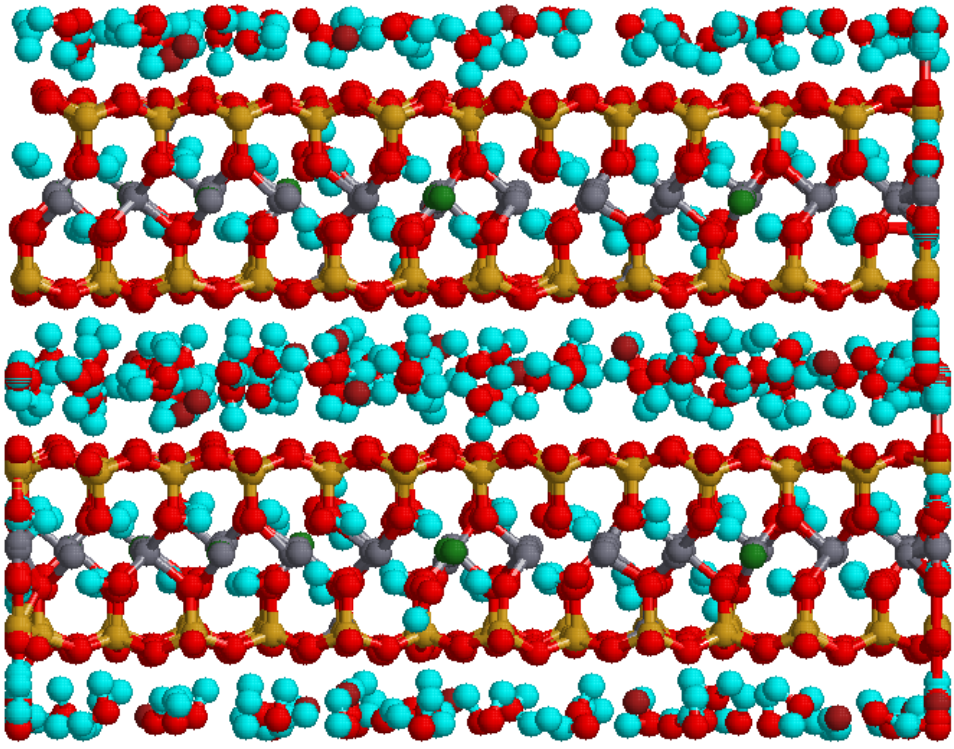

(b) At 0.3 GPa

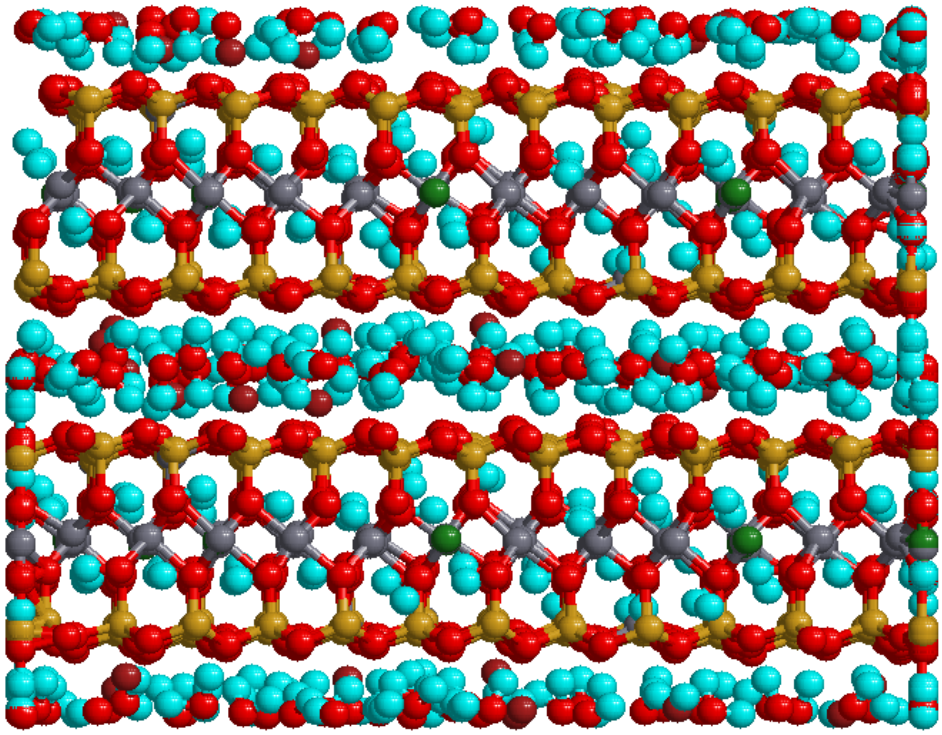

(c) At 20GPa

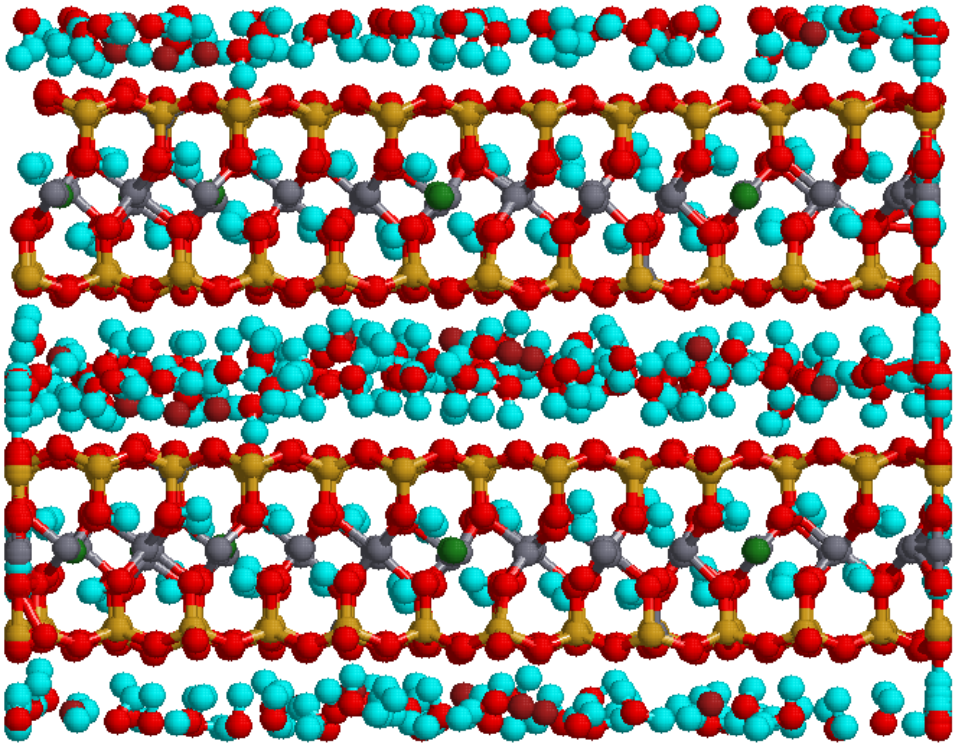

(d) Relax from 20GPa to 1 bar

Figure 5-8: The relaxed structure of monolayer hydrated Li-Wyoming montmorillonite at different pressure. (O-red, H-cyan, Si-golden, Al-grey, Mg-green, Li-brown)

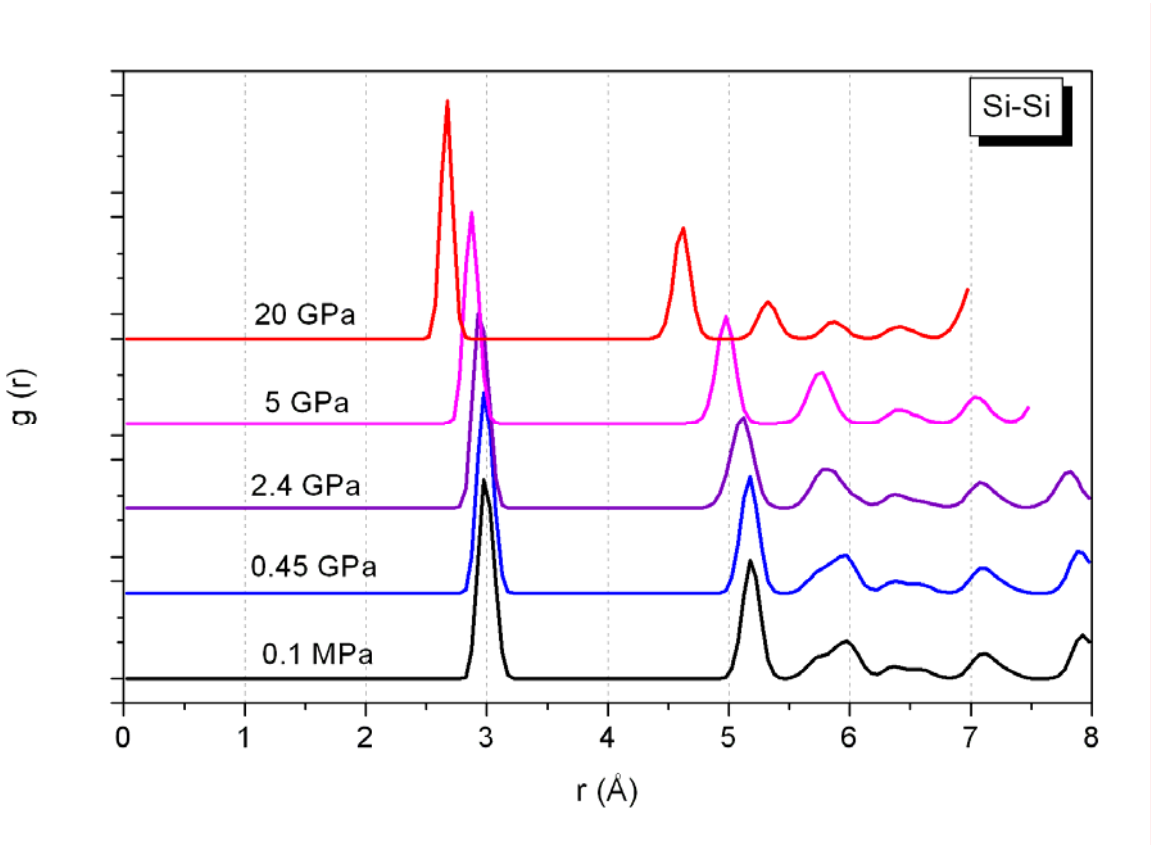


Figure 5-9: RDF of Si - Si pair in 3-layer hydrated Li–montmorillonite.

Detailed RDF study has been performed to all atom pairs in the systems at different hydrated states as well as different pressures. We show the RDF of Si-Si in 3-layer hydrated Li-montmorillonite in Figure 5-9 as the prototype example. According to the blue line in Figure 5-7, the curve of 3-layer hydrated clay, we consider the RDF of Si-Si of the initial state (at 0.1 MPa), the 'peak' point (0.45 GPa), two 'bottom' points (2.4 GPa and 5 GPa), and the point at 20 GPa. From Figure 5-9 we can see clearly that, the positions of the two main peaks in this RDF curve have no difference between the initial state and at the 'peak' pressure. Whereas, when the pressure continues to increase, the clay's structure begins to change that both the first and the second peak change towards the reducing direction. At 20 GPa, the position difference is very clear. When the clay relaxed from 20 GPa to atmospheric pressure, the RDF curve is the same as its initial one. From this RDF study, we can then obtain that the clay structure under pressure will change, but not exactly a phase transition.

### 5.3.3.3. Discussion

The possible phase transition pressure of different hydrated Li-montmorillonite, the pressure about the first peak in the bulk modulus-pressure variation, as well as their corresponding bulk modulus obtained by MC and MD simulations are shown in Table 5-4. Both MC and MD simulations show the same tendency that the bulk modulus of the clay reduces with hydrated degree. Comparing the results of Monte Carlo and Molecular Dynamic simulations, we can see that both of these two simulations can predict the possible phase transition pressures in hydrated clay not greater than 1GPa. Instead of the MC simulation, the MD simulation predicts the phase transition of dry clay at relative low pressure. And the phase transition pressures of different hydrated clay are not great difference which is different to MC results.

**Table 5-4: The possible phase Transition Pressure ($P_t$) and corresponding Bulk modulus (B) of different hydrated Li-montmorillonite by means of MC and MD simulation methods.**

| GPa | Dry | | 1-layer hydrate | | 2-layer hydrate | | 3-layer hydrate | |
|---|---|---|---|---|---|---|---|---|
| | $P_t$ | B | $P_t$ | B | $P_t$ | B | $P_t$ | B |
| MC | - | - | 0.8 | 146 | 0.3 | 25.6 | 0.08 | 11.3 |
| MD | 1.5 | 101 | 0.3 | 96 | 0.4 | 74 | 0.45 | 74 |

As we have found in section 5.3.2, Monte Carlo simulation results about the bulk modulus of different hydrated clay corresponding to possible phase transition pressure seems more reasonable than that of molecular dynamic simulation results. This tells us again that the frozen in the clay's framework during the simulation seems more representative to study the rigidity of clay.

It is clearly that the rigidity of clay increases under pressure. The compression process can be divided into two stages.

In the first stage, the clay is compressed under a certain range of low pressure. The interlayer space of the clay reduces with pressure and then the particles located in this space, such as water molecules and cations, will move to fill void in the interlayer space and rearrange themselves to find a more stable position. When the

pressure continues to increase, the interlayer space will be reduced till all void in this space filled by interlayer particles. During this process, the evolution of system's volume with pressure varies not monotonically that the bulk modulus, the derivation of pressure/volume according to equation(5.2), presents a fluctuation phenomenon.

Thereafter, with all void in the interlayer space filled by water and cations, the compression on the clay system begins the second stage, where the variation of clay's volume reduces monotonically with pressure. In this stage, both the interlayer particle and the clay's framework are compressed and the clay becomes denser and consequently more rigid. Then the bulk modulus of the clay system increases monotonically with pressure.

Under hydrostatic pressure, the isotropic decrease of the clay will induce a compacted structure and will decrease more and more the openness of the system. The atoms will closer until a critical situation where the first atomic positions are not appropriate. The atoms will rearrange themselves automatically looking for another situation, which should be more stable energetically. In fact the system obeys to a natural energetic equilibrium, since the initial energetic stability became high and the system will be instable. Then, the atoms will evolve to another situation, energetically more comfortable and more stable.

## 5.4. Conclusion

Monte Carlo and Molecular Dynamic simulations have been performed on compressing montmorillonite at 0-, 1-, 2- and 3-layer hydrated states to study the rigidity of this clay. Monovalent counterions such as $Li^+$, $Na^+$, $K^+$, $Rb^+$, $Cs^+$ and divalent cations such as $Ca^{2+}$, $Ni^{2+}$, $Zn^{2+}$ and $Pb^{2+}$ are considered including in montmorillonite to find the influence of cations especially some heavy metal cations on the bulk modulus of the clay. Based on the pressure-volume curves obtained from our simulation results, the evolution of bulk modulus of the clay system versus pressure can be then analysing.

Both Monte Carlo and Molecular Dynamic simulations show that the rigidity of clay increases under pressure.

The existence of water in the interlayer of montmorillonite has greatly effect the bulk modulus of clay that the bulk modulus decreases with rising hydrated degree. The cations including in the clay affect the bulk modulus of the clay.

The evolution of bulk modulus with pressure at low pressure shows a possible structural phase transition phenomenon. According to our analyse results, the possible phase transition pressure of hydrated montmorillonite is less than 1GPa in both MC and MD simulations. This quantity of dehydrated clay is predicted a little greater than 1GPa by MD simulation. However, the crystal and RDF study show change in the clay system, but not completely change of structure of clay.

To the best of our knowledge, simulation results of Monte Carlo method seem better than that of Molecular Dynamic method. This tells us that the fixed atoms in clay's framework may be more representative for studying clay's rigidity.

# *General Conclusion*

In this thesis, we have investigated the Wyoming-type montmorillonite containing different monovalent or divalent counterions by means of Monte Carlo and Molecular Dynamic simulation methods. Simulations have been performed to study: 1) the swelling and shrinking process of montmorillonite; 2) the diffusion coefficient of water molecules and counterions in the interlayer space of the clay; 3) the bulk modulus and phase transition pressure of different hydrated montmorillonite.

To be better search of the influence of counterions on the structural, dynamical and mechanical properties of montmorillonite, monovalent cations such as $Li^+$, $Na^+$, $K^+$, $Rb^+$, $Cs^+$, and divalent cations such as $Ca^{2+}$, $Ni^{2+}$, $Zn^{2+}$, $Pb^{2+}$ have been considered respectively. The favourable agreement between our simulation results with available experiment and/or preceding theoretical works on the common clay such as Li-, Na-, Ca-montmorillonite, have allowed us to predict the properties of the clay, especially, including heavy metal cations.

We have tested first the water model and potential model, and find that the SPC/E model works better in this study. So this model is employed to our remaining simulations.

In the study of swelling and shrinking behaviour of montmorillonite, we have found a general phenomenon of hysteresis in the hydrate/dehydrate process, which is more important in clay including divalent cations than monovalent ones and in clay including small cations than big ones. The quantities of counterions together with their solvation characteristics and their attraction capacities have an important influence on the swelling and shrinking behaviours of this clay.

Studies about the effect of temperature on this swelling and shrinking of clay show that a general hysteresis phenomenon can be found also in the warming/cooling process in different hydrated clay and with different cations. The effect of temperature is important in high hydrated clay and negligible in low hydrated ones. Moreover, the temperature effect is important in clay including monovalent cations.

In the study on the diffusion behaviour of water and cations, we have tested first the ensembles and find that the NVE ensemble works better in this study. This ensemble is then chosen to perform other simulations in our study.

We have found that at the same hydrated degree, water diffuses much faster than cations. Monovalent cations diffuse more quickly than divalent ones. Both water and cations' diffusion is speeded up by increasing hydrated degree. That means the increasing water content will release cations. However, heavy metal cations are always difficult to release. On the other hand, cations' size, weight and capacity of attracting water molecule affect the diffusion behaviour of water. The existence of heavy metal cations causes high diffusion of water in high hydrated clay.

The effect of temperature on the diffusion behaviour has been also studied. We have found that the diffusion behaviour of interlayer particles becomes important with the increasing of temperature. The temperature's effect is more important on diffusion of water than cations. This effect is significant in high hydrated clay than low hydrated ones. The influence of temperature is important on diffusion of monovalent cations and negligible for divalent ones. Pollutants, the heavy metal cations are always hard to release even at high temperature and high hydrated degree.

The investigation in the shrinking behaviour of different hydrated montmorillonite in the compressing process shows us the evolution of bulk modulus of the clay versus the pressure. This study allows us to shed light on the rigidity of this clay affected by the hydrated degree.

Both Monte Carlo and Molecular Dynamic simulations show that the rigidity of clay increases under pressure. The bulk modulus of clay decreases with hydrated degree. The evolution of bulk modulus with pressure shows a possible structural phase transition phenomenon occurred in hydrated clay with a phase transition pressure less than 1 GPa, whereas this value is a little greater than 1 GPa in dehydrated clay. However, the crystal and RDF studies show change in clay, but not completely change of clay's structure.

Monte Carlo simulations results seem better than Molecular Dynamic results, which tell us that the fixed atoms in clay's framework may be more representative for studying clay's rigidity.

Anyway, both hydrated and dehydrated clay becomes more rigid under pressure. According to our calculations the bulk modulus reaches extremely high values at modest pressures of ~20 GPa. This is likely to happen in a very different, and possibly quenchable to 1 atm, type of phases – such a possibility definitely needs to be explored in future work. It would open a route to a new family of ultra-

incompressible (and possibly ultra-hard) materials of clay composition. Such materials, and their superior mechanical properties and possibly low cost, could be practically attractive for a number of uses.

# Reference


1. Grim, R.E., *Clay Mineralogy*. 1968, New York: McGraw-Hill, Inc.
2. Martin, R.T., et al., *Report of the Clay Minerals Society Nomenclature Committee; Revised classification of clay materials.* Clays and Clay Minerals, 1991. **39**(3): p. 333-335.
3. C. Edmund Marshall, *The Physical Chemistry and Mineralogy of Soils. Volume 1: Soil Materials*. Soil Science. 1964.
4. Vincent, M., *Retrait-gonflement des sols argileux: un aléa géologique lié aux conditions climatiques*, in *Géosciences*. 2006. p. 50-55.
5. Newman, A.C.D. and G. Brown, *Chemistry of Clays and Clay Minerals*. Monograph (Mineralogical Society (Great Britain)); no. 6. 1987: Wiley.
6. Tsipursky, S.I. and V.A. Drits, *The distribution of octahedral cations in the 2: 1 layers of dioctahedral smectites studied by oblique-texture electron diffraction.* Clay Minerals, 1984. **19**(2): p. 177-193.
7. Delville, A., *Modeling the clay-water interface.* Langmuir, 1991. **7**(3): p. 547-555.
8. Delville, A., *Structure of liquids at a solid interface: an application to the swelling of clay by water.* Langmuir, 1992. **8**(7): p. 1796-1805.
9. Delville, A., *Monte Carlo Simulations of Surface Hydration: An Application to Clay Wetting.* The Journal of Physical Chemistry, 1995. **99**(7): p. 2033-2037.
10. Skipper, N.T., F.-R.C. Chang, and G. Sposito, *Monte Carlo simulation of interlayer molecular structure in swelling clay minerals; 1, Methodology.* Clays and Clay Minerals, 1995. **43**(3): p. 285-293.
11. Skipper, N.T., K. Refson, and J.D.C. McConnell, *Computer calculation of water-clay interactions using atomic pair potentials.* Clay Minerals, 1989. **24**(2): p. 411-425.
12. Skipper, N.T., G. Sposito, and F.-R.C. Chang, *Monte Carlo simulation of interlayer molecular structure in swelling clay minerals; 2, Monolayer hydrates.* Clays and Clay Minerals, 1995. **43**(3): p. 294-303.
13. Skipper, N.T., K. Refson, and J.D.C. McConnell, *Computer simulation of interlayer water in 2:1 clays.* The Journal of Chemical Physics, 1991. **94**(11): p. 7434-7445.
14. Sposito, G., S.H. Park, and R. Sutton, *Monte Carlo simulation of the total radial distribution function for interlayer water in sodium and potassium montmorillonites.* Clays and Clay Minerals, 1999. **47**(2): p. 192-200.
15. Chang, F.-R.C., N.T. Skipper, and G. Sposito, *Computer Simulation of Interlayer Molecular Structure in Sodium Montmorillonite Hydrates.* Langmuir, 1995. **11**(7): p. 2734-2741.
16. Chang, F.-R.C., N.T. Skipper, and G. Sposito, *Monte Carlo and Molecular Dynamics Simulations of Interfacial Structure in Lithium-Montmorillonite Hydrates.* Langmuir, 1997. **13**(7): p. 2074-2082.
17. Greathouse, J.A., K. Refson, and G. Sposito, *Molecular Dynamics Simulation of Water Mobility in Magnesium-Smectite Hydrates.* J. Am. Chem. Soc., 2000. **122**(46): p. 11459-11464.

18. Greathouse, J. and G. Sposito, *Monte Carlo and Molecular Dynamics Studies of Interlayer Structure in Li($H_2O$)$_3$-Smectites.* The Journal of Physical Chemistry B, 1998. **102**(13): p. 2406-2414.
19. Smith, D.E., *Molecular Computer Simulations of the Swelling Properties and Interlayer Structure of Cesium Montmorillonite.* Langmuir, 1998. **14**(20): p. 5959-5967.
20. Hartzell, C.J., R.T. Cygan, and K.L. Nagy, *Molecular Modeling of the Tributyl Phosphate Complex of Europium Nitrate in the Clay Hectorite.* The Journal of Physical Chemistry A, 1998. **102**(34): p. 6722-6729.
21. Cygan, R.T. and J.D. Kubicki, *Molecular modeling theory: applications in the geosciences*. 2001, Washington, DC: Mineralogical Society of America.
22. Sainz-Diaz, C.I., et al., *Quantum mechanical calculations of dioctahedral 2:1 phyllosilicates: Effect of octahedral cation distributions in pyrophyllite, illite, and smectite.* American Mineralogist, 2002. **87**(7): p. 958-965.
23. Cuadros, J., et al., *Analysis of Fe segregation in the octahedral sheet of bentonitic illite-smectite by means of FTIR, 27 Al MAS NMR and reverse Monte Carlo simulations.* American Journal of Science, 1999. **299**(4): p. 289-308.
24. Sainz-Díaz, C.I., J. Cuadros, and A. Hernández-Laguna, *Analysis of cation distribution in the octahedral sheet of dioctahedral 2:1 phyllosilicates by using inverse Monte Carlo methods.* Physics and Chemistry of Minerals, 2001. **28**(7): p. 445-454.
25. Matsuoka, O., E. Clementi, and M. Yoshimine, *CI study of the water dimer potential surface.* The Journal of Chemical Physics, 1976. **64**(4): p. 1351-1361.
26. Jorgensen, W.L., et al., *Comparison of simple potential functions for simulating liquid water.* The Journal of Chemical Physics, 1983. **79**(2): p. 926-935.
27. Berendsen, H.J.C., J.R. Grigera, and T.P. Straatsma, *The missing term in effective pair potentials.* The Journal of Physical Chemistry, 1987. **91**(24): p. 6269-6271.
28. Teleman, O., B. Jösson, and S. Engstrom, *A molecular dynamics simulation of a water model with intramolecular degrees of freedom.* Molecular Physics, 1987. **60**(1): p. 193-203.
29. Allen, M.P. and D.J. Tildesley, *Computer Simulation of Liquids, Clarendon*. 1987, Oxford.
30. Park, S.-H. and G. Sposito, *Monte Carlo Simulation of Total Radial Distribution Functions for Interlayer Water in Li-, Na-, and K-Montmorillonite Hydrates.* J. Phys. Chem. B, 2000. **104**(19): p. 4642-4648.
31. Boek, E.S., P.V. Coveney, and N.T. Skipper, *Monte Carlo Molecular Modeling Studies of Hydrated Li-, Na-, and K-Smectites: Understanding the Role of Potassium as a Clay Swelling Inhibitor.* J. Am. Chem. Soc., 1995. **117**(50): p. 12608-12617.
32. Dang, L.X. and D.E. Smith, *Comment on ``Mean force potential for the calcium--chloride ion pair in water'' [J. Chem. Phys. 99, 4229 (1993)].* The Journal of Chemical Physics, 1995. **102**(8): p. 3483-3484.
33. Whitley, H.D. and D.E. Smith, *Free energy, energy, and entropy of swelling in Cs-, Na-, and Sr-montmorillonite clays.* The Journal of Chemical Physics, 2004. **120**(11): p. 5387-5395.
34. Koneshan, S., et al., *Solvent Structure, Dynamics, and Ion Mobility in Aqueous Solutions at 25 C.* J. Phys. Chem. B, 1998. **102**(21): p. 4193-4204.

35. Rappe, A.K., et al., *UFF, a full periodic table force field for molecular mechanics and molecular dynamics simulations.* J. Am. Chem. Soc., 1992. **114**(25): p. 10024-10035.
36. Dang, L.X., Private communication.
37. Born, M. and T. von Karman, *Uber Schwingungen in Raumgittern.* Physik. Z, 1912. **13**: p. 297-309.
38. Metropolis, N., et al., *Equation of State Calculations by Fast Computing Machines.* The Journal of Chemical Physics, 1953. **21**(6): p. 1087-1092.
39. Gear, C.W., *The numerical integration of ordinary differential equations of various orders*. 1966: ANL-7126, Argonne National Lab., Ill.
40. Gear, C.W., *Numerical initial value problems in ordinary differential equations*. 1971: Prentice Hall PTR Upper Saddle River, NJ, USA.
41. Verlet, L., *Computer experiments on classical fluids. I. Thermodynamical properties of Lennard-Jones molecules.* Phys. Rev, 1967. **159**(1): p. 98-103.
42. Hockney, R.W., *The potential calculation and some applications.* Methods in Computational Physics, 1970. **9**(136-211).
43. Potter, D., *Computational physics*. 1973: Wiley New York.
44. Berend, I., *Les mécanismes d'hydratation de montmorillonites homoioniques pour des pressions relatives inférieures à 0. 95*, in *Institut national polytechnique de Lorraine, FRANCE (Université de soutenance)* 1991: Vandoeuvre-lès-Nancy.
45. Fu, M.H., Z.Z. Zhang, and P.F. Low, *CHANGES IN THE PROPERTIES OF A MONTMORILLONITE-WATER SYSTEM DURING THE ADSORPTION AND DESORPTION OF WATER: HYSTERESIS.* Clays and Clay Minerals, 1990. **38**(5): p. 485-492.
46. Calvet, R., *Hydration de la montmorillonite et diffusion des cations compensateurs. I. Saturation par des cations monovalents.* Annales Agronomiques, 1973. **24**: p. 77-133.
47. Zhang, Z.Z. and P.F. Low, *Relation between the heat of immersion and the initial water content of Li-, Na-, and K-montmorillonite.* Journal of colloid and interface science, 1989. **133**(2): p. 461-472.
48. Mooney, R.W., A.G. Keenan, and L.A. Wood, *Adsorption of Water Vapor by Montmorillonite. I. Heat of Desorption and Application of BET Theory.* J. Am. Chem. Soc., 1952. **74**(6): p. 1367-1371.
49. Mooney, R.W., A.G. Keenan, and L.A. Wood, *Adsorption of Water Vapor by Montmorillonite. II. Effect of Exchangeable Ions and Lattice Swelling as Measured by X-ray Diffraction.* Journal of the American Chemical Society, 1952. **74**(6): p. 1371-1374.
50. Boek, E.S., P.V. Coveney, and N.T. Skipper, *Molecular Modeling of Clay Hydration: A Study of Hysteresis Loops in the Swelling Curves of Sodium Montmorillonites.* Langmuir, 1995. **11**(12): p. 4629-4631.
51. Meleshyn, A. and C. Bunnenberg, *The gap between crystalline and osmotic swelling of Na-montmorillonite: A Monte Carlo study.* The Journal of Chemical Physics, 2005. **122**(3): p. 034705.
52. Meleshyn, A. and C. Bunnenberg, *Swelling of Na/Mg-montmorillonites and hydration of interlayer cations: A Monte Carlo study.* The Journal of Chemical Physics, 2005. **123**(7): p. 074706.
53. Smith, D.E., Y. Wang, and H.D. Whitley, *Molecular simulations of hydration and swelling in clay minerals.* Fluid Phase Equilibria, 2004. **222-223**: p. 189-194.

54. Chavez-Paez, M., et al., *Monte Carlo simulations of Wyoming sodium montmorillonite hydrates.* The Journal of Chemical Physics, 2001. **114**(3): p. 1405-1413.
55. Brindley, G.W. and G. Brown, *Crystal Structures of Clay Minerals and Their X-ray Identification*, ed. M. Society. Vol. Chapter 3. 1980: Mineralogical Society New York.
56. Suquet, H., C.d.l. Calle, and H. Pezerat, *Swelling and structural organization of saponite.* Clays and Clay Minerals, 1975. **23**(1): p. 1-9.
57. Cases, J.M., et al., *Mechanism of adsorption and desorption of water vapor by homoionic montmorillonite. 1. The sodium-exchanged form.* Langmuir, 1992. **8**(11): p. 2730-2739.
58. Keren, R. and I. Shainberg, *Water vapor isotherms and heat of immersion of Na/Ca-montmorillonite systems: I, Homoionic clay.* Clays and Clay Minerals, 1975. **23**(3): p. 193-200.
59. Skipper, N.T., *MONTE User's Manual.* Department of Physics and Astronomy, University College London, UK, 1996.
60. ZHENG, Y., A. ZAOUI, and I. SHAHROUR, *Swelling and Shrinking of Hydrated and Polluted Wyoming Montmorillonite Clay.* To be published.
61. ZHENG, Y., A. ZAOUI, and I. SHAHROUR, *Evolution of the Interlayer Space of Hydrated Montmorillonite under the Influence of Temperature.* To be published.
62. Hall, P.L., et al. *Dynamics of interlamellar water in divalent cation exchanged expanding lattice clays*. 1977.
63. Nye, P.H., *Diffusion of ions and uncharged solutes in soils and soil clays Adv.* Agron, 1979. **31**: p. 225-272.
64. Cebula, D.J., R.K. Thomas, and J.W. White, *Diffusion of water in Li-montmorillonite studied by quasielastic neutron scattering.* Clays and Clay Minerals, 1981. **29**(6): p. 241-248.
65. Sposito, G., *Single-particle motions in liquid water. II. The hydrodynamic model.* The Journal of Chemical Physics, 1981. **74**(12): p. 6943-6949.
66. Tuck, J.J., et al., *Quasi-elastic neutron-scattering studies of the dynamics of intercalated molecules in charge-deficient layers silicates. I: Temperature dependence of the scattering from water in Ca2+ -exchanged montmorillonite.* Journal of the Chemical Society. Faraday Transactions I, 1984. **80**(2): p. 309-324.
67. Poinsignon, C., et al., in *Proceedings of the International Clay Conference*, L.G. Schultz, H.v. Olphen, and F.A. Mumpton, Editors. 1985, The Clay Minerals Society: Denver. p. 284.
68. Chang, F.-R.C., N.T. Skipper, and G. Sposito, *Monte Carlo and Molecular Dynamics Simulations of Electrical Double-Layer Structure in Potassium-Montmorillonite Hydrates.* Langmuir, 1998. **14**(5): p. 1201-1207.
69. Spoel, D.v.d., P.J.v. Maaren, and H.J.C. Berendsen, *A systematic study of water models for molecular simulation: Derivation of water models optimized for use with a reaction field.* The Journal of Chemical Physics, 1998. **108**(24): p. 10220-10230.
70. Sutton, R. and G. Sposito, *Molecular Simulation of Interlayer Structure and Dynamics in 12.4 ?Cs-Smectite Hydrates.* Journal of colloid and interface science, 2001. **237**(2): p. 174-184.
71. Marry, V., et al., *Microscopic simulation of structure and dynamics of water and counterions in a monohydrated montmorillonite.* The Journal of Chemical Physics, 2002. **117**(7): p. 3454-3463.

72. Smith, W. and T.R. Forester, *DL_POLY_2.0: A general-purpose parallel molecular dynamics simulation package.* Journal of Molecular Graphics, 1996. **14**(3): p. 136-141.
73. Smith, W., C.W. Yong, and P.M. Rodger, *DL_POLY: application to molecular simulation.* Molecular Simulation, 2002. **28**(5): p. 385 - 471.
74. Smith, W., et al., *The DL POLY 2 User Manual*, in *CCLRC, Daresbury Laboratory, Daresbury, Warrington WA4 4AD, England*. 2006: Cheshire, U. K.
75. Nye, P.H., *Diffusion of ions and uncharged solutes in soils and soil clays Adv.* Agron, 1979. **31**: p. 225.
76. ZHENG, Y., A. ZAOUI, and I. SHAHROUR, *Molecular Dynamics Simulation Study on the Diffusions of Water and Different Counterions in Hydrated Montmorillonite.* To be published.
77. ZHENG, Y., A. ZAOUI, and I. SHAHROUR, *Molecular Dynamics Simulation Study on the Influence of Temperature on the Diffusions of Water and Some Counterions in Hydrated Montmorillonite.* To be published.
78. Vanorio, T., M. Prasad, and A. Nur, *Elastic properties of dry clay mineral aggregates, suspensions and sandstones.* Geophysical Journal International, 2003. **155**(1): p. 319-326.
79. Wang, Z.Z., H. Wang, and M.E. Cates, *Effective elastic properties of solid clays.* Geophysics, 2001. **66**(2): p. 428-440.
80. Hornby, B.E., L.M. Schwartz, and J.A. Hudson, *Anisotropic effective-medium modeling of the elastic properties of shales.* Geophysics, 1994. **59**(10): p. 1570-1583.
81. Stixrude, L., *Talc under tension and compression: Spinodal instability, elasticity, and structure.* J. Geophys. Res, 2002. **107**: p. 2327.
82. Fumagalli, P. and L. Stixrude, *The 10A phase at high pressure by first principles calculations and implications for the petrology of subduction zones.* Earth and Planetary Science Letters, 2007. **260**(1-2): p. 212-226.
83. Sato, H., et al., *First-principles studies on the elastic constants of a 1:1 layered kaolinite mineral.* American Mineralogist, 2005. **90**: p. 1824-1826.
84. Cygan, R.T., J.-J. Liang, and A.G. Kalinichev, *Molecular Models of Hydroxide, Oxyhydroxide, and Clay Phases and the Development of a General Force Field.* J. Phys. Chem. B, 2004. **108**(4): p. 1255-1266.
85. Berghout, A., D. Tunega, and A. Zaoui, *DFT study of the hydration steps of Na+/Mg2+/Ca2+/Sr2+/Ba2+-montmorillonites clays.* Clays and Clay Minerals, in press.

## *Abstract*

Clay mineral is widely distributed over the earth which impacts a wide variety of environmental and engineering processes. The swelling or shrinking of clay may generate extensive structural damage to constructing engineering. Whereas, the swelling clay is of great interest in geoenvironmental engineering as liners or constituents of the storage of radioactive waste, due to their low permeability to water, high swelling capacity, high surface area and high retention capacity for cations.

In this thesis, Monte Carlo and Molecular Dynamic simulation methods have been performed to study hydrated Wyoming-type montmorillonite, a naturally occurring swelling clay, including different monovalent or divalent counterions. The agreement of our simulation results on the clay containing some common cations such as $Li^+$, $Na^+$, $K^+$ and $Ca^{2+}$, with available experiment and preceding theoretical works, permitted us to extend our study to the clay with heavy metal ions, such as $Rb^+$, $Cs^+$, $Ni^{2+}$, $Zn^{2+}$ and $Pb^{2+}$,some of which have never been studied.

Besides, simulations have been also performed to investigate the swelling and shrinking behaviour of montmorillonite under the influence of water content, temperature and different counterions. We found a general phenomenon of hysteresis during both the hydrate/dehydrate and the warming/cooling processes. The quantities of counterions together with their solvation characteristics and their attraction capacities have an important influence on the swelling and shrinking behaviours of this clay. Moreover, investigations on the diffusion behaviours of water and counterions in the interlayer space of montmorillonite show the effect of hydrated degree and different existing cations especially the pollutants on the diffusion of water, as well as the effect of temperature on the diffusion of interlayer particles.

Finally, detailed studies on the shrinking behaviours of hydrated montmorillonite under pressure allowed us to shed light on the rigidity of this clay affected by the hydrated degree, where we found a phase transition phenomenon in hydrated montmorillonite with the phase transition pressure less than 1GPa.

According to our calculations the bulk modulus reaches extremely high values at modest pressures of ~20 GPa. This is likely to happen in a very different, and possibly quenchable to 1 atm, type of phases – such a possibility definitely needs to be explored in future work. It would open a route to a new family of ultra-incompressible (and possibly ultra-hard) materials of clay composition. Such materials, and their superior mechanical properties and possibly low cost, could be practically attractive for a number of uses.



## *Résumé*

Les sols argileux sont très présents à la surface de la terre et ont de grands impacts sur une large variété de processus d'environnement et d'ingénierie. Le gonflement ou dégonflement de l'argile peut causer des dégâts parfois importants aux constructions. Cependant, grâce à leur capacité de gonflement, leur faible perméabilité et leur grande aptitude de conservation des cations dans les espaces interlamellaires, les argiles gonflantes peuvent être utilisées pour le stockage de déchets radioactifs.

Dans cette thèse, les méthodes de Monte Carlo et Dynamique Moléculaire ont été utilisées pour étudier l'argile hydratée de type Wyoming-montmorillonite. Le bon accord de nos résultats de simulation concernant l'argile contenant $Li^+$, $Na^+$, $K^+$ et $Ca^{2+}$ avec les résultats expérimentaux et d'autres travaux théoriques nous a permis d'étendre notre étude à l'argile comportant des ions métalliques lourds, comme $Rb^+$, $Cs^+$, $Ni^{2+}$, $Zn^{2+}$ et $Pb^{2+}$.

Par ailleurs, les sols argileux se rétractent en période de sécheresse sous l'effet d'importante température, ce qui se traduit par des tassements différentiels qui peuvent occasionner des dégâts aux constructions. A cet effet nous avons examiné le comportement du gonflement et du dégonflement de la montmorillonite sous l'effet de la température, de la teneur en d'eau et de la nature des différents cations.

Un phénomène d'hystérésis a été constaté pendant le processus de gonflement/dégonflement ainsi que durant le processus de chauffage/refroidissement. La quantité de cations et leur capacité d'attraction ont un rôle important dans le processus de gonflement et du dégonflement de cette argile. En outre, l'étude de la diffusion de l'eau et des cations dans l'espace interlamellaire de la montmorillonite montre l'effet du degré d'hydratation et de la nature des cations (en particulier les polluants) sur la diffusion de l'eau, ainsi que l'effet de la température sur la diffusion des particules présentes dans les inter-couches.

Enfin l'étude détaillée de l'effet de la pression sur la montmorillonite montre la variation de la rigidité en fonction de la teneur en eau et permet de prédire des transitions de phase structurales inférieures à 1 GPa. Cette étude montre particulièrement que le module de rigidité peut atteindre des valeurs extrêmement élevées à des pressions relativement modestes d'environ 20 GPa. Ce résultat ouvre clairement la voie pour une nouvelle famille de matériaux ultra incompressible (et éventuellement ultra dures) composés d'argiles. Ce type de matériaux aux propriétés mécaniques spécifiques et de faibles coûts (abondance des argiles), peut être particulièrement attractif pour de nombreuses applications dans divers domaines.